

Below are concerns of each reviewer in italics, followed by the author's response and any actions that were taken to resolve it. At the end is a markup of the revised paper.

## **Response to Reviewer 1:**

### **Minor comments**

*line 109-112: what are the range of estimates for these numbers? You provided them for the Karion studies, but not these other two.*

Added the ranges of each to the paper.

*line 184: Perhaps cite the latest EPA greenhouse gas inventory*

We cited one from the previous year here because that was where the emission factor came from when this project was active. We cannot cite the most recent report here as the emission factors change from year to year and so the number may be different from the one we used.

*line 260-261: do these CH<sub>4</sub> sinks account for other reactive species in the atmosphere? If not, how would background or elevated levels of ethane or other gases affect these CH<sub>4</sub> losses?*

This is a fair point. Gases other than CH<sub>4</sub> are emitted from wells and could possibly decrease the reaction rate of OH with CH<sub>4</sub>. However, the purpose of this section is just to show that even in above average OH concentrations, the CH<sub>4</sub> sink is negligible. Unless the other gases released from well emissions lead to the production of additional OH, any gas released that will react with OH will only lower the sink's impact further.

Figure 2: if possible, it would be helpful to know where Bradford County was on this map

Updated the figure with the county highlighted in yellow

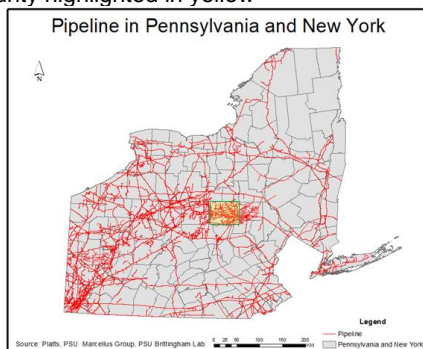
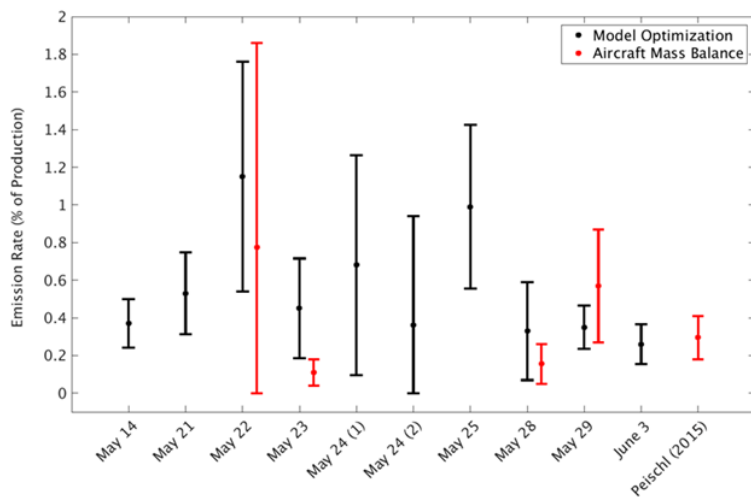


Figure 19: I would add the mean model optimization and aircraft mass balance emission rates to this graph, as well as the Omara and Peischl studies, along with their uncertainties. It seems like one advantage this study has, as mentioned in the introduction, is a narrowing of the uncertainties of these previous studies.

I did not add the mean for each as it made the plot a bit heavy and I want to emphasize the spread for each day. I also did not add Omara's number as it comes from emissions only from well production (no gathering emissions) and all wells from that study were measured in the southwest Marcellus, which has a much different composition compared to the northeast Marcellus. However, I did add the number from the Peischl study to the plot, as his study is a single mass balance flight in the region and so it fits in perfectly with the rest of the graph's content. I am not sure our final findings narrowed the uncertainties as intended so much as it discovered how uncertain the previous estimate may have been.



## Technical Comments

*The author numbering is not in order.*

Fixed

*line 48: Methane also has an atmospheric sink from chlorine chemistry.*

Clarified the sentence to imply the sink was mostly from OH.

*line 58: is "mining" the proper word for natural gas? It may be, I just can't say I've heard that before.*

Forget you heard it. It is not a good use of the word. Switched to "drilling and transportation of natural gas".

*line 64: add "of" to say "quality and quantity of its emission factors".*

Added.

*line 107: put "per day" before the abbreviation "MMSCFD", instead of after it.*

Switched the order.

## Response to Reviewer 2

Minor comments are addressed first. Major comments which have not been addressed through fixes in the minor comments are then addressed afterwards.

### Many Minor Comments:

*L51: Shouldn't you rather say that for emission rates larger than 3 %? Otherwise the sentence does not define a threshold.*

Changed to "greater than"

*L232-238: This paragraph should be directly in front of the one describing the data assimilation strategy finally used in the study (L246-253).*

Moved the paragraph accordingly

*L261: "The important time scale for the mass balance approach is not alone the flight duration but also the transport time from the upwind to the downwind interface of the box. Also the time from emission to sample should be discussed, as this is the crucial one for the inverse modelling."*

This segment is discussing how oxidation can decrease the background concentration of CH<sub>4</sub> during the duration of the flight. The emissions should not matter in this calculation because OH would be reacting with the entire CH<sub>4</sub> mole fraction (i.e., the background + enhancement), not just any enhancement in the region (a 40 ppb enhancement would change the CH<sub>4</sub> mole fraction by 2%, so changes to the reaction rate would be minimal). So it will be affecting all parts of the flight almost equally throughout the time of the flight and shouldn't have any relation to the distance the emissions are travelling from the well to the downwind transect.

However, I do agree that it is good to know the time it takes for emissions to travel to the downwind transect, if only to better understand how representative the upwind transect is of the air mass measured by the downwind transect. Given the range in wind speeds, it takes about 2-4 hours. This is mentioned briefly in the error analysis section.

*L312 and elsewhere: I don't like the terminology here. "observed CH<sub>4</sub> enhancement associated with upstream natural gas". The described quantity contains information from both model and observation and, thus, is not purely 'observed'. Maybe the term 'observation-based' or something else that identifies the real character of the data could be used instead.*

The term "observation-derived" replaces now "observed" across the entire document.

*L321: How frequent and how large are negative values of X<sub>GasO</sub>?*

Added sentence in paper describing negative values. 16% of the observation-derived enhancements are negative, but less than 3% are negative by 5 or more ppb.

L352: *“Were individual atmospheric densities for each flight neglected? Why?”*

They were not calculated, because a  $\pm 10$  change in the temperature produces a difference in the value (and thus the end result) of 3%. It's a similar change with a  $\pm 30$  hPa change in the pressure. For 10 flights during a 3 week period with no huge meteorological anomalies, calculating the exact density of the air in the ABL (which will have its own errors) based on a few vertical transects seemed unnecessary.

L416: *“If this is a good correlation coefficient, what is the range obtained for the other flights? Could this information be added to Table 4 or 5. It could also be used as part of the uncertainty assessment.”*

Correlation Coefficients for each flight have been added in a column under Table 5

L418f: *“Be a bit more specific concerning the near zero differences between model and observation. For the PBL height this statement may be true, however, it is also clear that the model is not able to capture the very sharp increase in potential temperature. I also wonder why the two profiles are shown separately, would be nice to have them on top of each other. Concerning the wind there is a directional shift of about  $+10$  degree in the model. You may call this small, but for the kind of plumes simulated here it might be of importance and should be mentioned.”*

I do not discuss the gradient of the potential temperature inversion or the offset in temperature between the model and observations because these factors do not impact the physics of the plume. For now, I would like to keep the two plots separated, as the important thing to emphasize with these plots are the ABL height similarities between the model and the observations which can be seen just fine with the plots as they currently are. Combining the plots would draw the reader's attention away from the ABL height and more towards the 1 K difference in temperature, which is not important to this discussion.

Changed L419-20 to reflect a difference in wind direction of 10 degrees.

L424ff: *“Please add a number for the average and maximum enhancement due to upstream natural gas sources at the northern transect to this discussion. From Figure 9 I would think these numbers are around 30 and 80 ppb. It puts the other contributions into perspective.”*

Adjusted line in the paper to give a range of the downwind enhancement.

L473ff: *“This discussion on the uncertainties due to shifts in the simulated wind direction is very hard to follow. Figure 16 does not speak for itself. You will need to explain in more detail what was done to derive the figure. This discussion should actually be given when the cost function is introduced.”*

Moved discussion of optimization technique and how it addresses transport uncertainties to methods section. Removed Figure 16 and wrote better explanation as to why sum of squares was not used as optimization technique. Simplified paragraph and associated figure is provided below.

“The decision to use a scalar cost function rather than the sum of squares is to account for possible misalignment between any observed CH<sub>4</sub> plume and modelled plumes. There are two potential ways in which misalignment may occur. One possibility is that the modelled wind direction differs from the true wind direction, leading to a plume in the model that is off-centre in relation to the observed plume. The other possibility relates to how the model treats emissions from natural gas as a uniform percent of production. In reality the emissions are more random in nature, and thus the plume may not always develop over the wells with the largest production values. If a cost function is used that minimizes the sum of the squares, any misalignment between the modelled and observed plume will result in the peak of the modelled plume aligning with the height of the tail of the observed plume (Figure 5). Unless the observed plume aligns perfectly with the modelled plume, the optimized emission rate using a sum of squares approach will always bias low. By using a scalar cost function, we solve for an optimized emission rate that results in a plume with the same area under the curve compared to the observed plume (Figure 5). This methodology is not impacted by any misalignment between the modelled vs. observed plumes, preventing the low biases associated with a sum of squares minimization.”

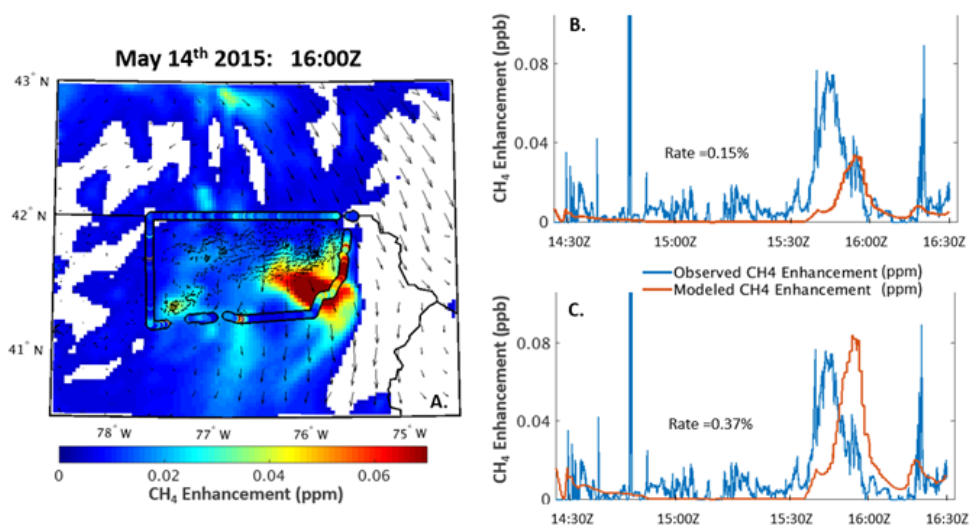


Figure 5: (a.) Observed vs model projected CH<sub>4</sub> enhancements during the May 14<sup>th</sup>, 2015 at 16Z. (b.) Comparison of observed natural gas enhancement to modelled natural gas enhancement along flight path, with upstream emission rate optimized by minimizing the absolute error between the datasets. (c.) Same as previous, but optimized by minimizing the sum of the error between the datasets.

L486: Should it be wind speed instead of wind direction?

It should be wind speed. Changed.

L498f: *“The way the wind speed error is assessed biases could be introduced. The average over all wind observations by the aircraft does not necessarily reflect the average wind speed within the boundary layer, since the sampling is not uniform (especially with height). It seems calculating an average vertical profile of wind speed from all the observations and comparing that to an average model profile generated from the same sampling locations should be more robust. Was this considered and decided that the aircraft sampling was sufficiently uniform?”*

Most of the time the aircraft is flying at a constant altitude. We have about 2-3 vertical profiles (mostly spirals) from the aircraft for most flights, but wind measurements can have large errors while the aircraft rises/falls and turns, both of which occur during a vertical spiral. So we cannot accurately construct a vertical profile of the winds in the ABL using the aircraft data. We could compare the model to surface station measurements in the area, but surface data poorly reflects on model inaccuracies within the boundary layer. Comparing the model directly to the aircraft observations when it is flying steady in the boundary layer is the best method we have of understanding the model's performance throughout the area, and also will capture all of the potential spatial variability as well. I do acknowledge though that due to a lack of wind measurements with height, if the model has a bias that is not uniform with height this will not be captured in the error analysis.

L506: *“There are more advanced techniques for estimating boundary layer heights from model and observational data than just ‘looking’ at the potential temperature. For example Bulk Richardson methods are quite useful in situations when potential temperature alone is not providing explicit results. The example shown here is an easy case but I wonder about the other situations mentioned in the text and especially how large the uncertainty of the estimates becomes in such situations.”*

Reading the sentence associated with this comment, I may have implied more uncertainty than there actually was. For all 10 flights, the potential temperature inversion could clearly be spotted in the model. This is also true for 9 of the aircraft flights. Only on one day (May 22nd, 2015) did the observational data not clearly show a large potential temperature gradient until ~3000m, with a smaller wiggle in the profile a bit lower. For this one though you could see a quick shift in the all of the trace gases at that wiggle, and so we could conclude that this represented the mixing height. We did not go into a more complicated methodology for deriving the ABL height because we felt it was unnecessary for our cases. Had the potential profiles been messier and vague, we would have then resorted to more complex methods of calculating the ABL height.

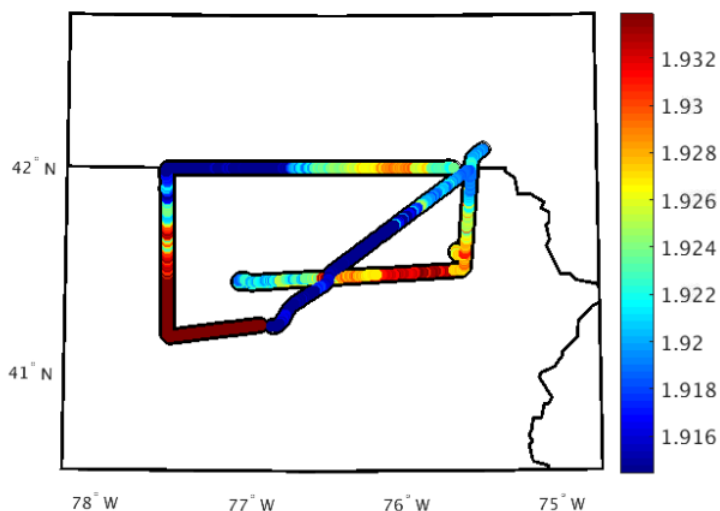
I have revised the sentence in the manuscript to make it more clear that there was little ambiguity in finding the ABL height.

L542f: *“How was this done exactly? Did you simply run 3 cases with 1) reference background, 2) background -5 ppb, 3) background +5 ppb? Or did you do a Monte Carlo approach where the +/- 5 ppb could be understood as the standard deviation of a normal distribution? Please clarify and justify the approach also in the light of possible non-linear effects that would not be covered by simply running 3 cases.”*

It was done by just running 3 cases to establish the limits because the effects changing the background has on the solution is nearly linear. Unlike using a sum of squares approach in our cost function, the cost function we use tries to minimize the difference between the area under the curve for the observations vs the model. Another way to think of it is that we are minimizing the total enhancement between the sum of the observation-derived enhancements and the sum of the modelled enhancements. By decreasing the background by 1 ppb, we are adding (1 ppb \* # of observations) to the total enhancement. By decreasing the background by 2 ppb, we are adding 2 ppb \* # of observations) to the total enhancement. The increase (or decrease) is linear, as is the effect on the cost function. The only effect that is non-linear occurs in the process the zeroing of any negative observation-based enhancements (of which you will have more of if you increase the background by 5 ppb), but the impact of this is small on the symmetry of the error bar. So a Monte Carlo approach was not needed due to the simple nature of the errors in this section.

L548f: *It is mentioned that the +/- 5 ppb assumption for the background uncertainty can have different impacts depending on the magnitude of the observed plume and this is related to wind speeds and PBL heights. How can you justify the use of a constant value for the background uncertainty? Shouldn't this also change with meteorological conditions? For example it is mentioned earlier that it will be large when there is more entrainment, which is usually the case while the PBL is still developing, and when plumes from other sources are advected. Wouldn't it make sense to take this variability in the background uncertainty into account?*

In truth, a lot of the changes we see in the background we just don't understand. Below are the methane observations from within the ABL for our flight on May 22nd.



This was a 3 hour flight between 1:30 pm-4:30pm local time. Winds were steady on this day and the boundary layer was deep throughout the duration of the flight. We should expect minimal changes in



the background in these conditions. But near the very beginning of the flight (bottom left), values were their largest despite being away from most sources. Meanwhile, values near the end of the flight suddenly drop off by 10 ppb despite having flown over the same area twice just one hour earlier. This is the most extreme example I can present of the randomness of the background variability, but in my experience with aircraft data, there are many instances in which sudden changes in the background can be observed which appear to be unrelated to entrainment or a simple calculation in how much the boundary layer changed. Much of the differences we see in the background values may have to do with heterogeneity of the large CH<sub>4</sub> plumes which develop regionally across the U.S.. As a curiosity, we ran WRF-Chem for 1 month at 27 km resolution using the EPA U.S. CH<sub>4</sub> emissions inventory (Maakkassers *et al.*, 2016) as input and found that the average difference in enhancement between two locations 71 km away in our study region was 5 ppb. These modelled differences are caused by the spatial gradients that naturally develop in the methane concentration field due to the transport of methane emissions across the central and eastern U.S.

In short, we picked a background variability of  $\pm 5$  ppb to represent a conservative estimate of how much variation we could see in a flight. We did not believe that any calculation we could perform with the data we had could sufficiently describe our uncertainty with the background value estimate, so we chose a range that seemed large without being unreasonable.

*L557f: "Again the question: is [the non-natural gas emissions adjustment] done by running by simply running 3 cases or in a Monte Carlo fashion. Did you scale all categories with the same factor at the same time or test combinations as well? How do you obtain symmetric uncertainties in the final emission rate when you use asymmetric uncertainties in the non-upstream natural gas emissions?"*

The 50-200% range was a typo and should have read 0-200%. However, we agree that the initial error analysis from the inventory could be improved upon. To improve this section, we followed the advice provided and ran a Monte Carlo simulation for 10,000 iterations, selecting a multiplier from a uniform distribution ranging from 0 to 2 for each of the 8 non-upstream gas sources. This allowed for a much more realistic understanding of the errors compared to assuming all sources were incorrect by the same multiplier. The resulting patterns for each day were close to Gaussian. For each day, we fit a Gaussian and took the 2 sigma range as the uncertainty. Most days did not see much of a change from the previous uncertainty assessment, but days where the coal plume interacted with the observations (May 24th May 25th) saw an increase in the error. The methodology for this has been updated in the paper.

*L505, L562: "Table 5 should already be referenced here and not only at the very end of the section."*

Added for L562. I didn't add a reference at L505. That's describing a different methodology related to Table 4. I did add another reference to both Table 4,5 when the error analysis is first introduced.

*L571: "The estimator for the model performance uncertainty is a normalised root mean square error (NRMS) and it should be called like this to reduce the confusion. However, I am not convinced that this is the best estimator for what you want to achieve. One problem is the use of the optimised simulation, which means you have already used the information contained in the observations and thus the uncertainty estimator is not independent anymore. Furthermore, NRMS is not a good measure of what you call "similarity of pattern". The Pearson correlation coefficient should be better suited for this*

purpose. Please justify your choice. If you stay with a RMS estimation it should be applied to the prior simulations and the bias should be removed before the RMS is estimated.”

We had originally looked at the correlation as a way to quantify uncertainty, but we found there were some interesting cases where the correlation did not accurately describe problems with the model vs. obs comparison. For a great example, look at Figure 17 (May 22nd Loop1 vs May 28 Loop2).

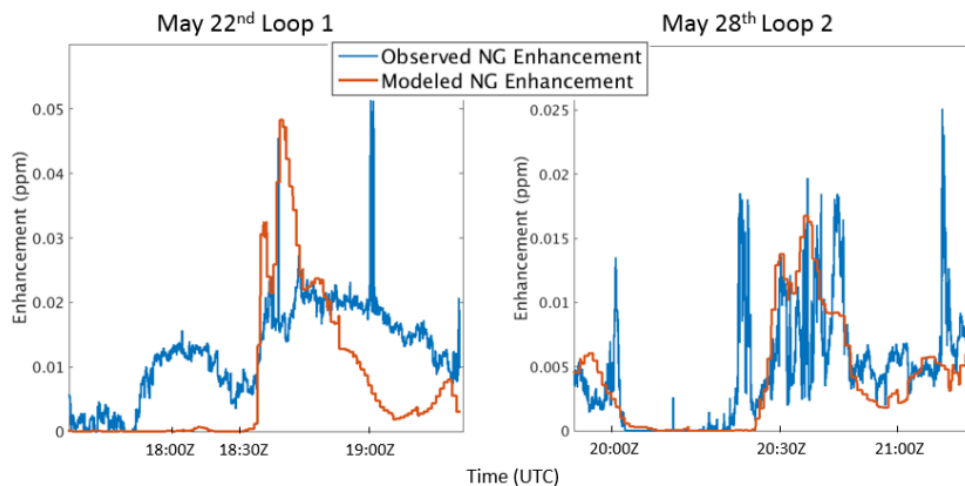


**Figure 17: Comparison of observed natural gas enhancement to modelled natural gas enhancement for segments along the (left) May 22nd flight and (right) May 28th flight. A distinct lack of representativeness of the observations in the modelled enhancement can be seen in the May 22nd flight compared to the May 28th flight.**

Anyone looking at the figures would immediately conclude that the observations on May 28th were modelled better than May 22nd. However, the May 22nd Loop1 flight actually has a correlation coefficient of 0.58 while the May 28th Loop2 flight has a correlation coefficient of 0.57. Of all the methods we tried, we found the NRMS method we use resulted in the error estimates that matched with a common-sense approach.

I do not fully understand the request to apply our methodology to the prior. Unlike an atmospheric inversion, our forward-based modeling experiment does not have a true prior. The number we selected for our first-guess emission rate (0.13% of production) has 0 bearing on the final results. It only provides the model with the spatial pattern the plume will take, and is scaled entirely by the observations. Had we started with a first-guess emission rate of 82,350% of production, the final result and uncertainties would not change.

Added a line addressing that the formula used is a modified NRMS to avoid confusion.

“L579f: You also assume Gaussian uncertainty distributions, which seems oversimpli- fied.”

As addressed above, the certainty of our background uncertainty parameter is very uncertain. The Monte Carlo for the non-natural gas emissions uncertainty produced mostly Gaussian-shaped distributions, but this was assuming an arbitrary range of variations in the emissions of each source which may also have spatial variabilities that we don't understand, and the model performance error is just a method we picked to try and best match our own understanding of what the errors associated with mismatch should look like. Assuming Gaussian uncertainty distributions is probably a stretch, but there was no methodology we could come up with where we would feel any more confident in our final error bounds.

To counteract the uncertainty in our uncertainty, it should be noted that we tried to be very conservative with our uncertainty parameters. A  $\pm 5$  ppb variation with the background is large. A 0-200% range in the emissions from non-natural gas sources is large. We did not want to underestimate the uncertainty, as is often done, so we tried to be as fair with our analysis as possible to produce a  $2\sigma$  range which would contain the true emission rate 95 times out of 100.

*L645: "Figure 18 can go into a supplement without any loss of information. Instead give the rate of change of the background with time as a number in the text."*

Added the rate of change in the text, and Figure 18 is in consideration to be moved to supplemental (see major comments below)

*L652: "Does this mean the final uncertainty estimate is the mean over the uncertainties for each flight?"*

From that sentence, we use the standard error from the four flights to come up with the uncertainty range.

*L663ff and Fig. 19: "The variability in emission rate estimates for individual days as shown in the figure are not discussed in any detail."*

This is a good point. Added a segment in the early part of the discussion section to discuss reasons for variability in the emission rate.

*Of special interest is the question of agreement between the two methods as it could lend some additional trust in the applied methods. However, the figure seems to raise more questions in the reliability. For example if 29 May is the golden day (as described earlier in the text), why are estimates from both methods so different?*

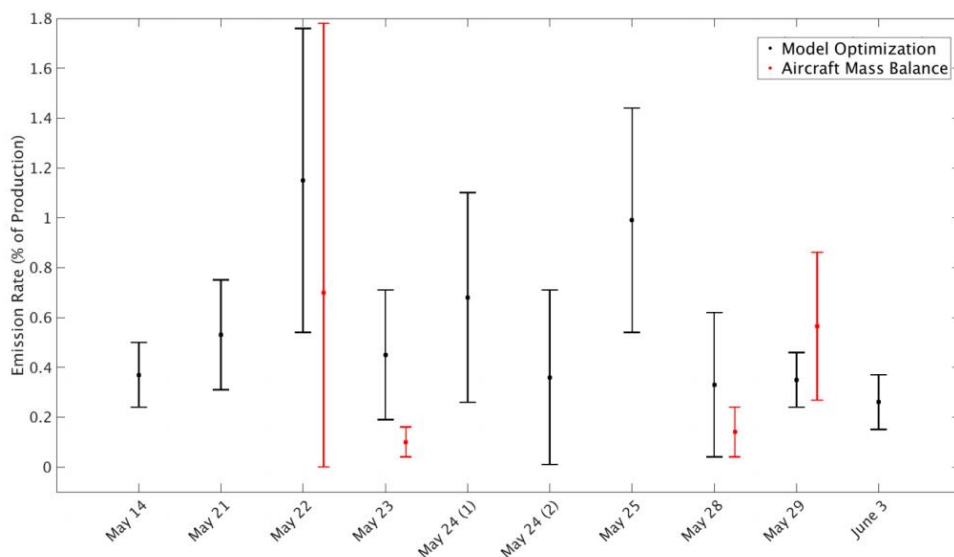


**Figure 19: Calculated upstream natural gas emission rates using (black) model optimization technique and (red) aircraft mass balance technique.**

The values on May 29th from the aircraft mass balance and model optimization are 0.57% and 0.35%, differing by 0.22% of production. They even fall within each other's error bars. Claiming the two values are "so different", is odd, and should not be used to question the reliability of the model optimization method. Furthermore, the aircraft mass balance method has sources of error which differ from errors associated with the model optimization technique. A perfect match between two methods each with their own unique sources of error is unlikely.

I do discuss briefly in the paper that the relative closeness of the results in these two methods gives credence to the model optimization technique. But that is not to say the aircraft mass balance method is the golden standard in the field. If the mass balance approach were flawless, bottom-up and top-down emission estimates would be in agreement at this point and there would be little need for this paper.

*Also there seems to be no agreement in the variability for the 4 common days. How could you explain the large variability from the point of the emission processes? Is there any dependency on the total production on these days (following the line of thought used later for the discussion of different basins)? Please speculate on this otherwise the reader is left with the impression that your given uncertainty estimate is rather optimistic."*

The topic of emissions variability is briefly touched upon in the introduction, but I've added a segment in the discussions to re-address some of the possible reasons for the variability in the totals. These reasons include the nature of natural gas releases from stochastic events such venting, flaring, liquids

unloading, ect., as well as the possibility that the days with large emission rates also have large uncertainties due to the complex scenarios from those days.

*L666f: Repeat the range of emission rates from other studies here.*

Added a line addressing this rate compared to other regions.

*L696ff: The flight described in this section and shown in Fig. 21 is not part of the main analysis of the paper and should be omitted as it does not provide any additional insights and aspects that have not or could not be shown on the other flight examples.*

On the contrary, this flight is the perfect example to demonstrate why it is so advantageous to model the plumes with a direct model instead of the backward adjoint model. Until this study, a mass balance from a single flight was the only top-down study performed in the northeastern Marcellus. There was little knowledge of how the coal plumes 500 km away would interact with the flight in this region. By running a transport model, we're able to see that the background of this flight is compromised by the heterogeneous nature of the coal plume, thus explaining the complex signals observed by the aircraft (it should be noted that the highest CH<sub>4</sub> values observed in *Peischl et. al.* 2015 were **upwind of the wells**). Even if someone does not plan to use the transport model to solve for the emissions in a region, it can still be useful to better understand the complexity of background plumes on a given day and decide whether a mass balance would be appropriate to use. By using the flight from *Peischl et. al.* (2015), we not only show the usefulness of using a transport model for future studies, but also emphasize the potential need to relook at flights from earlier studies and check for whether complex plume structures may be adding additional uncertainty to the regional emissions estimate.

### **Addressing the major concerns directly**

*Model optimisation technique (inverse modelling): The applied optimisation technique uses a very simple cost function to find an optimal factor between 'prior' and 'posterior' emission rates. Why did you not apply a Bayesian approach that could take uncertainties in the prior values and observations/simulations into account? Much of the following uncertainty assessment could then be used in the optimisation step and also more reliably give posterior uncertainties. Also, why do you not use sum of squares in the cost function as is commonly done? Some explanation is given later in the text, but without further discussion of Figure 16 this remains useless. Please discuss why your method should provide more reliable results as other similar studies that have used a Bayesian framework.*

As far as I'm aware, there are not any similar regional methane emission studies that have combined a Bayesian framework with an aircraft campaign. We know of few ongoing studies but to date, none of them have been published. Few top down studies used gas-to-gas ratios and backward footprints to estimate point source CO<sub>2</sub> emissions (e.g. Brioude et al., 2012) but without any prior emissions. One of the advantages of a Bayesian methodology is that it allows one to use and propagate their errors from a prior guess to the posterior estimate. However, it is for that same reason that a Bayesian approach would be inappropriate here. We have little information regarding the errors associated with this study. The background CH<sub>4</sub> values, the emissions inventory, and the model transport error are all poorly understood. This includes the 'prior' emissions estimate of natural gas as well, which is just the median

emission rate from 17 UNG wells in southwestern PA. Any Bayesian approach without reliable uncertainty estimates will not produce reliable results (Chevallier et al., 2006).

One of the greatest advantage to our forward-based modelling approach is that you are able to visualize plumes and partition the problem into components, directly observing the uncertainties associated with the optimization process. The forward modelling approach lets you directly see the structures of the different plumes on a given day and how they compare to observations. This makes it simple to know your problems for a specific day. If there are far-reaching plumes influencing the observations, you know to be cautious with the emissions estimate. If plumes appear to consistently misalign slightly between the observations and the model, you know there's likely a transport issue. If observations shift in regions where no plumes are modelled, you know you are dealing with either a missing source or background variability. And because emissions scale linearly with the resulting plumes, once the model is run it becomes easy to make adjustments to see how much impact changes can have on your results. These different aspects are purely and simply invisible in a backward mode, for which the adjoint only points to the simulated area of influence. The difficulty with the direct approach is to rigorously quantify the final uncertainties, but uncertainties obtained from a Bayesian will be no more reliable if the prior uncertainties are not known.

So while the approach we use in this study may be simplistic, we do not consider that to be a weakness. Rather, the ease-of-use associated with this method allows it to be readily applied to any other study, past, present, or future, so long as an emissions inventory can be compiled for the region.

We have responded to the "sum of squares" issue under minor comments. We have considered methods such as Nearest Neighbor Search (NNS) but found it tedious and unsatisfactory as it would look for surrounding pixels and would therefore require an adjoint model.

*Uncertainty assessment of obtained emission rates: The uncertainty assessment of the obtained emission rates for both the 'model optimisation' as well as the mass balance method contains a lot of arbitrary assumptions and does not seem to be statistically sound. Their seems to be an overall assumption of Gaussian uncertainties (although not explicitly mentioned), which does not seem to be justified for several of the sources of uncertainty. Also the way the uncertainties are propagated through the individual methods remains very vague and could be improved by using a Monte Carlo type uncertainty assessment. These concerns are repeated in detail below.*

We addressed this concern at multiple points under minor comments section. To summarize here, we have propagated errors when possible in the revised manuscript (non-Natural Gas sources), and found that our Gaussian assumption matches closely the exact error distribution in this case. For the other error terms, we have statistical information on transport errors (from other studies at similar scales, e.g. Deng et al., 2017) to confirm it, or reasons to use a Gaussian propagation of the standard deviations when the distribution remains unknown (e.g. prior errors on emissions). We also want to emphasize that the absence of known prior uncertainties for emissions will significantly impair our ability to diagnose the full error distributions with a Monte Carlo approach. Therefore, random sampling such as Monte Carlo would not solve the problem of unknown error distributions. In general, we have been very conservative in our estimates, using the high end of the error values. Unless more information on error sources becomes available, we think that propagating errors under Gaussian assumptions remains valid and perfectly justified.

*Length: With 21 figures, 8 tables and a total of 50 draft pages the manuscript is quite lengthy and it would profit from shortening and restructuring. Below I suggest a number of figures that could easily be omitted or moved into a supplement without loss of information. Furthermore, I strongly encourage to incorporate the description of the uncertainty assessment method, which is now given within the results section, into the methods section along with or following the description of emission rate estimation itself. In this was many repetitions could be avoided and the paper could really focus onto the results in section 3.*

A major restructure was done to move uncertainty assessment into methods section and eliminate duplications associated with having those split previously. Results are now concise and focused only on results, rather than methods. The number of figures has been reduced by combining Figures 1 and 20, and the removal of Figure 16. If the editor feels that the length of the paper is an issue, further changes can be made, such as moving Figure 4 and 18 to supplemental as well as the entire description of the mass balance method used in this paper. However, if the editor feels that length is not an issue, we would prefer to keep these sections in the paper to retain its flow.

#### **Technical Fixes**

*L26: Abbreviation (WRF-Chem) not introduced before. Do so on line 25.*  
Added abbreviation

*L48: "transforms" instead of "transform"*  
Due to interactions... which transform. Grammar is correct

*L59: Add "United States" in front of "Environmental Protection Agency".*  
Added

*L348: Why are the terms U, D, and L given in braces? Not necessary.*  
Braces removed.

*L496: "as long as" instead of "so long as".*  
Changed

*Fig. 7: Do not show wind arrows in center panel. Not visible anyway and one gets the general flow direction from the shape of the plumes. Show center panel with same size as the individual tracers. Also use exactly the same color scale for all sub-panels. It looks like the center plot does have fewer color levels than the others. Each panel (also the center panel) requires a label.*

We respectfully disagree with this comment and prefer to keep the wind arrows to illustrate the direction of the flow for this very specific case. The coal plume coming from far away is explained by the regional circulation. The arrows remain small and should not decrease the readability of the figure. We modified the colorscale to match better with individual tracer figures. Did not resize middle figure to match other figures. Middle figure is most important and thus should be drawn as such. I think the label being referred to each panel needing was lat/lon. Added to the main figure. Not added to smaller

figures as it makes things messy and unreadable. I would think the reader would have a good understanding of where they are in space using middle figure as reference.

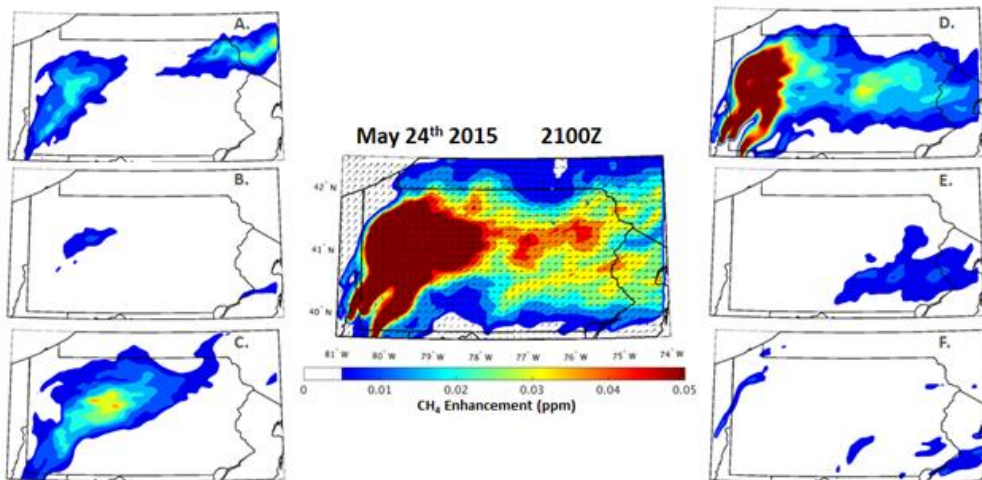


Fig. 11: Show observed and simulated profile on top of each other (see also comment above).

The purpose of the figure is to show an example of a theta profile for both the observations and the model and how the abl was found for each. The current figure accomplishes this fine.

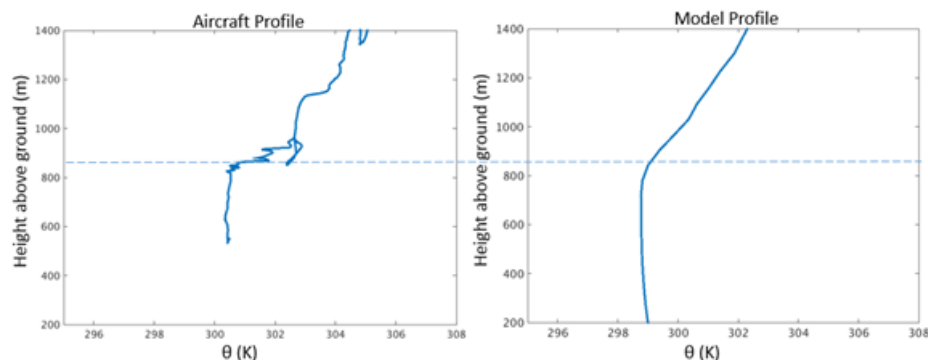


Fig. 12 and others: There is no mentioning of the wind arrows in the figure legend. Are these near surface or mean PBL winds? There is also no reference vector that would allow inferring



*the wind speeds from the arrow length. Choose a different color for the wind vectors. They are not well visible in the righthand figure.*

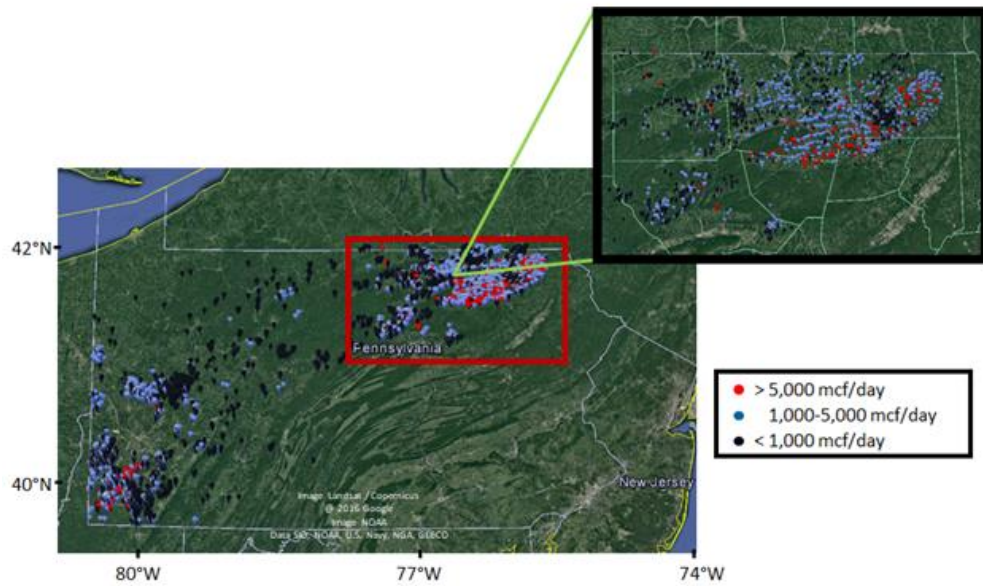
Added description of height level of model used in figure. Wind speed by arrow length changes in a complex manner from figure to figure with no easy way to retrieve its scale. Given the context of the figure, the reader will likely not be interested in small changes in the wind speed but rather the wind direction. If a reader wants more information on the wind speed, he can reference Table 3 which contains information on the mean wind speed for each flight. If the editor feels that a wind speed legend is necessary for these figures, then they will be added in. In terms of wind arrow color, it is difficult to pick a color that works everywhere due to the various colors on the plots associated with the plumes. For figure 12 this should not be an issue as it is a two panel figure where wind directions are clearly visible on the left panel. In figure 14 the wind direction is consistent throughout the domain and should not be too difficult for the reader to extrapolate the information.

*Fig. 19: Mention in the caption what error bars represent.*

Added description.

*Fig. 20: This information could also be merged into Fig. 1 and save the additional figure here.*

Merged well production information from Figure 20 into Figure 1. Removed Figure 20 from the paper.



### Other Changes

Fixed error in Corrected NG Emission Rate (Table 4: WS/ABL bias table), where errors were miscalculated.

Fixed error in calculation of mean and uncertainty regarding aircraft mass balance emission rate.

Minor text fixes.

# 1 Quantifying methane emissions from natural gas production in 2 northeastern Pennsylvania

3 Zachary R. Barkley<sup>1</sup>, Thomas Lauvaux<sup>1</sup>, Kenneth J. Davis<sup>1</sup>, Aijun Deng<sup>1</sup>, Yanni Cao<sup>1</sup>, ~~Colm Sweeney<sup>2</sup>;~~  
4 ~~Douglas Martins<sup>7</sup>;~~ Natasha L. Miles<sup>1</sup>, Scott J. Richardson<sup>1</sup>, ~~Thomas Murphy<sup>4</sup>;~~ ~~Guido Cervone<sup>5</sup>;~~ ~~Colm~~  
5 ~~Sweeney<sup>2</sup>;~~ Anna Karion<sup>2</sup>, ~~Stefan Schwietzke<sup>8</sup>;~~ Karion<sup>3</sup>, MacKenzie Smith<sup>3</sup> Smith<sup>4</sup>, Eric A. Kort<sup>3</sup> Kort<sup>4</sup>,  
6 ~~Stefan Schwietzke<sup>5</sup>;~~ Thomas Murphy<sup>6</sup>, Guido Cervone<sup>7</sup>, Douglas Martins<sup>8</sup>, Joannes D.  
7 ~~Maasakkers<sup>6</sup>;~~ ~~Maasakkers<sup>9</sup>~~

8 <sup>1</sup>Department of Meteorology, The Pennsylvania State University, University Park, PA 16802, United States

9 <sup>2</sup>NOAA/Earth Systems Research Laboratory, University of Colorado, Boulder, CO, 80305, United States

10 <sup>3</sup>~~Department~~ <sup>3</sup>National Institute of Standards and Technology, Gaithersburg, MD 20899, United States

11 <sup>4</sup>~~Department~~ of Climate and Space Sciences and Engineering, University of Michigan, Ann Arbor, MI, 48109, United States

12 <sup>4</sup>~~Marcellus~~ <sup>5</sup>Cooperative Institute for Research in Environmental Sciences, University of Colorado, Boulder, Colorado, USA,

13 <sup>6</sup>Marcellus Center for Outreach and Research, The Pennsylvania State University, University Park, PA 16802, United States

14 <sup>5</sup>~~Department~~ <sup>7</sup>Department of Geography, The Pennsylvania State University, University Park, PA 16802, United States

15 <sup>6</sup>School

16 <sup>8</sup>FLIR Systems, West Lafayette, IN 47906, United States

17 <sup>9</sup>School of Engineering and Applied Sciences, Harvard University, Pierce Hall, 29 Oxford Street, Cambridge, Massachusetts  
18 02138, United States

19 <sup>7</sup>FLIR Systems, West Lafayette, IN 47906, United States

20 <sup>8</sup>~~Cooperative Institute for Research in Environmental Sciences, University of Colorado, Boulder, Colorado, USA.~~

21

22

23 Correspondence to: Zachary R. Barkley (zrb5027@psu.edu)

24

25

26 **Abstract.** Natural gas infrastructure releases methane (CH<sub>4</sub>), a potent greenhouse gas, into the atmosphere. The estimated  
27 emission rate associated with the production and transportation of natural gas is uncertain, hindering our understanding of its  
28 greenhouse footprint. This study presents a new application of inverse methodology for estimating regional emission rates  
29 from natural gas production and gathering facilities in northeastern Pennsylvania. An inventory of CH<sub>4</sub> emissions was  
30 compiled for major sources in Pennsylvania. This inventory served as input emission data for the Weather Research and  
31 Forecasting model with chemistry enabled, (WRF-Chem), and atmospheric CH<sub>4</sub> mole fraction fields were generated at ~~3km~~  
32 ~~km~~ resolution. Simulated atmospheric CH<sub>4</sub> enhancements from WRF-Chem were compared to observations obtained from a  
33 three-week flight campaign in May 2015. Modelled enhancements from sources not associated with upstream natural gas  
34 processes were assumed constant and known and therefore removed from the optimization procedure, creating a set of  
35 observed enhancements from natural gas only. Simulated emission rates from unconventional production were then adjusted  
36 to minimize the mismatch between aircraft observations and model-simulated mole fractions for ten flights. To evaluate the

37 method, an aircraft mass balance calculation was performed for four flights where conditions permitted its use. Using the  
38 model optimization approach, the weighted mean emission rate from unconventional natural gas production and gathering  
39 facilities in northeastern Pennsylvania approach is found to be 0.36% of total gas production, with a  $2\sigma$  confidence interval  
40 between 0.27-0.45% of production. Similarly, the mean emission estimates using the aircraft mass balance approach is  
41 calculated to be 0.3440% of regional natural gas production, with a  $2\sigma$  confidence interval between 0.0608-0.6272% of  
42 production. These emission rates as a percent of production are lower than rates found in any other basin using a top-down  
43 methodology, and may be indicative of some characteristics of the basin that makes sources from the northeastern Marcellus  
44 region unique.

## 45 **1 Introduction**

46 The advent of hydraulic fracturing and horizontal drilling technology has opened up the potential to access vast reservoirs of  
47 natural gas previously inaccessible, shifting energy trends in the United States away from coal and towards natural gas (EIA,  
48 2016b). From a greenhouse gas (GHG) emissions perspective, natural gas has the potential to be a cleaner energy source  
49 than coal. For every unit of energy produced, half as much carbon dioxide (CO<sub>2</sub>) is emitted through the stationary  
50 combustion of natural gas in comparison to coal (EPA, 2016). However, during the process of extracting and distributing  
51 natural gas a percentage of the overall production escapes into the atmosphere through both planned releases and unintended  
52 leaks in infrastructure. Though these emissions may be small from an economic perspective, their climatological impacts are  
53 not negligible (Alvarez et al., 2012; Schwietzke et al., 2014). Methane (CH<sub>4</sub>), the main component of natural gas, is a potent  
54 greenhouse gas with a global warming potential over a 20-year period (GWP<sub>20</sub>) of 84 (Myhre et al., 2013). Over a 100-year  
55 period the GWP is reduced to 28 due mostly to interactions with the hydroxyl radical which transform the CH<sub>4</sub> molecule to  
56 CO<sub>2</sub>. Depending on which timespan is used, the relative climatological impacts of natural gas as an energy source compared  
57 to coal can vary. Using the GWP<sub>20</sub> value, it is estimated that a natural gas emission rate of only greater than 3% of total gas  
58 production would result in a natural gas power plant having a more negative impact on the climate than a coal-powered  
59 plant. Using the GWP<sub>100</sub> value, this emission rate threshold shifts to 10% of production (Schwietzke et al., 2014; Alvarez et  
60 al., 2012). Complicating matters further, the future climate impacts associated with an increased availability of natural gas  
61 extends well beyond a simple greenhouse gas footprint comparison against coal. Lower fuel prices linked to this new  
62 reservoir of energy can change the course of future energy development globally. With many states and countries attempting  
63 to find a suitable balance between their energy policies and greenhouse gas footprint, it is important for the scientific  
64 community to be able to quantify and monitor natural gas emission rates.

65 The miningdrilling and transfertransportation of natural gas can be broken down into five stages: production,  
66 processing, storage, transmission, and distribution. The United States Environmental Protection Agency (EPA) uses a  
67 bottom-up approach to quantify these emissions, estimating emission rates per facility or component (such as a compressor,  
68 unit length of pipeline, pneumatic device) or an average emission per event (such as a well completion or liquids unloading).

69 These “emission factors” are then multiplied by nationwide activity data containing the number of components or events  
70 associated with each emission factor, and a total emission rate is produced for the country (EPA, 2015b). This bottom-up  
71 approach is a practical methodology for estimating emissions over a large scale but has limitations. A bottom-up inventory  
72 depends on the quality and quantity of its emission factors and activity data. Emissions from sources in the natural gas  
73 industry can be temporally variable and have a wide range of values depending on a number of factors, such as the quality  
74 and age of the device and the gas pressure moving through the component. Furthermore, recent studies have shown that a  
75 majority of emissions comes from a small percentage of devices, often referred to as “super-emitters”, creating a long-tail  
76 distribution of emission sources (Brandt et al., 2014, Omara et al., 2016, Zavala-Araiza et al., 2015, 2017, Frankenberg et al.,  
77 2016). These ~~two~~ factors make it difficult to sample enough devices and adequately describe the mean emission rate, thus  
78 allowing for significant representation errors in the emission factors. Because emission factors are required for hundreds of  
79 different components, these errors can accumulate and lead to systematic biases in the total emissions estimate.

80 One way to ~~compare~~ complement results based on inadequate sample sizes in the bottom-up approach is to measure  
81 the aggregated enhancement in the atmospheric mole fraction at larger scales through a top-down approach. Instead of  
82 measuring emissions from individual devices and scaling up, a top-down approach takes atmospheric greenhouse gas  
83 concentrations measured downwind of a continent (e.g. Bousquet et al., 2006), a region (e.g. Lauvaux et al., 2008), a city  
84 (e.g. White et al., 1976, Mays et al., 2009, Lamb et al., 2016) or a facility (e.g. Ryerson et al., 2001) and uses inverse  
85 methodologies to attribute the enhancements to potential sources upwind. One of these methods, the aircraft mass balance  
86 technique, has been performed at many different oil and gas fields to characterize natural gas emissions (Petron et al., 2012,  
87 Karion et al., 2013, 2015, Peischl et al., 2015, Conley et al., 2016). While this methodology is able to capture surface fluxes  
88 over a large region, it remains difficult to attribute the emissions to any individual source (Cambaliza et al., 2014). Any  
89 sources from within the flux region that emit CH<sub>4</sub> will be measured in the downwind observations and be a part of the  
90 aggregated regional enhancement. Atmospheric observations ~~also may~~ include other sources of CH<sub>4</sub> unrelated to natural gas,  
91 such as anaerobic respiration from landfills and wetlands, enteric fermentation from cattle, anaerobic decomposition of  
92 manure, CH<sub>4</sub> seepage from coal mining, and many other smaller sources. If the purpose of the study is to solve for the  
93 emissions from the natural gas industry, emissions from all sources unrelated to natural gas must be known and removed  
94 from the regional flux estimate. Thus, top-down experiments require an accurate CH<sub>4</sub> inventory of the study area and any  
95 errors associated with the inventory will propagate into the final emissions estimate. A more advanced technique to separate  
96 out non-natural gas sources has been developed using ethane as a tracer for natural gas (Smith et al., 2015). However, such  
97 methods may struggle in dry gas basins where smaller ethane to methane ratios within the gas can make the ethane signature  
98 more difficult to separate out. or in regions where multiple ethane sources are present. And similar to bottom-up methods,  
99 top-down studies fail to address temporal variability, with observations from many of these studies having been collected  
100 during a limited number of 2 to 4 hour aircraft flights performed over a period of weeks.

101 In recent years, both bottom-up and top-down studies have aimed at calculating natural gas emission rates, with  
102 bottom-up studies generally finding smaller emission rates than their top-down counterparts (Brandt et al., 2014). The

Formatted: Font: 12 pt

103 discrepancy between the results from these two methodologies must be better understood if the true emission rate is to be  
104 known. Both the bottom-up and top-down approaches have their own inherent sources of error. For the bottom-up approach,  
105 a small sample size could result in the omission of any super-emitters, resulting in a low emissions bias. For the top-down  
106 approach, difficulty in attributing the measured enhancements to their correct sources can lead to errors when solving for the  
107 emissions of a particular sector.

108 Top-down emission estimates of individual basins have shown variation in the emission rate across the different  
109 basins. An aircraft mass balance performed over the Barnett shale in Texas found an emission rate between 1.3-1.9% of  
110 production (Karion et al., 2015), yet a similar mass balance study executed over unconventional wells in Uintah County,  
111 Utah, calculated an emission rate between 6.2-11.7% of production (Karion et al., 2013). Differences in regional emission  
112 rates can perhaps best be illustrated by recent studies in the Marcellus region. The Marcellus shale gas play is part of the  
113 Marcellus geological formation running close to the Appalachian mountain chain from West Virginia to southern New York  
114 and contains an estimated 140 billion cubic feet of technically recoverable natural gas (EIA, 2012). Reaching peak  
115 production by the end of 2015, the Marcellus is the largest producing shale in the U.S., producing 17,000 million standard  
116 cubic feet ~~per day~~ (MMSCFD) ~~per day~~ of natural gas (EIA, 2016a). A bottom-up study measuring emissions from 17  
117 unconventional well-sites in the Marcellus found a median emission rate from the wells of 0.13% of production, but  
118 estimated a mean emission rate ~~of between~~ 0.5338-0.86% of production due to the potential presence of super-emitters which  
119 would skew the mean emission rate towards values higher than the median (Omara et al., 2016). An aircraft mass balance  
120 study over northeastern Pennsylvania calculated an emission rate ~~of between~~ 0.3018-0.41%, a number that accounted for  
121 emissions from the production, processing, and transmission of the gas (Peischl et al., 2015). Both of these derived estimates  
122 fall below emission rates calculated throughout other basins and are below the 3% threshold required for natural gas to be a  
123 smaller climate pollutant in comparison to coal over a 20-year timescale. The low rates in the Marcellus compared to other  
124 regions could be the result of a systematic difference within the Marcellus that leads to a more efficient extraction of natural  
125 gas. However, while useful as a first-guess estimation, current studies performed in the region are based on relatively small  
126 sample sizes (1 aircraft mass balance and 88 individual well measurements). A more thorough analysis of the emission rate  
127 in the Marcellus would provide insight into regional differences in CH<sub>4</sub> emissions from different shale basins and help  
128 improve national estimates of emissions from natural gas.

129 This study seeks to provide confidence in the emission rate for the northeastern Marcellus by performing the most  
130 thorough top-down analysis of the northeastern Marcellus region to date. CH<sub>4</sub> measurements were taken from aircraft  
131 observations across 10 flights in northeastern Pennsylvania. A new implementation of modelling CH<sub>4</sub> mole fractions is  
132 developed to track complex plume structures associated with different emitters, and an optimal natural gas emission rate is  
133 solved for each of the 10 flights. An aircraft mass balance technique is also conducted for 4 of the flights and natural gas  
134 emission estimates from this method are compared to those calculated using the modelling technique. Using information on  
135 the uncertainty with both methods, a regional emission rate is calculated for the natural gas industry in the northeastern  
136 Marcellus region.

## 137 **2 Methods**

138 The objective of this study is to quantify CH<sub>4</sub> emissions coming from unconventional wells and compressor stations,  
139 henceforth referred to as upstream natural gas emissions, in the northeastern Marcellus region (defined as the area contain  
140 within 41.1-42.2°N 75.2-77.6°W, [see](#) Figure 1) through two different top-down methodologies. CH<sub>4</sub> observations from  
141 aircraft data are collected for ten (10) individual flights over a three-week period in May 2015. These data are used to solve  
142 for the upstream natural gas emission rate using an aircraft mass balance approach. Additionally, a CH<sub>4</sub> emissions inventory  
143 for the region is compiled and input into an atmospheric transport model described below. CH<sub>4</sub> concentrations are modelled  
144 for each flight, and the upstream natural gas emission rate within the model is optimized to create the best match between  
145 aircraft observations and model projected enhancement, providing another estimate for the upstream natural gas emission  
146 rate. The sections below detail the regional CH<sub>4</sub> inventory, the aircraft campaign, the transport model, the model  
147 optimization technique, and the mass balance approach used in this study.

148

### 149 **2.1 Regional Methane Emission Inventory**

150 In this study we characterize emissions from the natural gas industry into five different sectors: emissions from wells,  
151 emissions from compressor facilities, emissions from storage facilities, emissions from pipelines, and emissions in the  
152 distribution sector.

153 To estimate CH<sub>4</sub> emissions from the production sector of the natural gas industry, data were first obtained on the  
154 location and production rate of each unconventional well from the Pennsylvania Department of Environmental Protection  
155 Oil and Gas Reporting website (PADEP, 2016) and the West Virginia Department of Environmental Protection (WVDEP,  
156 2016). To convert the production rate into an emission rate, we need to assume a first-guess as to the expected leakage from  
157 wells in the area. A first-guess natural gas emission rate of 0.13% was applied to the production value of each of the 7000+  
158 producing unconventional wells based on the median rate from Omara et al., (2016). The natural gas emission rate was then  
159 converted to a CH<sub>4</sub> emission rate by assuming a CH<sub>4</sub> composition in the natural gas of 95% (Peischl et al., 2015).

160 In addition to unconventional wells, the domain also contains more than 100,000 shallow conventional wells.  
161 Annual conventional production rates for the year 2014 were obtained through the PADEP Oil and Gas Reporting website,  
162 the WVDEP, and the New York Department of Environmental Conservation (NYDEC, 2016). Despite the large number of  
163 wells, the average conventional well in PA produces 1% of the natural gas compared to its unconventional counterpart.  
164 However, it is speculated that the older age of these wells and a lack of maintenance and care for them results in a higher  
165 emission rate for these wells as a function of their production (Omara et al., 2016). A first-guess natural gas emission rate of  
166 11% was applied to the production values of the conventional wells based on the median emission rate from the wells  
167 sampled in Omara et al., (2016). Similar to the unconventional wells, the natural gas emission rate was then converted to a  
168 CH<sub>4</sub> emission rate by assuming a CH<sub>4</sub> composition in the natural gas of 95%.

169 Compressor stations located within the basin are responsible for collecting natural gas from multiple well locations,  
170 removing non-CH<sub>4</sub> hydrocarbons and other liquids from the flow, and regulating pressure to keep gas flowing along  
171 gathering and transmission pipelines, and can be a potential source for methane emissions. Data for compressor station  
172 locations and emissions comes from a dataset used in Marchese et al., (2015). A total of 489 compressor facilities are listed  
173 for Pennsylvania, with 87% of the listed facilities also containing location data. Emissions for each compressor station are  
174 calculated through two different methodologies. In the simplest case, a flat emission rate of 32.35 kg hr<sup>-1</sup> is applied for each  
175 station, the mean emission rate of a gathering facility in PA found in Marchese et al., (2015). In the more complex scenario,  
176 the same emissions total is used as in the flat rate case, but is distributed among the compressor stations linearly as a function  
177 of their energy usage. Wattage between compressors in our dataset can vary greatly, from 10 kW for small compressors to  
178 7000 kW or more at large gathering facilities. Using the wattage as a proxy for emissions allows us to account for the size  
179 and throughput of natural gas at each station and assumes larger stations will emit more natural gas compared to smaller  
180 stations (Marchese et al., 2015).

181 Data on locations of underground storage facilities were obtained from the United States Energy Information  
182 Administration (EIA, 2015). For each of these locations, a base emission rate of 96.7 kg hr<sup>-1</sup> was applied according to the  
183 average value emitted by a compressor station associated with an underground storage facility (Zimmerle et al., 2016).

184 To calculate pipeline emissions, data on pipeline locations needed to be collected. Information on transmission  
185 pipelines, which connect gathering compressors to distribution networks, is provided by the Natural Gas Pipelines GIS  
186 product purchased from Platts, a private organization which collects and creates various infrastructural layers for the natural  
187 gas and oil industry (Platts, 2016). Gathering pipeline data, corresponding to the transfer of gas from wellheads to gathering  
188 compressors, is nearly non-existent for PA with the exception of Bradford County, which maps out all gathering pipeline  
189 infrastructure within the county border. In PA, information on the location of a gathering pipeline elsewhere is only available  
190 where a gathering line crosses a stream or river. To account for gathering pipelines in the remainder of the state, a GIS model  
191 was created using Bradford County [pipelines map in addition to previously generated pipeline maps of Lycoming County](#)  
192 [\(Langlois et al., 2017\)](#) as a typical pattern to simulate connecting pipelines between unconventional wells throughout the  
193 state (Figure 2). The resulting pattern follows the valley of the Appalachian Mountains, with larger pipelines crossing  
194 through the state to connect the different branches of the network. These pipelines were then multiplied by an emission  
195 factor of 0.043 kg per mile of pipe, the factor used for gathering pipeline leaks in the Inventory of U.S. Greenhouse Gas  
196 Emissions and Sinks: 1990-2013 (EPA, 2015b).

197 CH<sub>4</sub> emissions from natural gas distribution sources, coal mines, and animal/animal waste were provided from  
198 Maasackers et al., (2016), which takes national scale emissions from the EPA's greenhouse gas inventory for the year 2012  
199 and transforms it into a 0.1° × 0.1° emissions map for the continental U.S. For natural gas distribution emissions, various  
200 pipeline data was collected at a state-level and emission factors were accounted for to calculate a total distribution emission  
201 for the state. This emissions total was then distributed within the state proportional to the population density. Emission  
202 estimates for coal are calculated using information from the Greenhouse Gas Reporting Program (GHGRP) for active mines



203 and the Abandoned Coal Mine Methane Opportunities Database for abandoned mines (EPA, 2008). State-level emissions  
204 missions from enteric fermentation and manure management are provided in the EPA's inventory. These emissions were  
205 segregated into higher resolutions using county-level data from the 2012 U.S. Census of Agriculture (USDA, 2012) and  
206 land-type mapping.

207 Finally, the EPA's Greenhouse Gas Reporting Program dataset for the year 2014 was used to capture all other major  
208 sources of CH<sub>4</sub> in the region otherwise unaccounted for, the majority of which are emissions from landfills and some  
209 industrial sources (EPA, 2015a). Sources within the GHGRP that overlap with natural gas sources already accounted for  
210 within our inventory were removed to prevent redundancy.

211 Although our emissions map used for the model runs did not account for potential CH<sub>4</sub> emissions from wetland  
212 sources, a series of wetlands emission scenarios was obtained for the region using data from Bloom, et al., (~~in review~~2017).  
213 From this dataset, wetland CH<sub>4</sub> emissions make up only 1% of all regional CH<sub>4</sub> emissions in the most extreme scenario, and  
214 thus we assume their impact is negligible to this study.

215

## 216 2.2 Aircraft Campaign

217 Observations for this project were obtained from a 3-week aircraft campaign during the period of May 14th-June 3rd, 2015-  
218 ~~and are available for public access (<https://doi.org/10.15138/G35K54>)~~. The campaign was led by the Global Monitoring  
219 Division (GMD) of the National Oceanic and Atmospheric Administration Earth Systems Research and Laboratory (NOAA  
220 ESRL), in collaboration with the University of Michigan. During this period, the NOAA Twin Otter aircraft flew throughout  
221 the northeast portion of Pennsylvania, providing a total of ten flights across nine days. The aircraft was equipped with a  
222 Cavity Ring-Down Spectroscopic analyser (Picarro G2401-m) measuring CH<sub>4</sub>, CO<sub>2</sub>, CO, and water vapour mole fractions at  
223 approximately 0.5Hz with a random error of 1 ppb, 0.1 ppm, 4 ppb, and 50 ppm respectively (Karion et al., 2013). GPS  
224 location, horizontal winds, temperature, humidity, and pressure were also recorded at ~~1Hz~~1 Hz. The majority of observations  
225 for each flight occurred during the afternoon hours at heights ~~generally~~lower than ~~4000~~1500 m above ground level. Each  
226 flight contains at least one vertical profile within and above the boundary layer, with temperature and water vapour  
227 observations from these profiles used to estimate the atmospheric boundary layer height and ensure that the aircraft sampled  
228 air within the boundary layer throughout the flight. Observations ~~taken~~~~suspected of being located~~ above the boundary layer  
229 top are flagged and removed from ~~calculation~~all calculations.

230 Flight paths, wind speeds, and CH<sub>4</sub> observations for each of the 10 flights can be seen in Figure 3. For six of the ten  
231 flights, a box pattern was flown around a large portion of unconventional natural gas wells in northeastern PA. These flights  
232 were performed typically on days with a strong, steady wind, with a clearly defined upwind and downwind transect intended  
233 for use in an aircraft mass balance calculation. Five of the six box-pattern flights were composed of two loops circling the  
234 gas basin, allowing for two separate calculations of the upstream natural gas emission rate for the flight. On the remaining

235 four flights, raster patterns were performed to help identify spatial complexities of CH<sub>4</sub> emissions within the basin. All ten  
236 flights were used in the model optimization calculation of the upstream natural gas emission rate.

### 237 **2.3 Transport Model**

238 The atmospheric transport model used in this study is the Advanced Weather Research and Forecasting (WRF) model  
239 (WRF-ARW, Skamarock et al., 2008) version 3.6.1. The WRF configuration for the model physics used in this research  
240 includes the use of: 1) the double-moment scheme (Thompson et al., 2004) for cloud microphysical processes, 2) the Kain-  
241 Fritsch scheme (Kain and Fritsch 1990, Kain 2004) for cumulus parameterization on the 9-km grid, 3) the Rapid Radiative  
242 Transfer Method for general circulation models (GCMs) (RRTMG, Mlawer et al., 1997, Iacono et al., 2008), 4) the level 2.5  
243 TKE-predicting MYNN planetary boundary layer (PBL) scheme (Nakanishi and Niino 2006), and 5) the Noah 4-layer land-  
244 surface model (LSM) that predicts soil temperature and moisture (Chen and Dudhia 2001, Tewari et al., 2004) in addition to  
245 sensible and latent heat fluxes between the land surface and atmosphere.

246 ~~The WRF modelling system used for this study also has four-dimensional data assimilation (FDDA) capabilities to  
247 allow meteorological observations to be assimilated into the model (Deng et al., 2009). With WRF FDDA, observations are  
248 assimilated through the entire simulation to ensure the optimal model solutions that combine both observation and the  
249 dynamic solution, a technique referred to as dynamic analysis. Data assimilation can be accomplished by nudging the model  
250 solutions toward gridded analyses based on observations (analysis nudging), or directly toward the individual observations  
251 (observation nudging), with a multiscale grid nesting assimilation framework typically using a combination of these two  
252 approaches (Deng et al., 2009; Rogers et al., 2013).~~

253 The WRF model grid configuration used in this research contains two grids: 9- and 3-km (Figure 4), each with a  
254 mesh of 202x202 grid points. The 9-km grid contains the mid-Atlantic region, the entire northeastern United States east of  
255 Indiana, parts of Canada, and a large area of the northern Atlantic Ocean. The 3-km grid contains the entire state of  
256 Pennsylvania and most of the state of New York. Fifty vertical terrain-following model layers are used, with the centre point  
257 of the lowest model layer located at ~10 m above ground level. The thickness of the layers stays nearly constant with height  
258 within the lowest 1 kilometre, with 26 model layers below 850 hPa (~1550 m AGL). One-way nesting is used so that  
259 information from the coarse domain translates to the fine domain but no information from the fine domain translates to the  
260 coarse domain.

261 ~~The WRF modelling system used for this study also has four-dimensional data assimilation (FDDA) capabilities to  
262 allow meteorological observations to be assimilated into the model (Deng et al., 2009). With WRF FDDA, observations are  
263 assimilated through the entire simulation to ensure the optimal model solutions that combine both observation and the  
264 dynamic solution, a technique referred to as dynamic analysis. Data assimilation can be accomplished by nudging the model  
265 solutions toward gridded analyses based on observations (analysis nudging), or directly toward the individual observations  
266 (observation nudging), with a multiscale grid-nesting assimilation framework typically using a combination of these two  
267 approaches (Deng et al., 2009; Rogers et al., 2013).~~

268 FDDA (Deng et al., 2009) was used in this research, with the same strategy as used in Rogers et al., (2013). Both  
269 analysis nudging and observation nudging were applied on the 9-km grid, and only observation nudging was applied on the  
270 3-km grid. In addition to assimilating observations and using the North America Regional Reanalysis model as initial  
271 conditions, we reinitialize the WRF model every five days, allowing 12 hours of overlapping period in consideration of  
272 model spin-up period to prevent model errors from growing over long periods. The observation data types assimilated  
273 include standard WMO surface and upper-air observations distributed by the National Weather Service (NWS), available  
274 hourly for surface and 12-hourly for upper air, and the Aircraft Communications Addressing and Reporting System  
275 (ACARS) commercial aircraft observations, available anywhere in space and time with low-level observations near the  
276 major airports.

277 The WRF model used in this study enables the chemical transport option within the model allowing for the  
278 projection of CH<sub>4</sub> concentrations throughout the domain. Surface CH<sub>4</sub> emissions used as input for the model come from our  
279 CH<sub>4</sub> emissions inventory and are all contained within the 3-km nested grid. Each source of CH<sub>4</sub> within our inventory is  
280 defined with its own tracer (Table 1), allowing for the tracking of each individual source's contribution to the overall  
281 projected CH<sub>4</sub> enhancement within the model. For this study, CH<sub>4</sub> is treated as an inert gas. The potential for interaction with  
282 the hydroxyl radical (OH), the main sink of CH<sub>4</sub>, is neglected. A calculation assuming an above-average OH mole fraction  
283 over a rural region of 0.5pptv (Stone et al., 2012) and a reaction rate of  $6.5 \times 10^{-15}$  (Overend et al., 1975) produces a  
284 CH<sub>4</sub> sink of 0.5ppb per hour. The duration of a flight can be up to 3 hours, leading to a potential loss of 1.5ppb over the  
285 course of a flight. This loss is small but not insignificant. CH<sub>4</sub> plumes associated with natural gas during each flight ranged  
286 between 15-70 ppb, and a change of 1.5ppb could theoretically impact observations by as much as 10% of the plume signal.  
287 However, this decrease in the CH<sub>4</sub> mole fraction would likely have equal impacts on both the background CH<sub>4</sub> values as well  
288 as the enhancement. Because emission calculations are based on the relative difference between the CH<sub>4</sub> background mole  
289 fraction and the enhancement downwind, it would take a gradient in the oxidation of OH to impact the results. Considering  
290 this relatively low destruction rate, the expected homogeneity of the sink across the region, and the difficulties associated  
291 with the simulation of chemical loss processes, we assumed that the CH<sub>4</sub> mass is conserved throughout the afternoon and  
292 therefore we ignored the impact of oxidation by OH.

293

## 294 **2.4 Model Optimization Technique**

### 295 **2.4.1 Model Optimization Methodology**

296 The objective of the model optimization technique is to solve for ~~a natural gas~~ emission rate as a percent of natural gas  
297 production that creates the best match between modelled CH<sub>4</sub> concentration maps, provided by the transport model, with  
298 actual CH<sub>4</sub> mole fraction observations, provided by the aircraft data. The optimization process in this study was originally  
299 designed to solve for natural gas emission from unconventional wells and emissions from compressor facilities separately.

300 Because the flow rate of natural gas being processed was not available for each compressor station, emissions at each facility  
301 were originally scaled based on the size of the station. However, when running the transport model using this emissions map,  
302 enhancements from the compressor stations produced plume structures nearly identical in shape to enhancements from the  
303 unconventional wells due to the similar spatial distributions of these two tracers. Without distinct differences between the  
304 enhancement patterns from each tracer, it becomes impossible to distinguish which emissions source must be adjusted to  
305 obtain the closest match to the observations. For this reason, emissions from compressor facilities are merged with  
306 unconventional well emissions in the optimized emission rate. Though the emission rate solved for in this experiment only  
307 uses the locations and production for the unconventional wells, this optimized rate represents emissions from both the wells  
308 and compressor facilities and ~~will be~~ referred to as the modelled upstream natural gas emission rate. Midstream and  
309 downstream natural gas processes (such as processing, transmission and distribution of the gas) and emissions from  
310 conventional wells are not solved for in this study due to their minimal contribution (less than 5%) to CH<sub>4</sub> emissions in the  
311 region encompassed by the aircraft campaign.

312 Using the transport model WRF-Chem, CH<sub>4</sub> atmospheric enhancements were generated for each flight using  
313 different tracers to track different components to the overall CH<sub>4</sub> enhancement (e.g. animal/animal waste, distribution sector,  
314 industries). From these concentration fields, the upstream natural gas emission rate was solved for each flight using a three-  
315 step model optimization technique. First, a background concentration was determined for each flight and subtracted from the  
316 observations to create a set of “observed CH<sub>4</sub> enhancements,” using

$$317 \quad X_{EnhO} = X_{Obs} - X_{bg} \quad , \quad (1)$$

318 where  $X_{Obs}$  is the CH<sub>4</sub> mole fraction observation from the aircraft,  $X_{bg}$  is a chosen background value for the flight, and  
319  $X_{EnhO}$  is the calculated CH<sub>4</sub> enhancement at each observation. In this study, the background value is defined as the ambient  
320 CH<sub>4</sub> mole fraction over the region not accounted for by any of the sources within the model, with each flight having a unique  
321 background value. Box-pattern flights containing 2 loops around the basin may have a different background value assigned  
322 for each loop. To determine the background mole fraction, we start with the value of the observed mole fraction in the lowest  
323 2nd percentile of all observations within the boundary layer for a given flight or loop. This chosen background value  
324 represents the CH<sub>4</sub> mole fraction across the flight path from sources that are outside of our model domain. Because the  
325 background value is meant to represent the CH<sub>4</sub> mole fraction outside the model domain ~~which that~~ is otherwise unaccounted  
326 for in our model, using the observations with the lowest CH<sub>4</sub> mole fraction is not always a sufficient definition for the  
327 background. On certain days, CH<sub>4</sub> enhancements from sources within the model domain can form plumes with wide spatial  
328 coverage that cover all observations during a flight. For example, during a flight the lowest CH<sub>4</sub> observations from the  
329 aircraft may be 1850 ppb, but the model simulation during that period indicates that all observations within the flight are  
330 being impacted by at minimum a 20 ppb enhancement. In this case, we would set our background value for the flight at 1830  
331 ppb, and say that our 1850 ppb observations from the flight are a combination of an 1830 ppb background in addition to a 20

332 ppb enhancement from sources within the model. By subtracting off this background value from our observations, we create  
 333 a set of “observed CH<sub>4</sub> enhancements” which can be directly compared to the model projected enhancements

334 The next step is to remove enhancements from this set that are not associated with emissions from upstream natural  
 335 gas using

$$336 \quad X_{GasO} = X_{EnhO} - X_{OtherM} \quad \text{_____} (2)$$

337 where  $X_{OtherM}$  is the modelled CH<sub>4</sub> enhancement at each observation from sources unrelated to upstream natural gas  
 338 processes, and  $X_{GasO}$  is the ~~observed~~ observation-derived CH<sub>4</sub> enhancement associated with upstream natural gas emissions  
 339 for each observation. In this step, each observed CH<sub>4</sub> enhancement has subtracted from it the projected non-natural gas  
 340 enhancement from the model (i.e. nearest grid point in space) using the corresponding model output time closest to the  
 341 observation within a 20-minute time interval. This creates a set of observed CH<sub>4</sub> enhancements related only to emissions  
 342 from upstream gas processes, filtering out potential signals from other CH<sub>4</sub> emitters and providing a set of observed  
 343 enhancements that can be directly compared to the projected upstream natural gas enhancement within the model. By  
 344 subtracting these other sources from the observations, we make the assumption that our emissions inventory is accurate for  
 345 non-natural gas sources and that the transport of these emissions is perfect, both of which are actually uncertain. Because  
 346 errors exist in both the emissions and transport, it is possible to ~~derive~~ create a negative ~~observed~~ observation-derived  
 347 upstream gas enhancement if model-projected enhancements from other sources are larger than the ~~observed~~ observation-  
 348 derived enhancement. From the 10 flights, 16% of the observation-derived enhancements are negative, but only 3% are  
 349 negative by more than 5 ppb. To avoid ~~such situations~~ solving for unrealistic negative values, these negative  
 350 ~~observed~~ observation-based upstream gas enhancements are set to 0. Errors associated with this issue and other uncertainties  
 351 with our inventory are examined further in the ~~results~~ uncertainly analysis section of this paper.

352 In the final step, the upstream natural gas emission rate within the model is adjusted to create the best match  
 353 between the modelled upstream gas enhancement and ~~observed~~ observation-derived upstream gas enhancement using

$$354 \quad J = \sum_{i=1}^n (x_i^{GasO} - X_{GasO} - C * x_i^{GasM} X_{GasM}) \text{_____}$$

355 (3)

356 where ~~n is the number of observations in the flight~~,  $x_i^{GasO}$  and  $x_i^{GasO}$  and  $x_i^{GasM} X_{GasM}$  are the observed and modelled  
 357 enhancement for each observation  $i$ . In this equation,  $J$  is a cost function we are trying to minimize by solving for a scalar  
 358 multiplier  $C$  which, when applied to the modelled natural gas enhancements, creates the smallest sum of the differences  
 359 between the ~~observed~~ observation-derived upstream gas enhancement and the modelled upstream enhancement. Because the  
 360 emission rate within the model is linearly proportional to the model enhancements, we can solve for the upstream natural gas  
 361 emission rate that minimizes the cost function using

$$362 \quad E = 0.13 C \quad \text{_____} (4)$$

363 where 0.13 was the first guess upstream emission rate (in percent of production) used in the model, and  $E$  is the optimized  
364 emission rate for the flight as a percentage of the natural gas production at each well. This final value represents an overall  
365 emission rate associated with both unconventional wells and compressor stations across the region.

366 The decision to use a scalar cost function rather than the sum of squares is to account for possible misalignment  
367 between any observed CH<sub>4</sub> plume and modelled plumes. There are two potential ways in which misalignment may occur.  
368 One possibility is that the modelled wind direction differs from the true wind direction, leading to a plume in the model that  
369 is off-centre in relation to the observed plume. The other possibility relates to how the model treats emissions from natural  
370 gas as a uniform percent of production. In reality the emissions are more random in nature, and thus the plume may not  
371 always develop over the wells with the largest production values. If a cost function is used that minimizes the sum of the  
372 squares, any misalignment between the modelled and observed plume will result in the peak of the modelled plume aligning  
373 with the height of the tail of the observed plume (Figure 5). Unless the observed plume aligns perfectly with the modelled  
374 plume, the optimized emission rate using a sum of squares approach will always bias low. By using a scalar cost function,  
375 we solve for an optimized emission rate that results in a plume with the same area under the curve compared to the observed  
376 plume (Figure 5). This methodology is not impacted by any misalignment between the modelled vs. observed plumes,  
377 preventing the low biases associated with a sum of squares minimization.  
378

#### 379 2.4.2 Model Optimization Uncertainty Assessment

380 For each of the ten flights, an uncertainty assessment was performed to obtain a range of likely upstream emission rates for  
381 any individual flight. Five different sources of error were considered in this assessment: model wind speed error, model  
382 boundary layer height error, CH<sub>4</sub> background error, CH<sub>4</sub> emission inventory error, and model/observation mismatch error.  
383 These five sources of error vary substantially from flight to flight depending on conditions, and each can have significant  
384 impacts on the total uncertainty (Table 4, 5).

385 Errors in the modelled wind speed and boundary layer height have impacts on our emission estimates that linearly  
386 impact the results. If we assume a constant wind speed, a constant boundary layer height, and no entrainment of air from the  
387 top of the boundary layer, we can use the following equation to understand their impacts.

$$388 \Delta C = \bar{F}_0 \left( \frac{\Delta x}{U \cdot D} \right) \quad (5)$$

389 where  $\Delta C$  is the total CH<sub>4</sub> enhancement of the column of air contained within the boundary layer,  $\bar{F}_0$  is the average emission  
390 rate over the path the parcel travelled,  $\Delta x$  is the distance the column of air travelled,  $U$  is the wind speed and  $D$  is the  
391 boundary layer height. Using this equation, we can see the linear relationship between the model wind speed, model  
392 boundary layer height, and the calculated emission rate. As an example, if wind speeds in the model are biased low, natural  
393 gas enhancements projected by the model would increase inversely. To compensate for this effect, the optimized emission  
394 rate would decrease proportionally. A similar case can be made for bias in the boundary layer height. Both errors in the wind

395 speed and boundary layer height have known impacts on the optimized emission rate which can be corrected for, as long as  
396 the errors of each are known.

397 To calculate the error in the model wind speed, we assume aircraft observations are truth and use

$$398 U_e = \frac{U_m - U_{obs}}{U_{obs}} \quad (6)$$

399 where  $\bar{U}_{obs}$  is the mean observed wind speed by the aircraft across all points within the boundary layer,  $\bar{U}_m$  is the mean  
400 modelled wind speed by the model across all points closest in time and space to each observation, and  $U_e$  is the wind speed  
401 error percentage.

402 To compute the error in the modelled boundary layer height, the observed boundary layer height for each flight is  
403 assumed to be the true boundary layer height and the boundary layer height percentage error,  $H_e$ , is estimated using:

$$404 H_e = \frac{H_m - H_{obs}}{H_{obs}} \quad (7)$$

405 where  $\bar{H}_{obs}$  is the average observed boundary layer height across each of the aircraft profiles for a given flight,  $\bar{H}_m$  is the  
406 model boundary layer height closest in time and space to the location of the observed profiles averaged over all profiles. For  
407 both the observation and the model, boundary layer heights were determined by locating height of the potential temperature  
408 inversion associated with the top of the boundary layer. On the May 22 flight where a potential temperature inversion could  
409 not easily be identified in the observations, changes in water vapour, CO<sub>2</sub> and CH<sub>4</sub> mixing ratios were used to identify the  
410 boundary layer top.

411 Errors in the model wind speed and boundary layer height are calculated for each of the ten flights. From these  
412 errors, a corrected optimized emission rate is calculated for each flight using Eq. (8):

$$413 E_{new} = \frac{E}{(1+U_e)(1+H_e)} \quad (8)$$

414 where  $E$  is the original emission rate and  $E_{new}$  is the corrected optimized upstream natural gas emission rate as a percent of  
415 production.

416 In addition to errors related to wind speed and boundary layer height, we quantify three other sources of error in  
417 each flight: errors in the selected CH<sub>4</sub> background value, errors in the CH<sub>4</sub> inventory, and errors associated with the overall  
418 model performance (Table 5). Unlike the wind speed and boundary layer errors which have easily computable impacts on  
419 the emission estimates, these other three sources of error and their impact on the optimized emission rate are more difficult  
420 to quantify.

421 The background error relates to the value chosen for each flight which represents the ambient CH<sub>4</sub> concentration in  
422 the boundary layer unrelated to emission sources within the model. In this study background values ranged from 1897-  
423 1923ppb. Though background values should not have high variability during a 2-3 hour mid-afternoon flight, entrainment  
424 from the boundary layer top can lead to the mixing in of tropospheric air that has different CH<sub>4</sub> mole fraction values from

425 those within the boundary layer, resulting in a change in the afternoon background value with time. Furthermore, for days on  
426 which all aircraft observations (including those upwind of the unconventional wells) are impacted by various CH<sub>4</sub> plumes  
427 predicted within the model, it is difficult to determine the background CH<sub>4</sub> concentration accurately. Additionally,  
428 observations corresponding to locations with no modelled enhancement may in fact have been impacted by missing sources  
429 in our inventory, highlighting the difficult nature of knowing with certainty where and what the background is for any given  
430 flight. Understanding this uncertainty is crucial; any error in subtracting off the background value directly impacts each  
431 observation's observed natural gas enhancement. For example, a background value of 1 ppb below the true background for a  
432 given flight would add 1 ppb to each observed natural gas enhancement for all observations, creating a high bias with the  
433 optimized upstream emission rate. To account for this error, each flight's optimization processes was rerun iterating the  
434 background value by ±5 ppb, and the ratio of the percent change in the emission rate compared to the original case was  
435 defined as the resulting error in the emission rate due to background uncertainty. This ±5 ppb background error range is an  
436 estimate at the range of possible error in the background based on changes observed in the upwind measurements from each  
437 of the flights and is meant to be a conservative estimate of the error. The impact this error can have in the emission rate  
438 varies depending on the magnitude of the observed downwind enhancements during a flight. A plume containing a CH<sub>4</sub>  
439 enhancement of 50 ppb will have a smaller relative error from a 5 ppb change compared to one with an enhancement of only  
440 10 ppb. Thus, days with high wind speeds and a high boundary layer height (and thus enhancements of a smaller magnitude)  
441 tend to be affected the most by background errors.

442 Similar to background errors, errors from the CH<sub>4</sub> emissions inventory are difficult to quantify. In the model  
443 optimization technique, we subtract out enhancements from sources unrelated to unconventional natural gas before solving  
444 for the upstream gas emission rate. In doing so, we are making the assumption that our emissions inventory for sources  
445 unrelated to upstream natural gas processes are accurate. In truth, each emission source in our inventory comes from a  
446 different dataset and has its own unique error bounds, many of which are unknown. To simulate the potential errors  
447 associated with unknowns in our inventory, we use a Monte Carlo approach and iterate the unconventional emissions  
448 optimization approach for each flight 10,000 times, applying a random multiplier between 0-2 for each of the different  
449 sources not associated with unconventional natural gas production. The resulting range of optimized natural gas emission  
450 rates was fit to a Gaussian distribution and the 2σ emission range was calculated. Despite varying the emissions used in the  
451 error analysis by 0 to 200% their original value, their impacts on the optimized natural gas emission rate are minimal on  
452 most days due to the northeastern Marcellus region having very few emission sources not related to upstream natural gas  
453 processes. Only for the flights on May 24<sup>th</sup> do we see errors from the inventory contribute significantly to the overall daily  
454 error, when the coal plume in southwestern PA enters the centre of the study region and has a large role in the upstream  
455 natural gas emission rate calculation for that day (Table 5).

456 The final source of error attempts to quantify the similarity of the pattern of modelled and observed natural gas  
457 enhancements, referred to here as the model performance error. Figure 6 shows an example of two days, one of which the  
458 model appears to recreate the observations, and the other of which the model poorly matches the shape of the observed



enhancements. Comparing these two simulations with no other information, we hypothesize that one should put more trust in the upstream natural gas emission rate calculated for the flight whose modelled upstream enhancements match structurally compared to the emission rate from the flight whose modelled enhancement bares little semblance to the observed enhancement. The model performance error is designed to account for the trustworthiness of the optimized upstream emission rate based on how well the model simulates a given day. The model performance error is calculated using a modified normalized root mean squared error formula given in Eq. (9):

$$e_{Perf} = \frac{\bar{\sigma}_{\Delta X}}{\Delta X_{gas}} \quad (9)$$

In this equation,  $\bar{\sigma}_{\Delta X}$  is the standard deviation of the difference between the modelled and observation-derived upstream natural gas CH<sub>4</sub> enhancement using the optimized emission rate, and  $\Delta X_{gas}$  is the observed magnitude of enhancement from the major natural gas plume observed in each flight. Here,  $\Delta X_{gas}$  serves as a normalization factor to account for the varying strength of the enhancement from flight to flight, and ensures that days with increased enhancements due to meteorological conditions or true daily fluctuations in the upstream natural gas emissions do not proportionally impact the performance error percentage. For example, a day with high winds and a deep boundary layer would produce smaller enhancements, leading to a small  $\bar{\sigma}_{\Delta X}$  regardless of model performance unless normalized by  $\Delta X_{gas}$ .

## 2.5 Aircraft Mass Balance Method and Uncertainty Assessment

An aircraft mass balance calculation was performed for four applicable flights from the aircraft campaign as an alternative method to calculate upstream natural gas emission rates independent of the transport model. The aircraft mass balance approach uses the CH<sub>4</sub> enhancement between a downwind and upwind transect to calculate the total CH<sub>4</sub> flux of the area contained between the two transects. We use the mass balance equation from Karion et al., (2013):

$$E = \bar{U} \cos(\bar{\theta}) \int_{-b}^b \Delta X \int_{z=0}^{z_{top}} n_{air} dz dx \quad (510)$$

where  $E$  is the total flux (in mol s<sup>-1</sup>) coming from the enclosed flight track,  $\bar{U}$  is the mean wind speed (in m s<sup>-1</sup>),  $\bar{\theta}$  is the mean angle of the wind perpendicular to the flight track,  $\Delta X$  is the CH<sub>4</sub> enhancement measured along the downwind flight track from  $-b$  to  $b$  (expressed as a mole fraction),  $n_{air}$  is the molar density of air within the boundary layer (in mol m<sup>-3</sup>), and each of the integrals represents the summing over all air being measured within our transect in both the horizontal ( $x$ ) and the vertical ( $z$ ). By simplifying further and using the mean enhancement along each downwind transect as the enhancement and choosing  $z_{top}$  to be the top of the boundary layer, we can transform the previous equation into the following:

$$E = 37.3(L)(D)(\bar{U})\Delta\bar{X}3LDU\Delta\bar{X}\cos(\bar{\theta}) \quad (11)$$

488 where L is the length of the transect (in meters), D is the depth of the boundary layer (in meters) found using observations  
489 from vertical ascents during each flight,  $\Delta\bar{x}$  is the mean enhancement across the transect (expressed as a mole fraction),  $\bar{U}$   
490 and  $\bar{\theta}$  are the mean wind speed (in m s<sup>-1</sup>) and wind direction relative to the angle of the transect, and 37.3 is the average  
491 molar density of dry air within the boundary layer (in mol m<sup>-3</sup>) assuming an average temperature and pressure of 290K and  
492 900hPa.

493 ~~Flights on May 22nd, May 23rd, May 28th, and May 29<sup>th</sup>, 2015 were selected for mass balance calculations based~~  
494 ~~on their box shaped flight patterns surrounding a large portion of the northeastern Marcellus gas basin, reasonable steady-~~  
495 ~~state wind conditions during the flight (this eliminated May 14<sup>th</sup> when a low pressure system was stationed over the region),~~  
496 ~~and a lack of strong CH<sub>4</sub> enhancements originating from outside of the box which could affect both the upwind and~~  
497 ~~downwind transects. Emission rates within the enclosed region were calculated from each of these flights, and emissions not~~  
498 ~~associated with unconventional gas production and gathering sources within the box were subtracted out using information~~  
499 ~~from our inventory. A ratio was taken of the calculated emission rate to the total production in the box, and an upstream~~  
500 ~~natural gas emission rate based on production was obtained. For each of the May 22nd, May 23rd, and May 28th flights, two~~  
501 ~~loops of similar structure and at similar altitudes were performed around the basin, allowing for two individual mass balance~~  
502 ~~calculations on these days. An emission rate is calculated for each of these loops and the two values are averaged to calculate~~  
503 ~~the daily emission rate.~~

504 Of the 6 days from the aircraft campaign with a clearly defined upwind and downwind transect, one day (May 14<sup>th</sup>)  
505 contained a surface high-pressure centre in the middle of the flight resulting in erratic wind patterns, and another day (May  
506 25<sup>th</sup>) had CH<sub>4</sub> plumes from southwestern PA affecting portions the flight observations. These days were not used for a mass  
507 balance, and calculations were performed for the remaining four box-pattern flights (May 22<sup>nd</sup>, May 23<sup>rd</sup>, May 28<sup>th</sup>, May  
508 29<sup>th</sup>). From this list of remaining flights, three of them contained two loops around a portion of the Marcellus basin. A mass  
509 balance was performed on each loop, resulting in a total of 7 mass balance calculations for the region across 4 days. Table 6  
510 summarizes the results from the mass balance flights.

511 For each flight, a total flux within the box encompassed was calculated using Eq. (11). Using this flux, a natural gas  
512 emission rate based on production from within the box was calculated using Eq. (12)

$$513 E_{\%} = \frac{E - E_{other}}{P} \quad (12)$$

514 where E is the total flux from Eq. (11) (in kg hr<sup>-1</sup>), E<sub>other</sub> are the emissions enclosed in the box from sources not  
515 related to upstream natural gas processes (in kg hr<sup>-1</sup>), P is the total CH<sub>4</sub> from natural gas being produced within the box (in  
516 kg hr<sup>-1</sup>), and E<sub>%</sub> is the resulting natural gas emission rate as a percent of total production within the box.

517 As an error analysis for the mass balance flight, we look at four potential sources of error (Table 7). One source of  
518 uncertainty comes from the observed wind speed used in Eq. (11). For our experiment, we take the mean observed wind  
519 speed from the aircraft and assume this value represents the mean wind speed within the entire box during the 2-4 hour  
520 period it would take for air to travel from the upwind transect to the downwind transect. To understand the uncertainty and

Formatted: Indent: First line: 0.5"

521 biases associated with this assumption, we recreate wind observations along the flight path using values from WRF-Chem,  
522 and compare the mean wind speed from the simulated observations to the mean model winds contained within the box  
523 integrated throughout the boundary layer during the 3 hour period closest to the flight time. By making this comparison, we  
524 are able to understand the representation error associated with treating the wind speed observations from the aircraft as the  
525 wind speed within the entire box during the period it would take for air to cross from the upwind transect to the downwind  
526 transect. On average, modelled wind speeds following the flight were 7% faster than integrated wind speeds within the box,  
527 due to the inability for aircraft observations to account for slower wind speeds closer to the surface. This bias was removed  
528 from each day's calculated wind speed. After accounting for the wind speed bias, the average error of the modelled wind  
529 speed following the flight path compared to the modelled winds within the box was 3%. This 3% uncertainty was applied to  
530 each flight and used as the potential uncertainty in the mean wind speed. Errors in the wind direction were neglected, as each  
531 flight used in the mass balance completely surrounded the basin using downwind transects at multiple angles, and thus small  
532 errors in the wind angle would result in a negligible net change on the total flux calculated.

533 Another source of uncertainty is error in the boundary layer height. For each flight, between 2-3 vertical profiles  
534 were performed, and the mean height was used in Eq. (11). The standard deviation of different heights from each transect  
535 was used as the uncertainty. On May 22<sup>nd</sup>, a boundary layer height could be interpreted from only one vertical transect. For  
536 this day, we assume an uncertainty of  $\pm 200$  m ( $\pm 9\%$ ).

537 Uncertainty in the CH<sub>4</sub> background mole fraction was estimated similar to the boundary layer height. On three of  
538 the four flights, two upwind transects were performed. The mean observed CH<sub>4</sub> mole fraction between the two transects was  
539 used as the background value for the entire flight, and the standard deviation between the loops was used as the uncertainty.  
540 On both the May 23<sup>rd</sup> and May 28<sup>th</sup> flights, background differences between the two transects were less than the instrument  
541 error of 1 ppb. On these days, we use the instrument error as the background error. On May 22<sup>nd</sup>, only one upwind transect  
542 was usable for the calculation. For this day, we assume a conservative estimate in the uncertainty of the background of  $\pm 5$   
543 ppb.

544 Finally, we assess uncertainty in the emissions inventory. After a CH<sub>4</sub> flux is calculated for each loop, emissions  
545 from sources contained within the box that are not associated with upstream natural gas processes must be subtracted out to  
546 solve for the upstream natural gas emission rate. Any errors associated with our inventory will result in a CH<sub>4</sub> source  
547 attribution error. To account for the potentially large uncertainty with the emission sources in our inventory, we vary these  
548 non-natural gas emissions by a factor of 2 to test the impact on the solved upstream natural gas emission rate. Because  
549 northeastern Pennsylvania contains few sources of CH<sub>4</sub> emissions outside of natural gas production, the impact of this  
550 uncertainty is typically less than 20% of the total emissions calculated within the box.

## 551 **3 Results**

### 552 **3.1 Methane Inventory**

553 From the [first-guess](#) CH<sub>4</sub> inventory created in this study, a total anthropogenic CH<sub>4</sub> emission rate of 2.76 Tg CH<sub>4</sub> year<sup>-1</sup> is  
554 projected within our inner model domain (Figure [57](#)) with values for individual source contributions shown in Table 2. This  
555 total emissions estimate assumes a leak rate of 0.13% of gas production for unconventional wells, and does not account for  
556 emissions from natural gas transmission and storage facilities outside of PA due to a lack of information available from other  
557 states. Within the model domain, the area encompassing southwestern PA and northeastern WV stands out as the largest  
558 contributor to CH<sub>4</sub> emissions, with emissions from conventional gas, unconventional gas, and coal mines all having  
559 significant contributions to the total. In particular, the large emissions from coal make this region unique in comparison to  
560 other shales. The EPA's Greenhouse Gas Reporting Program dataset for the year 2014 lists individual coal mines in the  
561 southwestern portion of our domain as 8 of the top 10 CH<sub>4</sub> emitting facilities across the entire United States. This large area  
562 source of CH<sub>4</sub> can have an impact on CH<sub>4</sub> concentrations hundreds of kilometres downwind and must be taken into account  
563 when winds are from the southwest (Figure [68](#)). Examples of this plume and its impacts on the aircraft campaign are  
564 discussed in Section 3.2.1.

### 566 **3.2 Model Optimization Results**

#### 567 **3.2.1 Case Studies**

568 From the aircraft campaign, a total of 10 flights across 9 days were used in the model optimization technique. For each one  
569 of these flights, CH<sub>4</sub> concentration fields were produced using WRF-Chem, and the emission rate from upstream gas  
570 processes was adjusted as outlined in the methods section to find the rate that best matches the total observed CH<sub>4</sub>  
571 enhancement. For box flights with two loops completed around the basin, emission rates were calculated for each loop  
572 independent from one another and then averaged for the flight. Table 3 provides the general meteorology for the 10 flights.

573 During each of the observational periods, we use the transport model to project the mole fraction enhancement  
574 across the region for each of the different CH<sub>4</sub> tracers (Figure [79](#)). From these projections, we see three common sources of  
575 CH<sub>4</sub> which can significantly influence the observed mole fractions in our study region of northeastern PA. The first is  
576 emissions from unconventional gas in northeastern PA. Although the first-guess total emissions from upstream production in  
577 the Marcellus are small compared to the overall contributions from other sources within the domain, their proximity to the  
578 aircraft track results in unconventional gas having the largest contribution to observed enhancements throughout the domain  
579 covered by most of the flights, often producing signals downwind of about 20-80 ppb above background levels. The second  
580 most influential source of enhancements in our study region comes from various sources of CH<sub>4</sub> emissions located in  
581 southwestern PA. Despite being more than 400 km away from our study region, large plumes from coal and other sources in  
582 the southwestern corner of the state can contribute enhancements as high as 50 ppb across portions of the flight when winds

583 are from the southwest, affecting background measurements and masking signals from the unconventional gas. One final,  
584 but less influential source of CH<sub>4</sub> enhancement is animal agriculture in southeastern PA. Lancaster County is home to  
585 roughly 20% of all cattle in the state, with more than 200,000 cattle and calves as of 2012. A southerly wind can result in a  
586 5-15 ppb enhancement across the flight path due to enteric fermentation and manure management from these cattle. Because  
587 of coal, conventional gas, and cattle sources located south of the basin, signals from flights with a southerly component to  
588 the wind can be difficult to interpret without modelling the projected plumes associated with these sources. Observations on  
589 these days contrast to days with a northerly wind component, where a lack of CH<sub>4</sub> sources north of the study region results in  
590 observations with a more clearly defined background and unconventional natural gas enhancement.

591 For each of the ten flights, variability in the model-observation offset was observed. The first loop of the May 29th  
592 flight is the best example of a case where comparisons between the modelled and observed enhancements match closely after  
593 optimization. For this flight, a box pattern was flown encompassing a majority of the unconventional wells in northeastern  
594 PA, and enhancements were observed along the western and northern transects of the flight. Modelled enhancements from  
595 sources unrelated to upstream gas emissions showed a broad CH<sub>4</sub> plume associated mostly with animal agriculture along the  
596 western edge of the flight, and a smaller enhancement on the eastern edge associated with two landfills in the  
597 Scranton/Wilkes-Barre urban corridor (Figure 810). Both of these enhancements are subtracted off from the observations to  
598 produce a set of ~~observed~~observation-derived enhancements due to upstream natural gas production and gathering facilities.  
599 Any enhancements in this new observational dataset are located almost entirely along the northern transect of the flight,  
600 directly downwind of the natural gas activity in the region. The ~~observed~~observation-derived upstream gas enhancement is  
601 then directly compared to the modelled upstream enhancement using its first guess emission rate, and an optimized upstream  
602 emission rate of 0.26% of production (i.e. a doubling of the first guess) is calculated by minimizing the difference between  
603 the two datasets (Figure 911).

604 The match between observed and modelled CH<sub>4</sub> enhancements on the first loop of the May 29<sup>th</sup> flight is closer than  
605 any other flight in the campaign, ~~with a correlation coefficient of 0.73.~~ The success of the model on this day is likely due to  
606 a number of ideal conditions. In general, inconsistencies between the modelled and observed mean wind speeds and  
607 boundary layer heights can have a linear bias on the projected enhancements, but for this flight differences between the  
608 observed and modelled wind speed and boundary layer height were near 0 for both loops (Figure ~~10,~~ 11, 12, 13). Observed  
609 wind directions throughout the course of the flight had little ~~spread~~directional spread and the averaged observed wind  
610 ~~direction was only 9° different compared to modelled values,~~ resulting in a transport of the CH<sub>4</sub> plumes that the model was  
611 able to match well. Furthermore, the observed mean wind speed was 4.6 m s<sup>-1</sup>, a moderate wind which allows for a steady  
612 transport of any enhancements towards the downwind transect, but not strong enough to dilute their magnitude, resulting in  
613 an easily observable enhancement downwind of the basin. Finally, intrusions from sources unrelated to upstream gas were  
614 small on this day due to favourable wind conditions, reducing the probability of incorrectly attributing the observed  
615 enhancements to the wrong source. Enhancements from upstream natural gas processes were ~~around 30~~between 15-40 ppb  
616 along our downwind transect. By comparison, enhancements from other sources were lower than 15 ppb along a majority of

617 the flight, and most of these enhancements were located west of the downwind transect, making them easier to identify and  
618 remove without unintentionally impacting enhancements from the natural gas plume. All of these different factors likely  
619 contributed to producing a situation where the model was successfully able to match CH<sub>4</sub> observations during the May 29<sup>th</sup>  
620 flight.

621 Flights that occurred on days with a southwest wind had a tendency to produce CH<sub>4</sub> observations that were  
622 intuitively difficult to interpret due to convolved CH<sub>4</sub> sources in southwestern Pennsylvania. One of these complex  
623 observation sets occurred during the late afternoon flight on May 24<sup>th</sup>, 2015 (Figure 1214). Observations on this day show a  
624 CH<sub>4</sub> enhancement-pattern that decreased with latitude, with higher CH<sub>4</sub> mole fractions observed farther south. Given the  
625 location of the wells in the middle of the flight path and the WSW wind pattern in the region, this north/south CH<sub>4</sub> gradient  
626 is unexpected and counterintuitive compared to where one would expect the enhancements to be based solely on the  
627 presence of the gas industry in northeastern PA. However, through modelling each of the many contributors of CH<sub>4</sub> within  
628 our inventory, we are able to recreate this latitudinal CH<sub>4</sub> gradient and better understand the observed patterns (Figure 1214).  
629 Throughout an 18-hour period leading up to the May 24<sup>th</sup> flight, winds from the SSW transport emissions from coal in  
630 southwestern PA northeastward until they reach the centre of the state, where a westerly wind then shifts the plume across  
631 the study region such that it only intersects the southern half of the flight path. Because of both the magnitude of the coal  
632 emissions and an accumulation that occurred in the southwestern portion of the state during the previous night, the modelled  
633 enhancement from the coal plume is substantial (>20 ppb) as it crosses over the flight path and covers up much of the signal  
634 from upstream gas emissions. Nonetheless, the transport model is able to account for these far-reaching sources and attempt  
635 to separate out their contribution to the observed enhancements. We are able to solve for the optimal upstream natural gas  
636 emission rate and recreate the May 24<sup>th</sup> flight observations more accurately than most other flights, with a correlation  
637 coefficient of 0.71 between the observations and model values. CH<sub>4</sub> values. Although the model successfully recreates the  
638 overall observed CH<sub>4</sub> pattern on this flight, attempting to match model vs. observation-derived enhancements specifically  
639 from upstream natural gas contributions is much more difficult. Contributions from non-natural natural gas sources are large  
640 such that they overwhelm much of the signal from local natural gas sources. After subtracting out non-natural gas sources  
641 from the observations, the correlation specifically between modelled and observation-derived upstream natural gas  
642 enhancements is only 0.11.

643 Despite the model's success at recreating observations from the May 24<sup>th</sup> late-afternoon flight, there is reason to be  
644 careful when interpreting results from day with observations influenced by distant sources. In particular, some transport  
645 error is unavoidable in atmospheric reanalyses, and the longer the time and distance a plume takes to reach the observations,  
646 the more its position and magnitude will be susceptible to these errors. During the early May 24<sup>th</sup> flight, a small 50 km shift  
647 in the location of the coal plume across the study region would change projected enhancements at some observations by as  
648 much as 20 ppb. Furthermore, errors in the transport speed could create scenarios where the coal plume either arrives in the  
649 study region too early or exits too late, creating a projected enhancement pattern that does not agree with the observations  
650 (Figure 1315). Additionally, inaccuracies with the emission estimates of non-unconventional gas sources in the inventory

651 will impact the magnitude of their CH<sub>4</sub> enhancements, creating additional errors in the optimization process when  
652 subtracting out these enhancements from the observations. The early-afternoon May 24<sup>th</sup> flight and May 25<sup>th</sup> flight are both  
653 examples where influences from CH<sub>4</sub> sources in southwest PA create complex structures in the enhancements, which the  
654 model is not able to match as well as the late-afternoon flight on May 24<sup>th</sup> (Figure 4416). And although observations and  
655 modelled enhancements closely match throughout portions of these two flights, a slight shift in the modelled wind direction  
656 can lead to vastly differing results due to the large offset small changes in the wind field can have on an emission source  
657 hundreds of kilometres away. Thus, results from the flights on May 24<sup>th</sup> and May 25<sup>th</sup> should be taken with caution. A deeper  
658 analysis of these errors can be found in Section 3.2.2.

659 ~~Though transport errors from far off sources can have significant impacts on the optimized emission rate, more~~  
660 ~~local transport error is handled more effectively in the model through use of the error minimization cost function discussed~~  
661 ~~in the methods section (Eq. 3). Through use of this cost function, we solve for an upstream emission rate that minimizes the~~  
662 ~~area under the curve between the observed and modelled enhancement. This analysis produces a compensation effect that~~  
663 ~~can adjust for misalignment between the observed natural gas CH<sub>4</sub> plume and the modelled plume, and works best for local~~  
664 ~~sources whose plume structure is similar between the model and observations but location is misaligned. The impact of this~~  
665 ~~effect can be seen best for the flight of May 14<sup>th</sup>, 2015 (Figure 15). During this day, high pressure was centred just north of~~  
666 ~~the flight track, creating diverging winds that were difficult for the transport model to simulate, and the major plume~~  
667 ~~associated with upstream gas emissions ends up south of a well defined plume in the observations. Despite this~~  
668 ~~misalignment, the model still simulates the correct magnitude and width of the plume, providing confidence that small errors~~  
669 ~~in the transport of local, well defined structures have only a small impact on the overall emission rate calculation for any~~  
670 ~~given flight. This assumption is corroborated by an analysis of simulated enhancements of an aircraft transecting a plume at~~  
671 ~~an angle of 45° with errors in the projected wind direction varying between ±20°. Such angle would produce errors in the~~  
672 ~~optimized emission rate ranging from ±30% (Figure 16). These errors become smaller as the angle of the aircraft's path with~~  
673 ~~the axis of the major plume approach 90°. Because the downwind transect of most flights is often close to perpendicular with~~  
674 ~~the plume from upstream gas sources, and differences between modelled and observed winds are often less than 20°,~~  
675 ~~emission estimate errors associated with incorrect transport of the CH<sub>4</sub> plumes would be less than 30%.~~

### 676 3.2.2 Emission Rates and Uncertainty Assessment

677 ~~For each of the ten flights, an uncertainty assessment was performed to obtain a range of likely upstream emission rates for~~  
678 ~~any individual flight. Five different sources of error were considered in this assessment: model wind speed error, model~~  
679 ~~boundary layer height error, CH<sub>4</sub> background error, CH<sub>4</sub> emission inventory error, and model/observation mismatch error.~~  
680 ~~These five sources of error vary substantially from flight to flight depending on conditions, and each can have significant~~  
681 ~~impacts on the total uncertainty.~~

682 ~~Errors in the modelled wind direction and boundary layer height have impacts on our emission estimates which~~  
 683 ~~have a linear impact on the results. If we assume a constant wind speed, a constant boundary layer height, and no~~  
 684 ~~entrainment of air from the top of the boundary layer, we use the following equation to understand these impacts:-~~

$$685 \Delta C = \bar{F}_U \left( \frac{\Delta x}{U \cdot D} \right) \quad (5)$$

686 ~~where  $\Delta C$  is the total  $\text{CH}_4$  enhancement of the column of air contained within the boundary layer,  $\bar{F}_U$  is the average emission~~  
 687 ~~rate over the path the parcel travelled,  $\Delta x$  is the distance the column of air travelled,  $U$  is the wind speed and  $D$  is the~~  
 688 ~~boundary layer height. Using this equation, we can see the linear relationship between the model wind speed, model~~  
 689 ~~boundary layer height, and the calculated emission rate. As an example, if wind speeds in the model are biased low, natural~~  
 690 ~~gas enhancements projected by the model would increase inversely. To compensate for this effect, the optimized emission~~  
 691 ~~rate would decrease proportionally. A similar case can be made for bias in the boundary layer height. Both errors in the wind~~  
 692 ~~speed and boundary layer height have known impacts on the optimized emission rate which can be corrected for, so long as~~  
 693 ~~the errors of each are known.~~

694 To calculate the error in the model wind speed, we assume aircraft observations are truth and use

$$695 U_e = \frac{U_m - U_{obs}}{U_{obs}} \quad (6)$$

696 where  $\bar{U}_{obs}$  is the mean observed wind speed by the aircraft across all points within the boundary layer,  $\bar{U}_m$  is the mean  
 697 modelled wind speed by the model across all points closest in time and space to each observation, and  $U_e$  is the wind speed  
 698 error percentage.

699 To compute the error in the modelled boundary layer height, the observed boundary layer height for each flight is  
 700 assumed to be the true boundary layer height and the boundary layer height percentage error,  $H_e$ , is estimated using:

$$701 H_e = \frac{H_m - H_{obs}}{H_{obs}} \quad (7)$$

702 where  $\bar{H}_{obs}$  is the average observed boundary layer height across each of the aircraft profiles for a given flight,  $\bar{H}_m$  is the  
 703 model boundary layer height closest in time and space to the location of the observed profiles averaged over all profiles. For  
 704 both the observation and the model, boundary layer heights were determined by locating height of the potential temperature  
 705 inversion associated with the top of the boundary layer (Figure 11). In cases where a potential temperature inversion could  
 706 not easily be identified, changes in water vapour,  $\text{CO}_2$  and  $\text{CH}_4$  mixing ratios were used to identify the boundary layer top.

707 Errors in the model wind speed and boundary layer height are calculated for each of the ten flights. From these  
 708 errors, a corrected optimized emission rate is calculated for each flight using Eq. (8):

$$709 E_{new} = \frac{E}{(1+U_e)(1+H_e)} \quad (8)$$



710 ~~where  $E$  is the original emission rate and  $E_{\text{opt}}$  is the corrected optimized upstream natural gas emission rate as a~~  
711 ~~percent of production.~~ Table 4 shows the wind speed and boundary layer height errors for each flight as well as the  
712 optimized and corrected natural gas emission rates. On days where model performance was poor in regards to the wind speed  
713 and boundary layer height, we can see changes in the corrected emission rate. For most days, this change is less than 20%  
714 different than the original optimized emission rate. However, both May 14<sup>th</sup> and May 25<sup>th</sup> have corrected emission rates  
715 which are around a factor of 2 different from their original value. Whether these corrected emission rates are more accurate  
716 than the original optimized rates is debatable. To calculate these alternative emission rates, we must assume that the wind  
717 speeds and boundary layer heights from our limited number of observations are the true values in the atmosphere, which may  
718 not be the case. Regardless of which rate is more accurate for each flight, the overall 16% high bias in the model wind speed  
719 and the ~~\_\_\_~~-12% low bias in the model boundary layer result in compensating errors that cancel out, and the mean emission  
720 rates across all flights end up ~~equal~~similar. Thus, any errors associated with these two meteorological variables has a trivial  
721 impact on the overall calculated emission rate for the region and the uncorrected emission rates are used for the final mean  
722 and uncertainty calculations.

723 ~~In addition to errors related to wind speed and boundary layer height, we quantify three other sources of error in~~  
724 ~~each flight: errors in the selected  $\text{CH}_4$  background value, errors in the  $\text{CH}_4$  inventory, and errors associated with the overall~~  
725 ~~model performance (Table 5). Unlike the wind speed and boundary layer errors which have easily computable impacts on~~  
726 ~~the emission estimates, these other three sources of error and their impact on the optimized emission rate are more difficult~~  
727 ~~to quantify.~~

728 ~~The background error relates to the value chosen for each flight which represents the ambient  $\text{CH}_4$  concentration in~~  
729 ~~the boundary layer unrelated to emission sources within the model. In this study background values ranged from 1897~~  
730 ~~1923ppb. Though background values should not have high variability during a 2-3 hour mid-afternoon flight, entrainment~~  
731 ~~from the boundary layer top can lead to the mixing in of tropospheric air that has different  $\text{CH}_4$  mole fraction values from~~  
732 ~~those within the boundary layer, resulting in a change in the afternoon background value with time. Furthermore, for days on~~  
733 ~~which all aircraft observations (including those upwind of the unconventional wells) are impacted by various  $\text{CH}_4$  plumes~~  
734 ~~predicted within the model, it is difficult to determine the background  $\text{CH}_4$  concentration accurately. Additionally,~~  
735 ~~observations corresponding to locations with no modelled enhancement may in fact have been impacted by missing sources~~  
736 ~~in our inventory, highlighting the difficult nature of knowing with certainty where and what the background is for any given~~  
737 ~~flight. Understanding this uncertainty is crucial; any error in subtracting off the background value directly impacts each~~  
738 ~~observation's observed natural gas enhancement. For example, a background value of 1 ppb below the true background for a~~  
739 ~~given flight would add 1 ppb to each observed natural gas enhancement for all observations, creating a high bias with the~~  
740 ~~optimized upstream emission rate. To account for this error, each flight's optimization processes was rerun iterating the~~  
741 ~~background value by  $\pm 5$  ppb, and the ratio of the percent change in the emission rate compared to the original case was~~  
742 ~~defined as the resulting error in the emission rate due to background uncertainty. This  $\pm 5$  ppb background error range is an~~  
743 ~~estimate at the range of possible error in the background based on changes observed in the upwind measurements from each~~

744 of the flights and is meant to be a conservative estimate of the error. The impact this error can have in the emission rate  
745 varies depending on the magnitude of the observed downwind enhancements during a flight. A plume containing a CH<sub>4</sub>  
746 enhancement of 50 ppb will have a smaller relative error from a 5 ppb change compared to one with an enhancement of only  
747 10 ppb. Thus, days with high wind speeds and a high boundary layer height (and thus enhancements of a smaller magnitude)  
748 tend to be affected the most by background errors.

749 Similar to background errors, errors from the CH<sub>4</sub> emissions inventory are difficult to quantify. In the model  
750 optimization technique, we subtract out enhancements from sources unrelated to unconventional natural gas before solving  
751 for the upstream gas emission rate. In doing so, we are making the assumption that our emissions inventory for sources  
752 unrelated to upstream natural gas processes are accurate. In truth, each emission source in our inventory comes from a  
753 different dataset and has its own unique error bounds, many of which are unknown. Because of the potential for errors in  
754 these emission estimates, we take a conservative approach and iterate the unconventional emissions optimization approach  
755 for each flight, varying the emissions from other unsolved for emission sources in the model by a factor of 2 in each  
756 direction, thus applying a range of 50-200% to the emissions inventory values to assess its impact on the calculated upstream  
757 natural gas emission rate. Despite the extensive range of emissions used in the error analysis, its impact is minimal on most  
758 days due to the northeastern Marcellus region having very few emission sources not related to upstream gas processes. Only  
759 for the flights on May 24<sup>th</sup> do we see errors from the inventory contribute significantly to the overall daily error, when the  
760 coal plume in southwestern PA enters the centre of the study region and has a large role in the upstream emission rate  
761 calculation for that day.

762 The final source of error accounted for attempts to quantify the similarity of the pattern of modelled and observed  
763 natural gas enhancements, referred to here as the model performance error. Figure 17 shows an example of two days, one of  
764 which the model appears to recreate the observations, and the other of which the model poorly matches the shape of the  
765 observed enhancements. Comparing these two simulations with no other information, we hypothesize that one should put  
766 more trust in the upstream natural gas emission rate calculated for the flight whose modelled upstream enhancements match  
767 structurally compared to the emission rate from the flight whose modelled enhancement bares little resemblance to the  
768 observed enhancement. The model performance error is designed to account for the trustworthiness of the optimized  
769 upstream emission rate based on how well the model simulates a given day. The model performance error is calculated using  
770 Eq. (9):

$$771 \sigma_{\text{MPE}} = \frac{\sigma_{\text{diff}}}{\Delta X_{\text{gas}}} \quad (9)$$

772 In this equation,  $\sigma_{\text{diff}}$  is the standard deviation of the difference between the modelled and observed upstream natural gas CH<sub>4</sub>  
773 enhancement using the optimized emission rate, and  $\Delta X_{\text{gas}}$  is the observed magnitude of enhancement from the major  
774 natural gas plume observed in each flight. Here,  $\Delta X_{\text{gas}}$  serves as a normalization factor to account for the varying strength of  
775 the enhancement from flight to flight, and ensures that days with increased enhancements due to meteorological conditions

~~or true daily fluctuations in the upstream natural gas emissions do not proportionally impact the performance error percentage. For example, a day with high winds and a deep boundary layer would produce smaller enhancements, leading to a small  $\bar{\sigma}_{\text{up}}$ , regardless of model performance unless normalized by  $\Delta V_{\text{gas}}$ .~~

Table 5 summarizes the background error, inventory error, and model performance error, and assumes independence between the three error sources to calculate the total ~~error uncertainty~~ for each flight. The largest ~~error occurred during uncertainty exists for~~ the May 22<sup>nd</sup> flight, where an unexplained enhancement along the northern transect led to a poor match between the modelled enhancements and the observed enhancements. This may explain the anomalously high optimized emission rate for that day. Other flights with large ~~error uncertainty~~ are those ~~which that~~ occurred on May 24<sup>th</sup> ~~and May 25<sup>th</sup>, both days,~~ where enhancements from southwestern PA are believed to be influencing large portions of the observations.

Based on the conservative methodology used to calculate these ~~error uncertainties~~, we assume the total ~~error uncertainty~~ for each flight represents a  $2\sigma$  range of possible emission rates and calculate a weighted mean and a  $2\sigma$  confidence interval for the overall upstream emission rate across the ten flights. From this approach, we find a mean upstream emission rate of 0.36% of production and a  $2\sigma$  confidence interval from 0.27-0.45% of production.

### 3.3 Aircraft Mass Balance Results

~~In addition to the model emission optimization, a simplified aircraft mass balance technique was used to calculate upstream natural gas emission rates for flights with a box pattern, a consistent wind direction within the box, and minimal intrusion of CH<sub>4</sub> enhancements from outside the study region that would affect both the upwind and downwind transects. Of the 6 days with box patterned flights from the aircraft campaign, one day (May 14<sup>th</sup>) contained a surface low pressure centre in the middle of the flight resulting in erratic wind patterns, and another day (May 25<sup>th</sup>) had CH<sub>4</sub> plumes from southwestern PA affecting portions the flight observations. These days were not used for a mass balance, and calculations were performed for the remaining box pattern flights (May 22<sup>nd</sup>, May 23<sup>rd</sup>, May 28<sup>th</sup>, May 29<sup>th</sup>). Of the four remaining flights, three of these flights contained two loops around a portion of the Marcellus basin. A mass balance was performed on each loop, resulting in a total of 7 mass balance calculations for the region across 4 days. Table 6 summarizes the results from the mass balance flights.~~

~~For each flight, a total flux within the box encompassed was calculated using Eq. (6). Using this flux, a natural gas emission rate based on production from within the box was calculated using Eq. (10)~~

$$\frac{E}{\mu} = \frac{E - E_{\text{other}}}{\mu} \quad (10)$$

~~where  $E$  is the total flux from Eq. (6) (in kg hr<sup>-1</sup>),  $E_{\text{other}}$  are the emissions enclosed in the box from sources not related to upstream natural gas processes (in kg hr<sup>-1</sup>),  $D$  is the total CH<sub>4</sub> from natural gas being produced within the box (in kg hr<sup>-1</sup>), and  $E_{\text{up}}$  is the resulting natural gas emission rate as a percent of total production within the box.~~ Calculated emission rates varied extensively between flights used for the mass balance analysis, ranging from 0.11% to 1.04% of natural gas

Formatted: Indent: First line: 0.5"

808 production- (Table 6). Comparing emission rates between loops on the same day, we see more consistency in the values.  
809 This result is not surprising, as on each of the days with multiple loops, upwind and downwind CH<sub>4</sub> concentrations patterns  
810 tended to be similar between loops. Thus, differences in the total emission rate are likely due to either errors specific to each  
811 day (such as background variability, errors in meteorology) or real daily variability in the upstream natural gas emission rate.

812 ~~As an error analysis for the mass balance flight, we look at four potential sources of error (Table 7). One source of~~  
813 ~~uncertainty comes from the observed wind speed used in Eq. (6). For our experiment, we take the mean observed wind speed~~  
814 ~~from the aircraft and assume this value represents the mean wind speed within the entire box during the 2-3 hour period it~~  
815 ~~would take for air to travel from the upwind transect to the downwind transect. To understand the uncertainty and biases~~  
816 ~~associated with this assumption, we recreate wind observations along the flight path using values from WRF Chem, and~~  
817 ~~compare the mean wind speed from the simulated observations to the mean model winds contained within the box integrated~~  
818 ~~throughout the boundary layer during the 2-hour period closest to the flight time. By making this comparison, we are able to~~  
819 ~~understand the representation error associated with treating the wind speed observations from the aircraft as the wind speed~~  
820 ~~within the entire box during the period it would take for air to cross from the upwind transect to the downwind transect. On~~  
821 ~~average, modelled wind speeds following the flight were 7% faster than integrated wind speeds within the box, due to the~~  
822 ~~inability for aircraft observations to account for slower wind speeds closer to the surface. This bias was removed from each~~  
823 ~~day's calculated wind speed. After accounting for the wind speed bias, the average error of the modelled wind speed~~  
824 ~~following the flight path compared to the modelled winds within the box was 2%. This 2% uncertainty was applied to each~~  
825 ~~flight and used as the potential uncertainty in the mean wind speed. Errors in the wind direction were neglected, as each~~  
826 ~~flight used in the mass balance completely surrounded the basin using downwind transects at multiple angles, and thus small~~  
827 ~~errors in the wind angle would result in a negligible net change on the total flux calculated.~~

828 ~~Another source of uncertainty is error in the boundary layer height. For each flight, between 2-3 vertical profiles~~  
829 ~~were performed, and the mean height was used in Eq. (6). The standard deviation of different heights from each transect was~~  
830 ~~used as the uncertainty. On May 22<sup>nd</sup>, a boundary layer height could be interpreted from only one vertical transect. For this~~  
831 ~~day, we assume an uncertainty of  $\pm 200\text{m}$  ( $\pm 9\%$ ).~~

832 ~~Uncertainty in the CH<sub>4</sub> background mole fraction was estimated similarly to the boundary layer height. On three of~~  
833 ~~the four flights, two upwind transects were performed. The mean observed CH<sub>4</sub> mole fraction between the two transects was~~  
834 ~~used as the background value for the entire flight, and the standard deviation between the loops was used as the uncertainty.~~  
835 ~~On both the May 23<sup>rd</sup> and May 28<sup>th</sup> flights, background differences between the two transects were less than the instrument~~  
836 ~~error of 1 ppb. On these days, we use the instrument error as the background error. On May 22<sup>nd</sup>, only one upwind transect~~  
837 ~~was usable for the calculation. For this day, we assume a conservative estimate in the uncertainty of the background of  $\pm 5$~~   
838 ~~ppb.~~

839 ~~Finally, we assess uncertainty in the emissions inventory. After a CH<sub>4</sub> flux is calculated for each loop, emissions~~  
840 ~~from sources contained within the box that are not associated with upstream natural gas processes must be subtracted out to~~  
841 ~~solve for the upstream natural gas emission rate. Any errors associated with our inventory will result in a CH<sub>4</sub> source~~

~~attribution error. To account for the potentially large uncertainty with the emission sources in our inventory, we vary these non natural gas emissions by a factor of 2 to test the impact on the solved upstream natural gas emission rate. Because northeastern Pennsylvania contains few sources of CH<sub>4</sub> emissions outside of natural gas production, the impact of this uncertainty is typically less than 20% of the total emissions calculated within the box.~~

From Table 7, we can see the largest ~~relative errors occur~~error with regards to the absolute uncertainty in the emission rate occurs on the May 22<sup>nd</sup> flight. It is on this day where we have the largest uncertainty in the background value, with observations towards the end of the flight becoming unusable due to a rapid and unexplained decrease in the CH<sub>4</sub> mole fraction ~~with time of 8 ppb over a 30 minute period~~ (Figure ~~48~~17). This day also features the highest boundary layer height and fastest winds of all flights done in this study, reducing the magnitude of the enhancement associated with the natural gas plume and thus amplifying the effects an uncertain background has on the overall uncertainty of the calculated CH<sub>4</sub> flux. Uncertainty across the other three flights is smaller, and results between individual loops on the May 23<sup>rd</sup> and May 28<sup>th</sup> flight provide more confidence in the calculated flux for those days.

Using the mean estimated CH<sub>4</sub> emissions and uncertainty for each loop, we calculate a daily mean emission rate and uncertainty for each of the four days. We then solve for an unweighted mean across the four flights to derive our overall emissions estimate from the aircraft mass balance approach, and use the standard error of the flights to estimate the uncertainty. In doing so, we derive a natural gas emission rate from upstream processes of ~~0.3440~~0.3440% of production, with a 2 $\sigma$  confidence interval from ~~0.0608-0.6272~~0.0608-0.6272% of production. Here, we use the arithmetic mean rather than a weighted mean due to the linear relationship between the size of the emission rate and the size of the errors. Because errors associated with ABL height and wind speed have a proportional impact on the calculated emissions within the box, days with a high emissions estimate produce large uncertainties relative to days with a small emission rate. Using a weighted mean approach assigns more weight to the days with low estimated emissions, and produces an overall emission estimate too low and certain to have confidence in (0.12 $\pm$ 0.02 percent of gas production).

## 4 Discussion

### 4.1 Upstream Emission Rate

From this study, we estimate with a 2 $\sigma$  confidence interval an emission rate between 0.27-0.45% of gas production using the model optimization method and 0.06-0.62% of gas production using the aircraft mass balance. Figure ~~49~~18 provides the emission range estimates from upstream natural gas processes using both the model optimization technique and mass balance technique when applicable. ~~These~~Top-down studies of other basins in the U.S. have all found emission ~~rate estimates as a~~percent rates greater than 1% of production, ~~and thus the rates calculated for the northeastern Marcellus basin~~are the lowest observed ~~from top-down measurements of different basins in the U.S., and raise yet, raising~~questions as to why these the values in ~~the northeastern Marcellus this~~region appear to be low. One possibility may be related to the well efficiency of the

874 northeastern Marcellus region compared to other major shale plays (Table 8). In terms of gas production per unconventional  
875 well, the Marcellus is the highest of all major basins in the U.S. Furthermore, the gas production per well increases by nearly  
876 a factor of two when focusing specifically on Susquehanna and Bradford Counties in northeastern Pennsylvania where the  
877 majority of the wells from this study are located (Figure 201). The large difference in production per well between the  
878 northeastern Marcellus and other shales may partly explain the low emission rates as a percentage of production. Throughout  
879 this study, we normalize natural gas emissions as a percentage of total production under the assumption that higher  
880 throughput of natural gas in a system should lead to higher emissions in the system. However, if leaks are more influenced  
881 by the number of pneumatic devices components in operation rather than the throughput passing through the device wells, a  
882 high-efficiency production-per-well system such as the unconventional wells in the northeastern Marcellus could end up  
883 having a very low emission rate as a percentage of production, but a similar emission rate compared to other basins based on  
884 the number of wells, compressors, etc. A thorough bottom-up study of the Marcellus region measuring emissions on a device  
885 level could provide an answer to this hypothesis.

886 Although we calculate a low emission rate for this region, rates calculated for May 22 and May 25 stand out as  
887 outliers where emissions fall well-above our uncertainty bounds. It is possible that emissions from natural gas sources were  
888 higher on these days compared to others. Releases of natural gas into the atmosphere from short timeframe events such as  
889 liquids unloading and venting can add a temporal component to the emission rate. Such events occurring at an increased  
890 frequency during the May 22 and May 25 flights could be responsible for the higher emission rates. However, these two days  
891 both have issues that could have affected the optimized emission rate. On May 22, we observe a sudden drop in the observed  
892 CH<sub>4</sub> values that is nearly as large as the main plume on that day, creating concerns about background concentrations. On  
893 May 25, a southwesterly wind was present, and while the model showed the coal plume to be west of the flight path, a small  
894 shift in the model wind direction would shift the coal plume over the region. For these reasons we are sceptical but not  
895 dismissive of the high emission rates found during these two flights.

896  
897

#### 898 **4.2 Advantages of Combining Observations with Model Output**

899 One of the major advantages of using a chemical transport model to solve for natural gas emission rates compared to a  
900 standard mass-balance approach is that the transport model is able to account for the complex and oftentimes non-uniform  
901 plume structures originating from sources outside the flight path that can affect observations. When performing a mass  
902 balance over a basin, it is assumed that the upwind transect is representative of the air exiting the downwind transect after  
903 subtracting out all sources within the box. However, this assumption is only true if winds contained within the flight path are  
904 in perfect steady state during the time it take for air to move from the upwind transect to the downwind transect, and that  
905 measurements from the downwind transect occurred at a much later time so that the air being measured is the same air  
906 measured from the upwind transect. These conditions are not easily achieved for regional scale mass balances due to the long

907 times needed for the air from the upwind transect to reach the downwind transect. As an example, from the four mass  
908 balance flights performed for this study the average time for air to move from the upwind transect to the downwind transect  
909 was 4 hours whereas the average time between the aircraft's upwind and downwind measurements was ~40 minutes. The  
910 aircraft observations can be thought of as a snapshot in time, which can be problematic if large scale plumes from outside the  
911 domain are moving through the region and impacting only certain portions of the observations during the flight's short  
912 timeframe. By using a transport model for a domain much larger than that of the flight paths, we are able to track these far-  
913 reaching plumes and identify situations where the background CH<sub>4</sub> concentrations may be spatially heterogeneous.

914 The potential usefulness of using a transport model alongside a mass balance calculation can best be demonstrated  
915 from observations taken over the Marcellus during a 2013 aircraft campaign (Peischl et. al 2015). During this flight the  
916 prevailing winds were from the WSW, and the largest CH<sub>4</sub> enhancements were observed along the western edge of the flight  
917 path, upwind of the unconventional wells. Using our transport model, we are able to recreate the day of flight and attempt to  
918 use our inventory and explain this feature (Figure 2+19). Comparisons between modelled output and observations show a 60  
919 ppb CH<sub>4</sub> enhancement from coal and conventional wells in southwest PA stretching close to the western edge of the aircraft  
920 observations, a plume structure similar to the one observed during the May 24<sup>th</sup> flight from our own study. Though this  
921 plume does not initially align with the observed transect with the largest enhancements, we recognize that the coal and gas  
922 plume travels for more than 20 hours (a distance of 400 km) from its source before reaching the flight path. If we allow for a  
923 10% error in the transport speed and therefore advance the transport model by an additional two hours past the time in which  
924 the aircraft observed these high values, we are able to line up the centre of the plume with the largest observed CH<sub>4</sub> mole  
925 fractions along the western edge of the flight. In addition to the 60 ppb enhancement along the centre of the plume, the  
926 model projects 20 ppb enhancements along the edges and in front of the plume centre. These smaller enhancements have an  
927 influence along different portions of the flight which varies in magnitude, making it difficult to assess a proper background  
928 CH<sub>4</sub> value upwind of the wells and potentially masking natural gas enhancements downwind of them. But by using a  
929 transport model, we are able to see the potential impact of these far-reaching sources which would otherwise not be  
930 considered in a regional mass balance and better understand the complex CH<sub>4</sub> plume structures which can occur in a given  
931 region under specific wind conditions.

## 932 **5 Conclusion**

933 Using the model optimization technique presented in this study, we find a weighted mean natural gas emission rate from  
934 unconventional production and gathering facilities of 0.36% of production with a 2 $\sigma$  confidence interval from 0.27-0.45% of  
935 production. This emission rate is supported by four mass balance calculations, which produce a mean of 0.3440% and a 2 $\sigma$   
936 confidence interval from of 0.0608-0.6272% of production. Applied to all the wells in our study region, this mean rate  
937 results in a leakage rate of 20 Mg CH<sub>4</sub> hr<sup>-1</sup> for the year 2015. The emission rate found in this top-down study quantified as a  
938 percent of production is significantly lower than rates found using top-down methodology at any other basin, and indicates

939 the presence of some fundamental difference in the northeastern Marcellus gas industry that is resulting in more efficient  
940 extraction and processing of the natural gas.

941 The ten flights that took place in this study reveal large regional variations in the CH<sub>4</sub> enhancement patterns  
942 depending on the prevailing wind direction. On days with a northwest wind, observed enhancements come primarily from  
943 ~~the natural gas industry sources~~, and a small plume associated with it can be seen on the downwind leg of each flight with  
944 few enhancements upwind of the wells. Flights ~~which that~~ took place with winds conditions predominantly from the  
945 southwest were more difficult to interpret. Plumes associated with coal and other potential sources of CH<sub>4</sub> in the  
946 southwestern Pennsylvania create complex enhancement patterns affecting both the upwind and downwind portions of the  
947 flight, making both the background CH<sub>4</sub> mole fraction and enhancements from the gas industry difficult to interpret. The  
948 stark difference between observations ~~which that~~ occurred with a northwest wind compared to a southwest wind illustrates  
949 the importance of having multiple flights across days with various wind conditions to better understand the major influences  
950 on CH<sub>4</sub> concentrations throughout a region. The regional influences in Pennsylvania also demonstrate the utility of deriving  
951 an emissions inventory that provides input data to drive a transport model, allowing one to forecast CH<sub>4</sub> mole fractions on  
952 difficult days and better understand the daily uncertainties associated with heterogeneous background conditions.

953 Though this study presented observations from ten flights over a three-week period, it is not able to account for the  
954 potential of long term temporal variability in the emission rates. In May 2015 when the flights took place, the entire  
955 Marcellus basin was nearing peak production and active drilling and hydraulic fracturing was still ongoing in the region. By  
956 mid-2016, the rate of drilling of new wells in the northeast Marcellus had decreased and natural gas production had begun to  
957 decline in the area. A snapshot of the emission rate during one month of a basin in its peak production is insufficient to  
958 characterize emissions from an area that is likely to be producing and transporting gas at various intensities for decades. We  
959 need to quantify the long-term climatological impacts of gas production. Future work examining the temporal variability of  
960 CH<sub>4</sub> emissions within natural gas basins would complement short-term, high-intensity studies such as this one, and aid with  
961 understanding how well the calculated emission rates represent the gas basin over the course of time.

## 962 **Acknowledgements**

963 This work has been funded by the U.S. Department of Energy National Energy Technology Laboratory (project DE-  
964 FE0013590). We thank in-kind contributions from the Global Monitoring Division of the National Oceanic and Atmospheric  
965 Administration, and from the Earth and Environmental Systems Institute, the Department of Meteorology and Atmospheric  
966 Science, and the College of Earth and Mineral Science of The Pennsylvania State University. We also want to thank the  
967 Pennsylvania College of Technology in Williamsport, PA for access to their Technology Aviation Center facilities during  
968 the aircraft campaign. We also want to thank Lillie Langlois from the Department of Ecosystem Science and  
969 Management for sharing pipeline information, Anthony J. Marchese and Dan Zimmerle (Colorado State University) for  
970 information on compressor stations, Jeff Peischl for sharing data from his 2013 flight campaign, and Bernd Haupt (Penn



971 State University) for data processing and management during the project. Finally, we would like to thank Dennis and Joan  
972 Thomson for their creation and continued support of the Thomson Distinguished Graduate Fellowship.

973 **References**

- 974 Alvarez, R. A., Pacala, S. W., Winebrake, J. J., Chameides, W. L., and Hamburg, S. P.: Greater focus needed on methane  
975 leakage from natural gas infrastructure, *Proceedings of the National Academy of Sciences*, 109, 6435-6440,  
976 10.1073/pnas.1202407109, 2012.
- 977
- 978 Bloom, A. A., Bowman, K., Lee, M., Turner, A. J., Schroeder, R., Worden, J. R., Weidner, R., McDonald, K. C., and Jacob,  
979 D. J.: A global wetland methane emissions and uncertainty dataset for atmospheric chemical transport models,  
980 *Geosci. Model Dev. Discuss.*, doi:10.5194/gmd-2016-224, in review, 2016-2017, 2017.
- 981
- 982 Bradford County: Maps of Natural Gas Development in Bradford County, available at:  
983 <http://www.bradfordcountypa.org/index.php/natural-gas-information>.
- 984
- 985 Bousquet, P., Ciais, P., Miller, J. B., Dlugokencky, E. J., Hauglustaine, D. A., Prigent, C., Van der Werf, G. R., Peylin, P.,  
986 Brunke, E. G., Carouge, C., Langenfelds, R. L., Lathiere, J., Papa, F., Ramonet, M., Schmidt, M., Steele, L. P.,  
987 Tyler, S. C., and White, J.: Contribution of anthropogenic and natural sources to atmospheric methane variability,  
988 *Nature*, 443, 439-443, [http://www.nature.com/nature/journal/v443/n7110/supinfo/nature05132\\_S1.html](http://www.nature.com/nature/journal/v443/n7110/supinfo/nature05132_S1.html), 2006.
- 989
- 990 Brandt, A. R., Heath, G. A., Kort, E. A., O'Sullivan, F., Pétron, G., Jordaan, S. M., Tans, P., Wilcox, J., Gopstein, A. M.,  
991 Arent, D., Wofsy, S., Brown, N. J., Bradley, R., Stucky, G. D., Eardley, D., and Harriss, R.: Methane Leaks from  
992 North American Natural Gas Systems, *Science*, 343, 733-735, 10.1126/science.1247045, 2014.
- 993
- 994 Cambaliza, M. O. L., Shepson, P. B., Caulton, D. R., Stirm, B., Samarov, D., Gurney, K. R., Turnbull, J., Davis, K. J.,  
995 Possolo, A., Karion, A., Sweeney, C., Moser, B., Hendricks, A., Lauvaux, T., Mays, K., Whetstone, J., Huang, J.,  
996 Razlivanov, I., Miles, N. L., and Richardson, S. J.: Assessment of uncertainties of an aircraft-based mass balance  
997 approach for quantifying urban greenhouse gas emissions, *Atmos. Chem. Phys.*, 14, 9029-9050, 10.5194/acp-14-  
998 9029-2014, 2014.
- 999
- 1000 Chen, F., and Dudhia, J.: Coupling an Advanced Land Surface-Hydrology Model with the Penn State-NCAR MM5  
1001 Modeling System. Part I: Model Implementation and Sensitivity, *Monthly Weather Review*, 129, 569-585,  
1002 10.1175/1520-0493(2001)129<0569:caalsh>2.0.co;2, 2001.
- 1003
- 1004 Conley, S., Franco, G., Faloon, I., Blake, D. R., Peischl, J., and Ryerson, T. B.: Methane emissions from the 2015 Aliso  
1005 Canyon blowout in Los Angeles, CA, *Science*, 10.1126/science.aaf2348, 2016.
- 1006
- 1007 Deng, A., Stauffer, D., Gaudet, B., Dudhia, J., Hacker, J., Bruyere, C., Wu, W., Vandenberghe, F., Liu, Y., and Bourgeois,  
1008 A.: Update on WRF-ARW end-to-end multi-scale FDDA system, 10th Annual WRF Users' Workshop, Boulder,  
1009 CO, June 23, 2009.
- 1010
- 1011 Deng, A., Gaudet, B., Dudhia, J., and Alapaty, K.: Implementation and Evaluation of a New Shallow Convection Scheme in  
1012 WRF, 94th American Meteorological Society Annual Meeting, Atlanta, GA, February 2-6, 2014.
- 1013
- 1014 EIA: Annual Energy Outlook 2012 with Projections to 2035, available at:  
1015 [http://www.eia.gov/forecasts/aeo/pdf/0383\(2012\).pdf](http://www.eia.gov/forecasts/aeo/pdf/0383(2012).pdf), 2012.
- 1016
- 1017 EIA: Layer Information for Interactive State Maps, available at: [https://www.eia.gov/maps/layer\\_info-m.cfm](https://www.eia.gov/maps/layer_info-m.cfm), 2015
- 1018
- 1019 EIA: Shale in the United States, available at: [https://www.eia.gov/energyexplained/index.cfm?page=natural\\_gas\\_where](https://www.eia.gov/energyexplained/index.cfm?page=natural_gas_where),  
1020 2016a
- 1021

Formatted: Tab stops: 5.09", Left

1022 EIA: Monthly Energy Review: June 2016. [Available online at  
1023 <http://www.eia.gov/totalenergy/data/monthly/archive/00351607.pdf>, 2016b.  
1024

1025 EPA: Abandoned Coal Mine Methane Opportunities Database, available at: [https://www.epa.gov/cmop/abandoned-](https://www.epa.gov/cmop/abandoned-underground-mines)  
1026 [underground-mines](https://www.epa.gov/cmop/abandoned-underground-mines), 2008.  
1027

1028 EPA: Greenhouse Gas Reporting Program 2014, available at: [https://www.epa.gov/ghgreporting/ghg-reporting-program-](https://www.epa.gov/ghgreporting/ghg-reporting-program-data-sets)  
1029 [data-sets](https://www.epa.gov/ghgreporting/ghg-reporting-program-data-sets), 2015a.  
1030

1031 EPA: Inventory of US Greenhouse Gas Emissions and Sinks: 1990-2013 Annex 3.6, available at:  
1032 <https://www.epa.gov/ghgemissions/inventory-us-greenhouse-gas-emissions-and-sinks-1990-2013>, 2015b.  
1033

1034 EPA: Inventory of US Greenhouse Gas Emissions and Sinks: 1990-2014 Annex 2.2, available at:  
1035 <https://www.epa.gov/ghgemissions/inventory-us-greenhouse-gas-emissions-and-sinks-1990-2014>, 2016.  
1036

1037 Frankenberg C., Thorpe, A. K., Thompson, D. R., Hulley, G., Kort, E. A., Vance, N., Borchardt, J., Krings, T., Gerilowski,  
1038 K., Sweeney, C., Conley, S., Bue, B. D., Aubrey, A. D., Hook, S., and Green, R. O.: Airborne methane remote  
1039 measurements reveal heavy-tail flux distribution in Four Corners region, *Proceedings of the National Academy of*  
1040 *Sciences*, 113, 9734-9739, 2016.  
1041

1042 Hughes, J. D.: *Drilling Deeper: A Reality Check on US Government Forecasts for a Lasting Tight Oil & Shale Gas Boom*,  
1043 Post Carbon Institute, Santa Rosa, California, 2014.  
1044

1045 Iacono, M. J., Delamere, J. S., Mlawer, E. J., Shephard, M. W., Clough, S. A., and Collins, W. D.: Radiative forcing by long-  
1046 lived greenhouse gases: Calculations with the AER radiative transfer models, *Journal of Geophysical Research:*  
1047 *Atmospheres*, 113, 10.1029/2008jd009944, 2008.  
1048

1049 Jimenez, P. A., Hacker, J. P., Dudhia, J., Haupt, S. E., Ruiz-Arias, J. A., Gueymard, C. A., Thompson, G., Eidhammer, T.,  
1050 and Deng, A.: WRF-Solar: Description and Clear-Sky Assessment of an Augmented NWP Model for Solar Power  
1051 Prediction, *Bulletin of the American Meteorological Society*, 97, 1249-1264, 10.1175/bams-d-14-00279.1, 2016.  
1052

1053 Jiménez, P. A., Alessandrini, S., Haupt, S. E., Deng, A., Kosovic, B., Lee, J. A., and Monache, L. D.: The Role of  
1054 Unresolved Clouds on Short-Range Global Horizontal Irradiance Predictability, *Monthly Weather Review*, 144,  
1055 3099-3107, 10.1175/mwr-d-16-0104.1, 2016.  
1056

1057 Kain, J. S., and Fritsch, J. M.: A One-Dimensional Entraining/Detraining Plume Model and Its Application in Convective  
1058 Parameterization, *Journal of the Atmospheric Sciences*, 47, 2784-2802, 10.1175/1520-  
1059 0469(1990)047<2784:aodepm>2.0.co;2, 1990.  
1060

1061 Kain, J. S.: The Kain-Fritsch Convective Parameterization: An Update, *Journal of Applied Meteorology*, 43, 170-181,  
1062 10.1175/1520-0450(2004)043<0170:tkcpau>2.0.co;2, 2004.  
1063

1064 Karion, A., Sweeney, C., Pétron, G., Frost, G., Michael Hardesty, R., Kofler, J., Miller, B. R., Newberger, T., Wolter, S.,  
1065 Banta, R., Brewer, A., Dlugokencky, E., Lang, P., Montzka, S. A., Schnell, R., Tans, P., Trainer, M., Zamora, R.,  
1066 and Conley, S.: Methane emissions estimate from airborne measurements over a western United States natural gas  
1067 field, *Geophysical Research Letters*, 40, 4393-4397, 10.1002/grl.50811, 2013.  
1068

1069 Karion, A., Sweeney, C., Kort, E. A., Shepson, P. B., Brewer, A., Cambaliza, M., Conley, S. A., Davis, K., Deng, A.,  
1070 Hardesty, M., Herndon, S. C., Lauvaux, T., Lavoie, T., Lyon, D., Newberger, T., Pétron, G., Rella, C., Smith, M.,

1071 Wolter, S., Yacovitch, T. I., and Tans, P.: Aircraft-Based Estimate of Total Methane Emissions from the Barnett  
1072 Shale Region, *Environmental Science & Technology*, 49, 8124-8131, 10.1021/acs.est.5b00217, 2015.  
1073  
1074 Lamb, B. K., Cambaliza, M. O. L., Davis, K. J., Edburg, S. L., Ferrara, T. W., Floerchinger, C., Heimbürger, A. M. F.,  
1075 Herndon, S., Lauvaux, T., Lavoie, T., Lyon, D. R., Miles, N., Prasad, K. R., Richardson, S., Roscioli, J. R., Salmon,  
1076 O. E., Shepson, P. B., Stirm, B. H., and Whetstone, J.: Direct and Indirect Measurements and Modeling of Methane  
1077 Emissions in Indianapolis, Indiana, *Environmental Science & Technology*, 50, 8910-8917,  
1078 10.1021/acs.est.6b01198, 2016.  
1079  
1080 [Langlois, L. A., Drohan, P. J., and Brittingham, M. C.: Linear infrastructure drives habitat conversion and forest](#)  
1081 [fragmentation associated with Marcellus shale gas development in a forested landscape. \*Journal of Environmental\*](#)  
1082 [Management](#). 197, 167-176. 10.1016/j.jenvman.2017.03.045. 2017.  
1083  
1084 Lauvaux, T., Uliasz, M., Sarrat, C., Chevallier, F., Bousquet, P., Lac, C., Davis, K. J., Ciais, P., Denning, A. S., and Rayner,  
1085 P. J.: Mesoscale inversion: first results from the CERES campaign with synthetic data, *Atmos. Chem. Phys.*, 8,  
1086 3459-3471, 10.5194/acp-8-3459-2008, 2008.  
1087  
1088 Maasakkers, J. D., Jacob, D. J., Sulprizio, M. P., Turner, A. J., Weitz, M., Wirth, T., Hight, C., DeFigueiredo, M., Desai, M.,  
1089 Schmeltz, R., Hockstad, L., Bloom, A. A., Bowman, K. W., Jeong, S., and Fischer, M. L.: Gridded National  
1090 Inventory of U.S. Methane Emissions, *Environmental Science & Technology*, 50, 13123-13133,  
1091 10.1021/acs.est.6b02878, 2016.  
1092  
1093 Marchese, A. J., Vaughn, T. L., Zimmerle, D. J., Martinez, D. M., Williams, L. L., Robinson, A. L., Mitchell, A. L.,  
1094 Subramanian, R., Tkacik, D. S., Roscioli, J. R., and Herndon, S. C.: Methane Emissions from United States Natural  
1095 Gas Gathering and Processing, *Environmental Science & Technology*, 49, 10718-10727, 10.1021/acs.est.5b02275,  
1096 2015.  
1097  
1098 Mays, K. L., Shepson, P. B., Stirm, B. H., Karion, A., Sweeney, C., and Gurney, K. R.: Aircraft-Based Measurements of the  
1099 Carbon Footprint of Indianapolis, *Environmental Science & Technology*, 43, 7816-7823, 10.1021/es901326b, 2009.  
1100  
1101 Mlawer, E. J., Taubman, S. J., Brown, P. D., Iacono, M. J., and Clough, S. A.: Radiative transfer for inhomogeneous  
1102 atmospheres: RRTM, a validated correlated-k model for the longwave, *Journal of Geophysical Research:*  
1103 *Atmospheres*, 102, 16663-16682, 10.1029/97jd00237, 1997.  
1104  
1105 Myhre, G., Shindell, D., Bréon, F.-M., Collins, W., Fuglestedt, J., Huang, J., Koch, D., Lamarque, J.-F., Lee, D., and  
1106 Mendoza, B.: Anthropogenic and natural radiative forcing, *Climate change*, 423, 2013.  
1107  
1108 Nakanishi, M., and Niino, H.: An improved Mellor–Yamada level-3 model: Its numerical stability and application to a  
1109 regional prediction of advection fog, *Boundary-Layer Meteorology*, 119, 397-407, 2006.  
1110  
1111 NYDEC: NY 2014 Oil & Gas Production Data: available at: <http://www.dec.ny.gov/energy/36159.html>, 2016.  
1112  
1113 Omara, M., Sullivan, M. R., Li, X., Subramanian, R., Robinson, A. L., and Presto, A. A.: Methane Emissions from  
1114 Conventional and Unconventional Natural Gas Production Sites in the Marcellus Shale Basin, *Environmental*  
1115 *Science & Technology*, 50, 2099-2107, 10.1021/acs.est.5b05503, 2016.  
1116  
1117 Overend, R. P., Paraskevopoulos, G., and Cvetanović, R. J.: Rates of OH Radical Reactions. I. Reactions with H<sub>2</sub>, CH<sub>4</sub>,  
1118 C<sub>2</sub>H<sub>6</sub>, and C<sub>3</sub>H<sub>8</sub> at 295 K, *Canadian Journal of Chemistry*, 53, 3374-3382, 10.1139/v75-482, 1975.  
1119

1120 PADEP: PA Oil and Gas Well Historical Production Report, available at:  
1121 [http://www.depreportingservices.state.pa.us/ReportServer/Pages/ReportViewer.aspx?%2fOil\\_Gas%2fOil\\_Gas\\_Wel](http://www.depreportingservices.state.pa.us/ReportServer/Pages/ReportViewer.aspx?%2fOil_Gas%2fOil_Gas_Wel)  
1122 [l\\_Historical\\_Production\\_Report](http://www.depreportingservices.state.pa.us/ReportServer/Pages/ReportViewer.aspx?%2fOil_Gas%2fOil_Gas_Wel), 2016.  
1123

1124 Peischl, J., Ryerson, T. B., Aikin, K. C., de Gouw, J. A., Gilman, J. B., Holloway, J. S., Lerner, B. M., Nadkarni, R.,  
1125 Neuman, J. A., Nowak, J. B., Trainer, M., Warneke, C., and Parrish, D. D.: Quantifying atmospheric methane  
1126 emissions from the Haynesville, Fayetteville, and northeastern Marcellus shale gas production regions, *Journal of*  
1127 *Geophysical Research: Atmospheres*, 120, 2119-2139, 10.1002/2014jd022697, 2015.  
1128

1129 Pétron, G., Frost, G., Miller, B. R., Hirsch, A. I., Montzka, S. A., Karion, A., Trainer, M., Sweeney, C., Andrews, A. E.,  
1130 Miller, L., Kofler, J., Bar-Ilan, A., Dlugokencky, E. J., Patrick, L., Moore, C. T., Ryerson, T. B., Siso, C.,  
1131 Kolodzey, W., Lang, P. M., Conway, T., Novelli, P., Masarie, K., Hall, B., Guenther, D., Kitzis, D., Miller, J.,  
1132 Welsh, D., Wolfe, D., Neff, W., and Tans, P.: Hydrocarbon emissions characterization in the Colorado Front Range:  
1133 A pilot study, *Journal of Geophysical Research: Atmospheres*, 117, ~~n/a-n/a~~, 10.1029/2011jd016360, 2012.  
1134

1135 Platts: Maps and Geospatial Data: available at: <http://www.platts.com/maps-geospatial>, 2016.  
1136

1137 Rogers, R., Deng, A., Stauffer, D., Jia, Y., Soong, S., Tanrikulu, S., Beaver, S., and Tran, C.: Fine particulate matter  
1138 modeling in Central California. Part I: Application of the Weather Research and Forecasting model, 91th Annual  
1139 Meeting, 2011.  
1140

1141 Ryerson, T. B., Trainer, M., Holloway, J. S., Parrish, D. D., Huey, L. G., Sueper, D. T., Frost, G. J., Donnelly, S. G.,  
1142 Schaufli, S., Atlas, E. L., Kuster, W. C., Goldan, P. D., Hübler, G., Meagher, J. F., and Fehsenfeld, F. C.:  
1143 Observations of Ozone Formation in Power Plant Plumes and Implications for Ozone Control Strategies, *Science*,  
1144 292, 719-723, 10.1126/science.1058113, 2001.  
1145

1146 Schwietzke, S., Griffin, W. M., Matthews, H. S., and Bruhwiler, L. M. P.: Natural Gas Fugitive Emissions Rates Constrained  
1147 by Global Atmospheric Methane and Ethane, *Environmental Science & Technology*, 48, 7714-7722,  
1148 10.1021/es501204c, 2014.  
1149

1150 Smith, M. L., Kort, E. A., Karion, A., Sweeney, C., Herndon, S. C., and Yacovitch, T. I.: Airborne Ethane Observations in  
1151 the Barnett Shale: Quantification of Ethane Flux and Attribution of Methane Emissions, *Environmental Science &*  
1152 *Technology*, 49, 8158-8166, 10.1021/acs.est.5b00219, 2015.  
1153

1154 Skamarock, W. C., Klemp, J. B., Dudhia, J., Gill, D. O., Barker, D. M., Wang, W., and Powers, J. G.: A description of the  
1155 advanced research WRF version 2, DTIC Document, 2005.  
1156

1157 Stone, D., Whalley, L. K., and Heard, D. E.: Tropospheric OH and HO<sub>2</sub> radicals: field measurements and model  
1158 comparisons, *Chemical Society Reviews*, 41, 6348-6404, 10.1039/c2cs35140d, 2012.  
1159

1160 [Sweeney, C., Karion, A., Kort, E. A., Smith, M. L., Newberger T., Schwietzke, S., Wolter, S., and Lauvaux, T.: Aircraft](https://doi.org/10.15138/G35K54)  
1161 [Campaign Data over the Northeastern Marcellus Shale, May-June 2015, Version: 2017-03-29, Path:](https://doi.org/10.15138/G35K54)  
1162 [https://doi.org/10.15138/G35K54, 2015](https://doi.org/10.15138/G35K54)  
1163

1164 Tewari, M., Chen, F., Wang, W., Dudhia, J., LeMone, M., Mitchell, K., Ek, M., Gayno, G., Wegiel, J., and Cuenca, R.:  
1165 Implementation and verification of the unified NOAA land surface model in the WRF model, 20th conference on  
1166 weather analysis and forecasting/16th conference on numerical weather prediction, 2004.  
1167

1168 Thompson, G., Field, P. R., Rasmussen, R. M., and Hall, W. D.: Explicit Forecasts of Winter Precipitation Using an  
1169 Improved Bulk Microphysics Scheme. Part II: Implementation of a New Snow Parameterization, Monthly Weather  
1170 Review, 136, 5095-5115, 10.1175/2008mwr2387.1, 2008.  
1171  
1172 USDA: Census Ag Atlas Maps, available at:  
1173 [https://www.agcensus.usda.gov/Publications/2012/Online\\_Resources/Ag\\_Atlas\\_Maps/Livestock\\_and\\_Animals/](https://www.agcensus.usda.gov/Publications/2012/Online_Resources/Ag_Atlas_Maps/Livestock_and_Animals/),  
1174 2012.  
1175  
1176 White, W. H., Anderson, J. A., Blumenthal, D. L., and Wilson, W. E., Formation and transport of secondary air-pollutants:  
1177 Ozone and aerosols in St. Louis urban plume: Science 194, 187-189, 10.1126/science.959846, 1976.  
1178  
1179 WVDEP: WV Oil and Gas Database and Map Information, available at: [http://www.dep.wv.gov/oil-and-](http://www.dep.wv.gov/oil-and-gas/databaseinfo/Pages/default.aspx)  
1180 [gas/databaseinfo/Pages/default.aspx](http://www.dep.wv.gov/oil-and-gas/databaseinfo/Pages/default.aspx), 2016.  
1181  
1182 Zavala-Araiza, D., Lyon, D., Alvarez, R. A., Palacios, V., Harriss, R., Lan, X., Talbot, R., and Hamburg, S. P.: Toward a  
1183 Functional Definition of Methane Super-Emitters: Application to Natural Gas Production Sites, Environmental  
1184 Science & Technology, 49, 8167-8174, 10.1021/acs.est.5b00133, 2015  
1185  
1186 Zavala-Araiza, D., Alvarez, R. A., Lyon, D. R., Allen, D. T., Marchese, A. J., Zimmerle, D. J., and Hamburg, S. P.: Super-  
1187 emitters in natural gas infrastructure are caused by abnormal process conditions, Nature Communications, 8, 14012,  
1188 10.1038/ncomms14012, 2017.  
1189  
1190 Zimmerle, D. J., Williams, L. L., Vaughn, T. L., Quinn, C., Subramanian, R., Duggan, G. P., Willson, B., Opsomer, J. D.,  
1191 Marchese, A. J., Martinez, D. M., and Robinson, A. L.: Methane Emissions from the Natural Gas Transmission and  
1192 Storage System in the United States, Environmental Science & Technology, 49, 9374-9383,  
1193 10.1021/acs.est.5b01669, 2015.

**Table 1: List of tracers used in the transport model.**

Tracer #	Name	Description of source
1	Unconventional Wells	Emissions from unconventional wells.
2	Storage Facilities	Emissions from compressors associated with natural gas storage.
3	Pipelines	Emissions from gathering and transmission pipelines
4	Distribution	Emissions from the distribution sector of the natural gas industry.
5	Conventional Wells	Emissions from conventional wells.
6	Landfills/Other	Emissions from landfills and uncharacterized industrial sources.
7	Coal	Emissions from active and abandoned coal mining.
8	Animals/Waste	Emissions from enteric fermentation and manure management
9	Production Compressors (HP)	Emissions from compressor stations characterized as “production”. Emissions scaled linearly with wattage.
10	Gathering Compressors (HP)	Emissions from compressor stations characterized as “gathering”. Emissions scaled linearly with wattage.
11	Other Compressors (HP)	Emissions from all other compressor stations. Emissions scaled linearly with wattage.
12	Production Compressors (C)	Emissions from compressor stations characterized as “production”. Emissions constant among compressors.
13	Gathering Compressors (C)	Emissions from compressor stations characterized as “gathering”. Emissions constant among compressors.
14	Other Compressors (C)	Emissions from all other compressor stations. Emissions constant among compressors.

**Table 2: Annual emission rate totals from anthropogenic sources within the innermost model domain based on values from the inventory within this study**

Source	Total Emission Rate (Gg CH <sub>4</sub> year <sup>-1</sup> )
Unconventional Wells	125
Conventional Wells	607
Gathering Compressor Facilities	118
Storage Facilities	69
Gathering/Transmission Pipelines	8
Natural Gas Distribution	213
Underground, Surface, and Abandoned Coal Mines	831
Enteric Fermentation/Manure Management	371
Landfills	420
<b>Total</b>	<b>2762</b>

**Table 3: Meteorological statistics from the May 2015 flight campaign.**

Day	Flight Pattern	# of Loops	# of Vertical Profiles	ABL Depth (m)	Mean Observed Wind Speed (m/s)	Mean Observed Wind Direction	Model Background Value (ppm)
May 14	Box	1	2	1300	2.9	30°	1.908
May 21	Raster	N/A	2	1300	3.9	231°	1.905
May 22	Box	2	2	2300	10.1	300°	1.910
May 23	Box	2	2	1400	4.4	276°	1.906
May 24 <sup>1</sup>	Other	N/A	2	1500	4.4	270°	1.923
May 24 <sup>2</sup>	Raster	N/A	2	2050	4.8	272°	1.907
May 25	Box	1	2	1800	9.0	217°	1.920
May 28	Box	2	3	1400	7.1	322°	1.897
May 29	Box	2	2	1000	4.6	195°	1.899
June 3	Raster	N/A	1	1250	2.7	149°	1.898



**Table 4: Optimized natural gas emission rates for each flight as well as corrected emission rates adjusting for errors in the model wind speed and boundary layer height For wind speed and boundary layer height error, a negative value represents a model value less than the observations.**

Day	Optimized NG Emission Rate (% of production)	Wind Speed Error (6)	Boundary Layer Height Error (7)	Corrected NG Emission Rate (% of production)
May 14	0.37	-31%	-33%	<u>0.4780</u>
May 21	0.53	3%	39%	<u>0.7637</u>
May 22	1.15	37%	-18%	<u>1.3902</u>
May 23	0.45	34%	-9%	<u>0.5537</u>
May 24	0.68	48%	-21%	<u>0.8058</u>
May 24	0.36	48%	-21%	<u>0.4230</u>
May 25	0.99	3%	-43%	<u>0.58169</u>
May 28	0.33	-4%	-8%	<u>0.2937</u>
May 29	0.35	4%	1%	<u>0.3733</u>
June 3	0.26	19%	-8%	<u>0.2924</u>
<b>Average</b>	<b>0.55</b>	<b>16%</b>	<b>-12%</b>	<b><u>0.5561</u></b>

**Table 5: Emission rates and potential errors associated with the model optimization technique. r-values represent the correlation between the model and observation-derived upstream natural gas enhancements.**

Day	Optimized Upstream Emission Rate (% of production)	<u>r-value Model vs Obs NG Sources</u>	Background Error	Non-Upstream Gas Inventory Error	Model Performance Error	Total Error	2σ Confidence Interval (% of Production)
May 14	0.37	<u>0.20</u>	±24%	<u>±2019%</u>	±17%	<u>±3635%</u>	±0.13
May 21	0.53	<u>0.31</u>	±24%	<u>±1713%</u>	±30%	<u>±4241%</u>	±0.22
May 22	1.15	<u>0.47</u>	±38%	<u>±65%</u>	±37%	±53%	±0.61
May 23	0.45	<u>0.10</u>	±39%	±13%	±42%	±59%	±0.26
May 24 <sup>1</sup>	0.68	<u>0.31</u>	±24%	<u>±5481%</u>	±17%	<u>±6486%</u>	±0.4258
May 24 <sup>2</sup>	0.36	<u>0.11</u>	±51%	<u>±78150%</u>	±31%	<u>±98161%</u>	±0.3557
May 25	0.99	<u>0.43</u>	±29%	<u>±1915%</u>	±30%	<u>±4644%</u>	±0.4544
May 28	0.33	<u>0.33</u>	±76%	<u>±3612%</u>	±20%	<u>±8679%</u>	±0.2926
May 29	0.35	<u>0.58</u>	±24%	<u>±911%</u>	±19%	<u>±3233%</u>	±0.4412
June 3	0.26	<u>0.37</u>	±31%	<u>±4012%</u>	±24%	<u>±4041%</u>	±0.11

Formatted Table

Inserted Cells

**Table 6: Emission rates from mass balance calculations on applicable days, with emission ranges associated with a  $\pm 5$ ppb error in the background value.**

Flight	CH <sub>4</sub> Production within box (Gg hr <sup>-1</sup> )	Mass Balance CH <sub>4</sub> Flux (kg hr <sup>-1</sup> )	Non-Upstream CH <sub>4</sub> Emissions (kg hr <sup>-1</sup> )	Calculated Upstream Emission Rate (% of production)	2 $\sigma$ Confidence Interval (% of Production)
May 22 <sub>1</sub>	4.96	53800	2250	1.04	$\pm 1.09$
May 22 <sub>2</sub>	4.96	27400	2250	0.51	$\pm 1.08$
May 23 <sub>1</sub>	4.05	5600	934	0.11	$\pm 0.07$
May 23 <sub>2</sub>	4.05	5500	934	0.11	$\pm 0.07$
May 28 <sub>1</sub>	3.73	7100	706	0.17	$\pm 0.11$
May 28 <sub>2</sub>	3.73	6000	843	0.14	$\pm 0.10$
May 29 <sub>1</sub>	4.63	27900	1622	0.57	$\pm 0.30$

**Table 7: Relative error associated with the different sources of uncertainty in the aircraft mass balance.**

Flight	Wind Speed Error	Background Error	ABL Error	Inventory Error	Total Error ( $1\sigma$ )	Upstream Emission Rate (% of Production) w/ $2\sigma$ Confidence Interval
May 22 <sub>1</sub>	±3%	±56%	±9%	±5%	±57%	1.04 ±1.09
May 22 <sub>2</sub>	±3%	±121%	±9%	±8%	±121%	0.51 ±1.08
May 23 <sub>1</sub>	±3%	±24%	±7%	±20%	±32%	0.11 ±0.07
May 23 <sub>2</sub>	±3%	±26%	±7%	±21%	±34%	0.11 ±0.07
May 28 <sub>1</sub>	±3%	±31%	±7%	±11%	±34%	0.17 ±0.11
May 28 <sub>2</sub>	±3%	±33%	±7%	±16%	±38%	0.14 ±0.10
May 29 <sub>1</sub>	±3%	±28%	±20%	±8%	±36%	0.57 ±0.30

**Table 8: Production statistics from mid-2014 for various shales across the United States (Hughes 2014).**

	Barnett	Fayetteville	Haynesville	Marcellus	Bradford/ Susquehanna County, PA
# of Producing Wells	16100	4500	3100	7000	1558
Total Production (Bcf day <sup>-1</sup> )	5.0	2.8	4.5	12	5.01
Production per well (MMcf day <sup>-1</sup> )	0.31	0.56	1.25	1.71	3.22

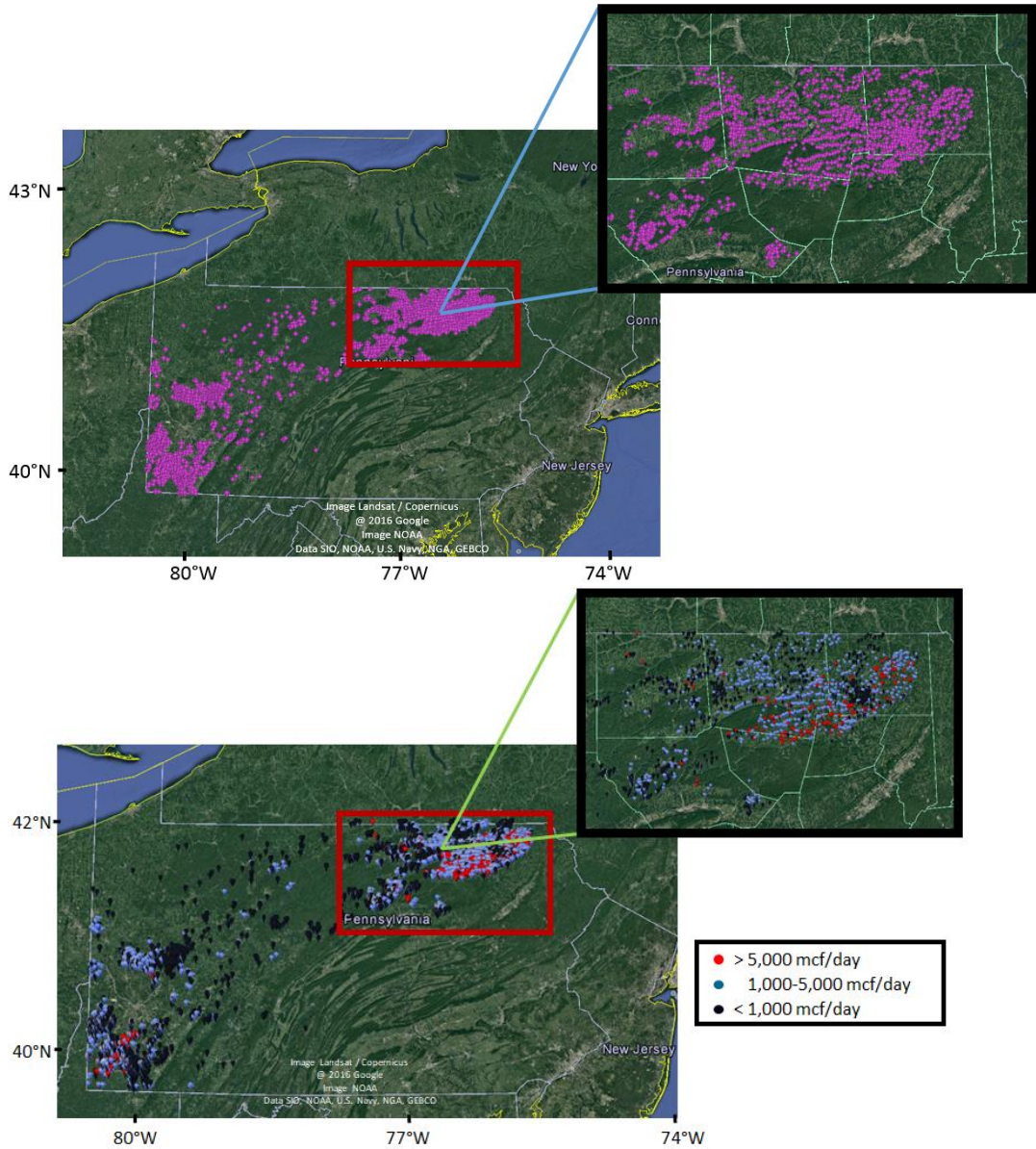
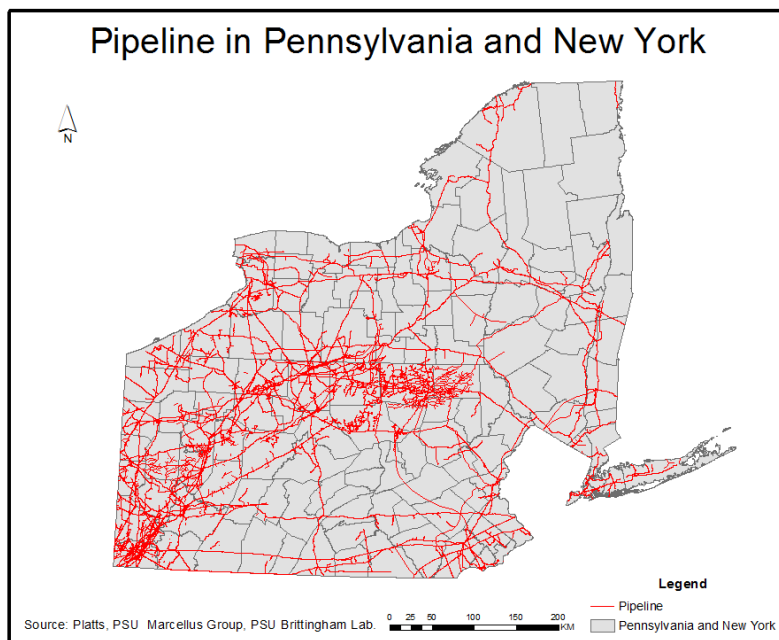


Figure 1: A map of the unconventional wells in Pennsylvania dotted in purple. Production values of wells for May 2015 are indicated by the marker colour. Red rectangle and zoom-in show the region of focus for this study, 41.1-42.2°N 75.2-77.6°W.



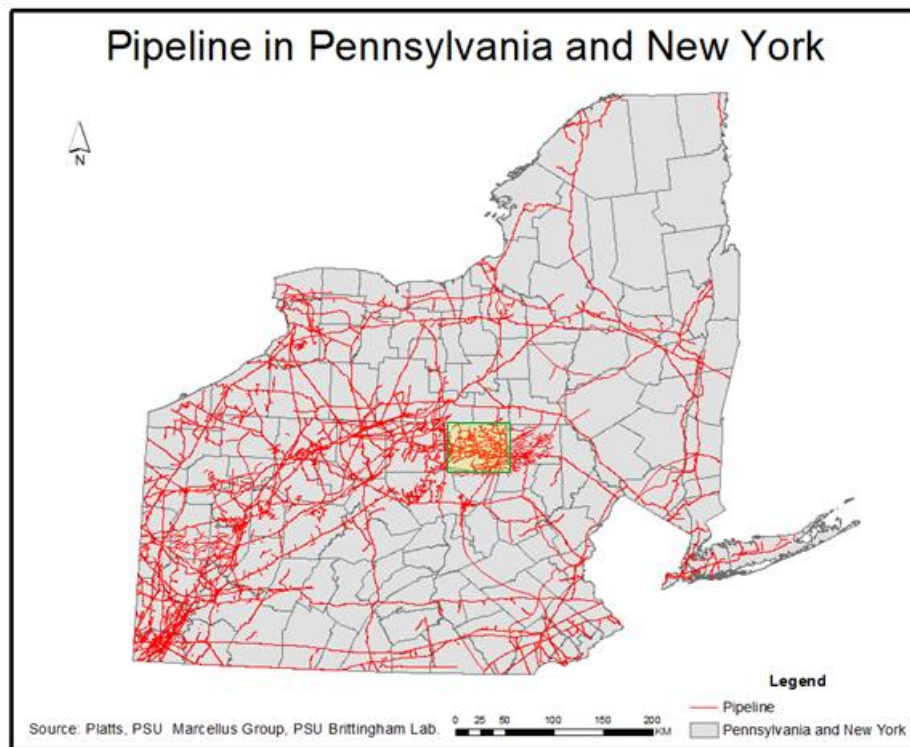


Figure 2: A map of transmission and gathering pipelines for the state of PA and NY. Transmission pipelines are provided by Platts Natural Gas Pipelines product. Gathering pipelines associated with unconventional wells in PA are extrapolated using information on existing gathering pipelines provided by Bradford County, PA: (highlighted in yellow).

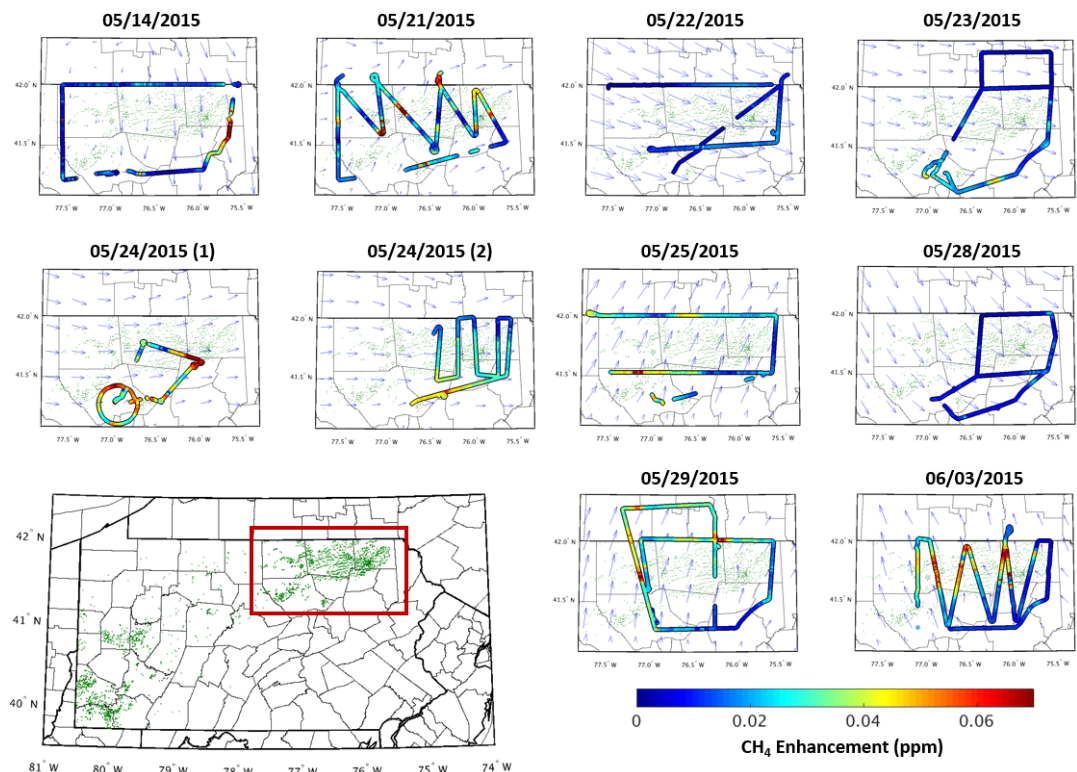


Figure 3: Observed CH<sub>4</sub> enhancements within the boundary layer from each of the 10 afternoon flights used in this study, with green dots showing the location of unconventional wells in PA and blue arrows showing the modelled wind direction during the time of the flight. CH<sub>4</sub> enhancements are calculated by taking the observed CH<sub>4</sub> mole fraction values and subtracting off the flight's background CH<sub>4</sub> value shown in Table 3.

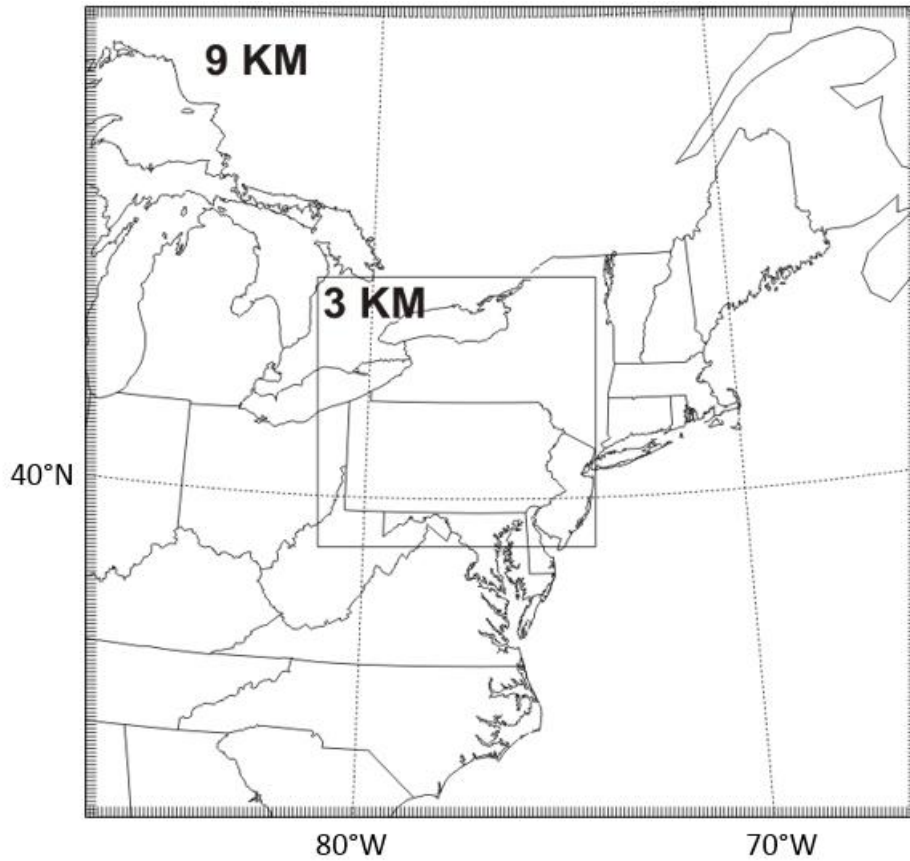


Figure 4: Model domain and resolutions used within the transport model. All emissions used for this study are contained within the 3 km resolution domain.



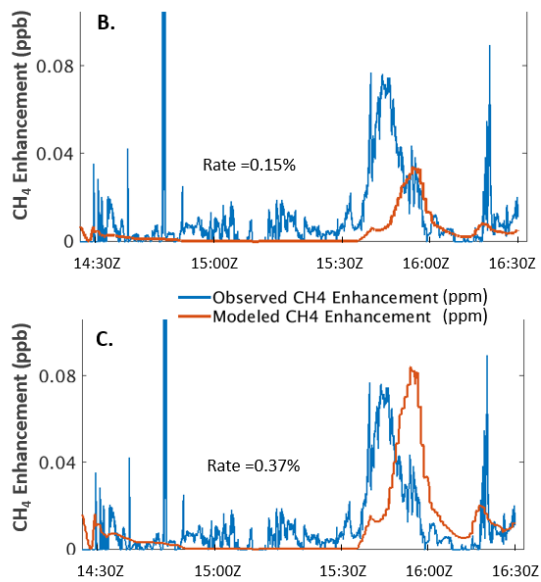
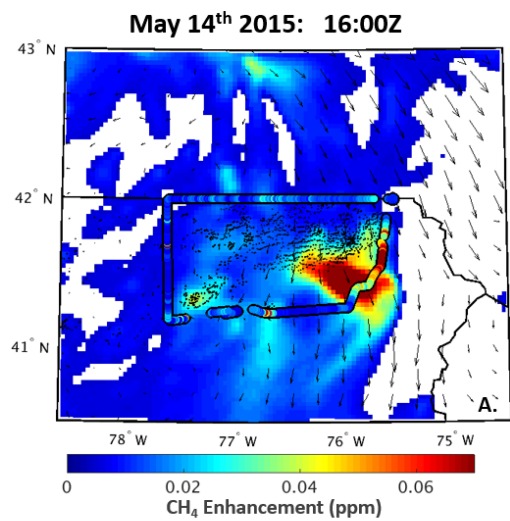
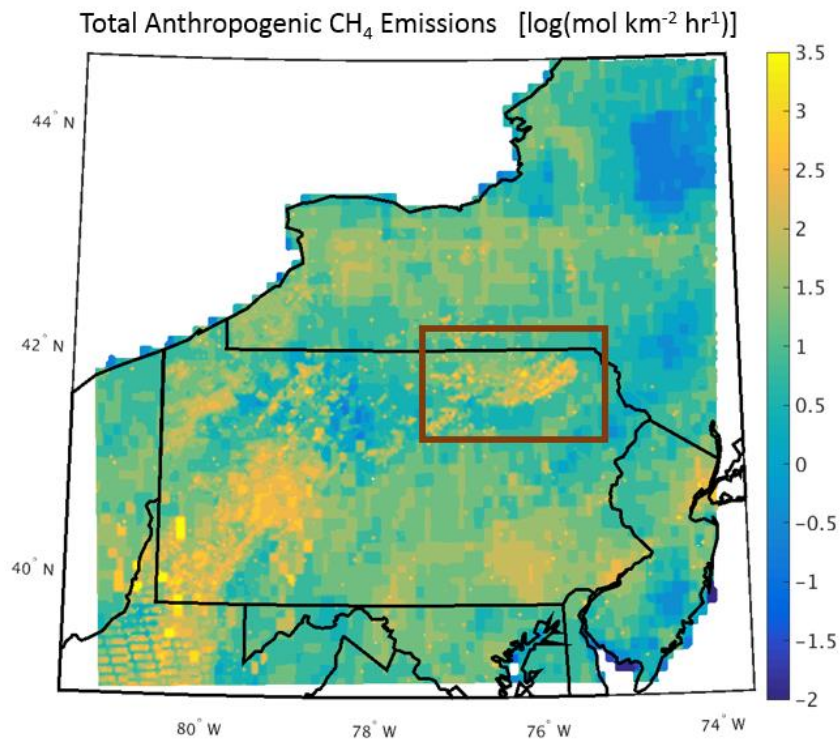
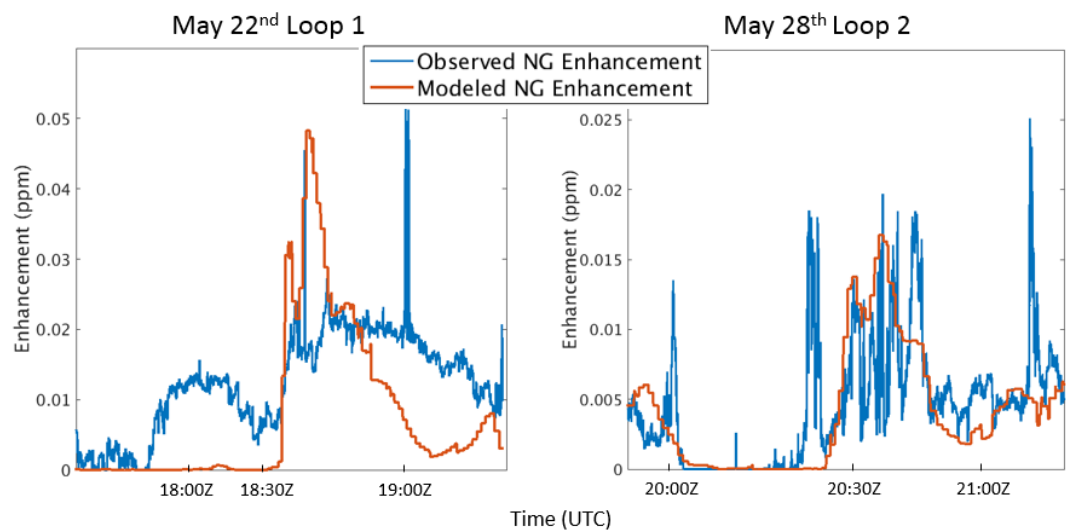


Figure 5: (a.)



**Figure 5** Observed vs model projected CH<sub>4</sub> enhancements during the May 14<sup>th</sup>, 2015 at 16Z. (b.) Comparison of observed natural gas enhancement to modelled natural gas enhancement along flight path, with upstream emission rate optimized by minimizing the absolute error between the datasets. (c.) Same as previous, but optimized by minimizing the sum of the error between the datasets.

**Formatted:** Font: Bold



**Figure 6:** Comparison of observed natural gas enhancement to modelled natural gas enhancement for segments along the (left) May 22<sup>nd</sup> flight and (right) May 28<sup>th</sup> flight. A distinct lack of representativeness of the observations in the modelled enhancement can be seen in the May 22<sup>nd</sup> flight compared to the May 28<sup>th</sup> flight.

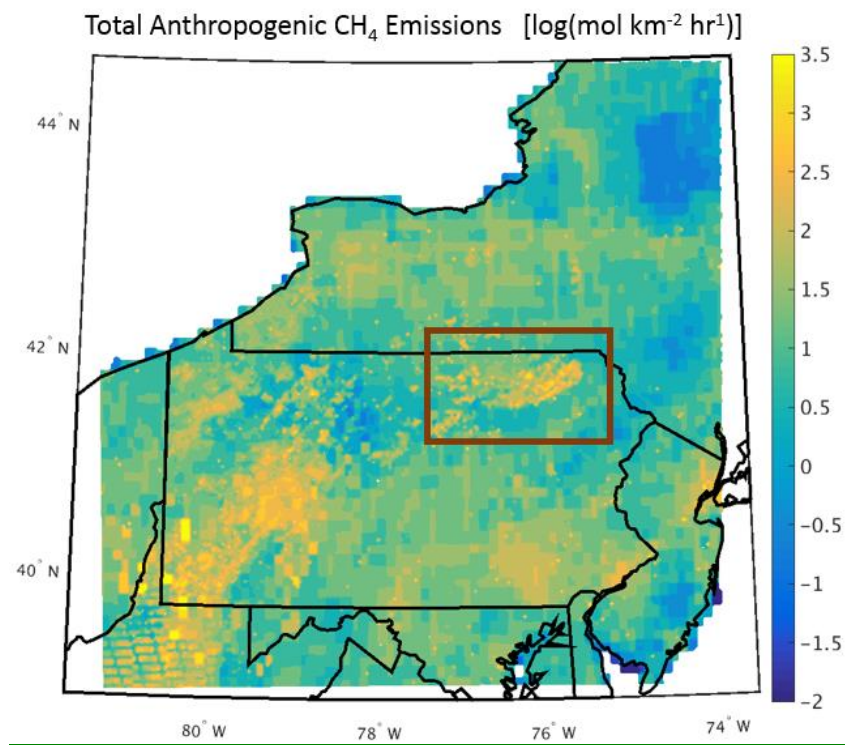


**Figure 7:** A log scale contour of the anthropogenic CH<sub>4</sub> emissions inventory from this study used within the transport model. The red rectangle surrounds the study region where the aircraft campaign took place.

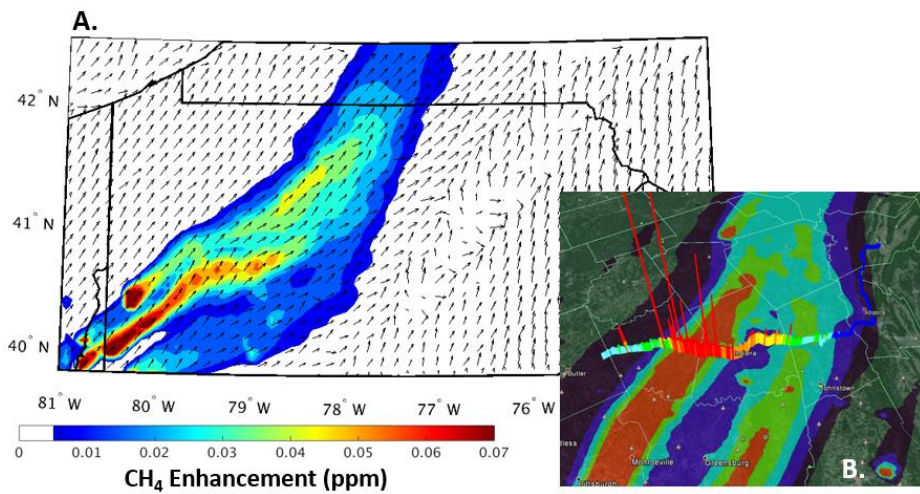


Figure 68: (a.) Model projected CH<sub>4</sub> enhancement at the surface associated with underground, surface, and abandoned coal mines on May 27<sup>th</sup>, 2015 at 19Z, with the shaded regions showing the CH<sub>4</sub> enhancement and the arrows representing the wind direction. (b.) Projected enhancement from a. mapped over measured CH<sub>4</sub> enhancement from a driving campaign. The height and colour of the bars represents the scale of the CH<sub>4</sub> enhancement.

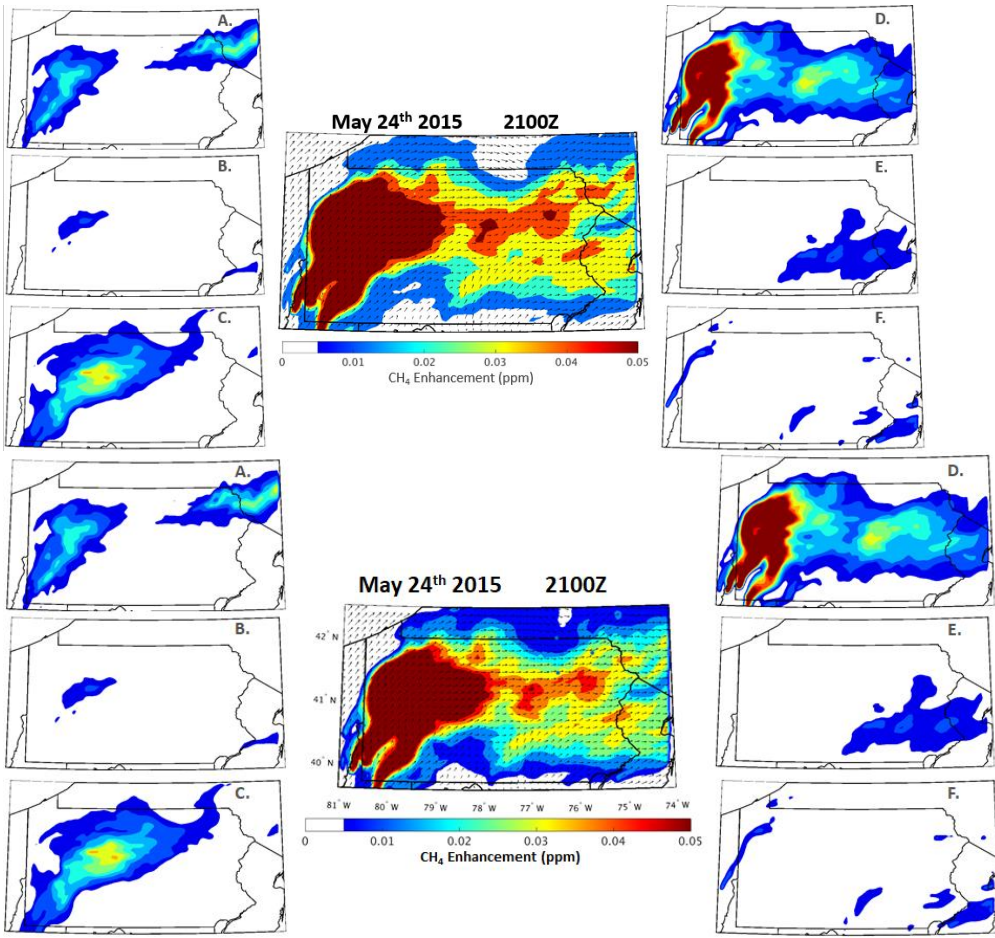


Figure 79: Projected CH<sub>4</sub> enhancements during the late afternoon flight of May 24<sup>th</sup>, 2015 at 2100Z, 700m above ground level from (A) upstream unconventional gas processes (B) downstream unconventional gas processes (C) conventional production (D) coal mines (E) animal emissions and (F) landfills and other sources within the EPA GHG Inventory Report. The centre figure is a map of the combined enhancement from sources A-F.

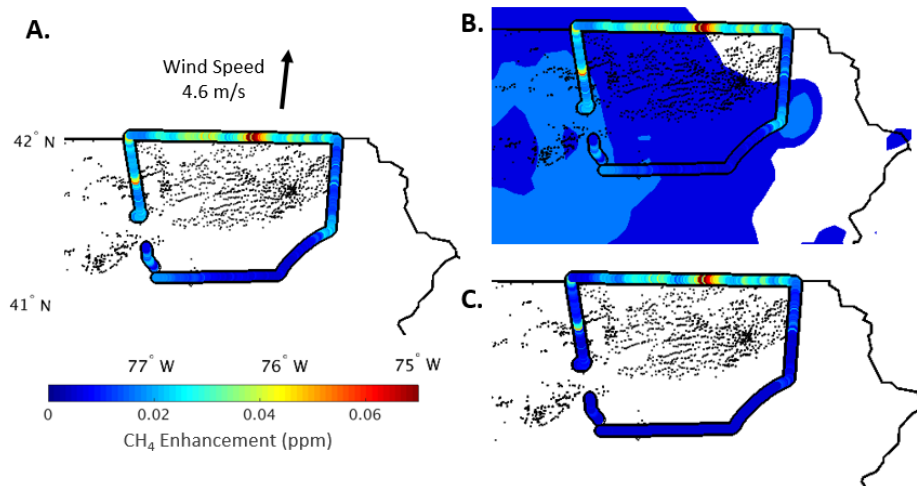


Figure 810: (a.) Observed CH<sub>4</sub> enhancements from within the boundary layer during the first loop of the May 29<sup>th</sup> aircraft campaign. (b.) Aircraft observations laid overtop modelled CH<sub>4</sub> concentrations at 700 m from sources unrelated to emissions from upstream gas production. (c.) Observed CH<sub>4</sub> enhancements from the May 29<sup>th</sup> flight after subtracting off modelled sources in b. The new set of observations represent the ~~observed~~ observation-derived upstream gas enhancement during the flight.



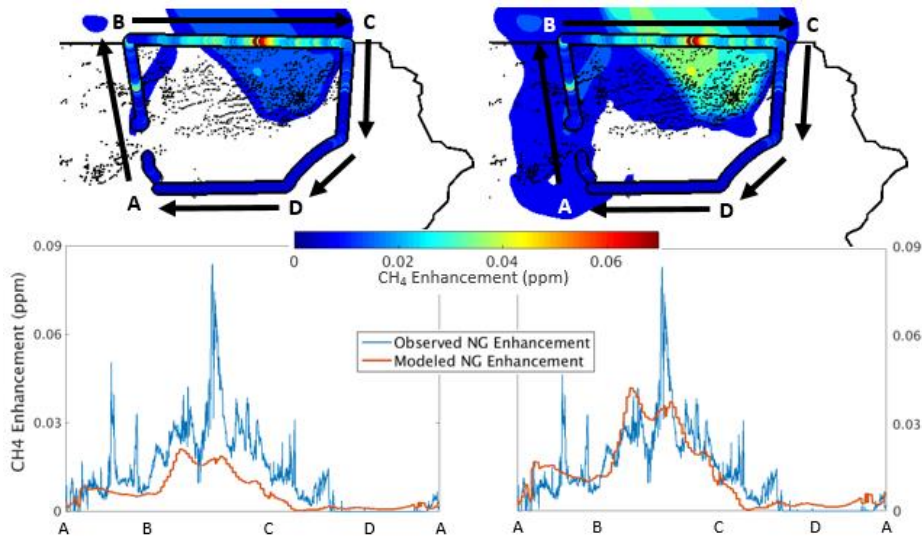


Figure 911: (top-left) Observed enhancement from unconventional natural gas production overtop projected upstream natural gas enhancements at 700 m from the first loop of the May 29<sup>th</sup> flight, using an upstream gas emission rate of 0.13% of production. (bottom-left) Direct comparison of the observed natural gas enhancement vs. the modelled enhancement following the path from A-D using an unconventional emission rate of 0.13%. (top-right, bottom-right). Same as left figures, except using the optimized upstream emission rate of 0.26%

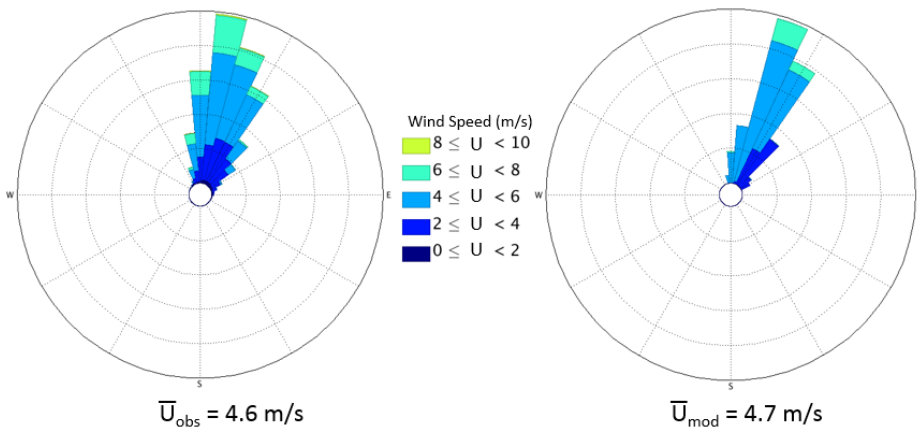


Figure 1012: Wind rose of aircraft observations (left) within the boundary from the first loop of the May 29<sup>th</sup> flight compared to modelled winds following the flight path (right).



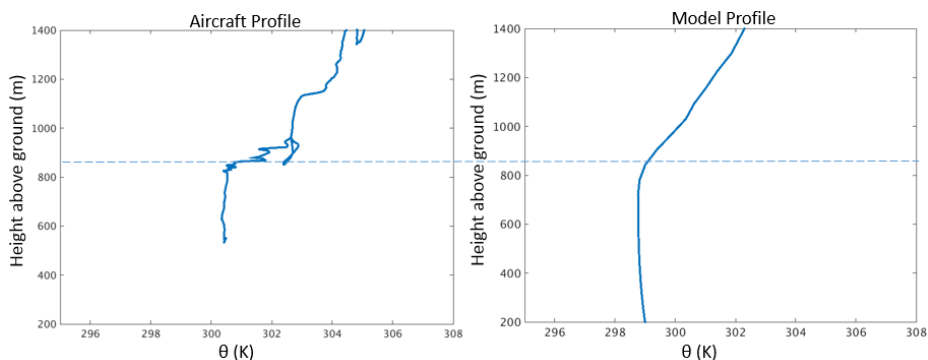


Figure 413: (left) Observed potential temperature profile with height from the first aircraft spiral on the May 29<sup>th</sup> flight at 17Z. (right) Modelled potential temperature at the location and time at which the aircraft spiral occurred. In both cases, an inversion in the potential temperature profile begins to occur around 850m.

### May 24<sup>th</sup> 2015: Late-Afternoon Flight

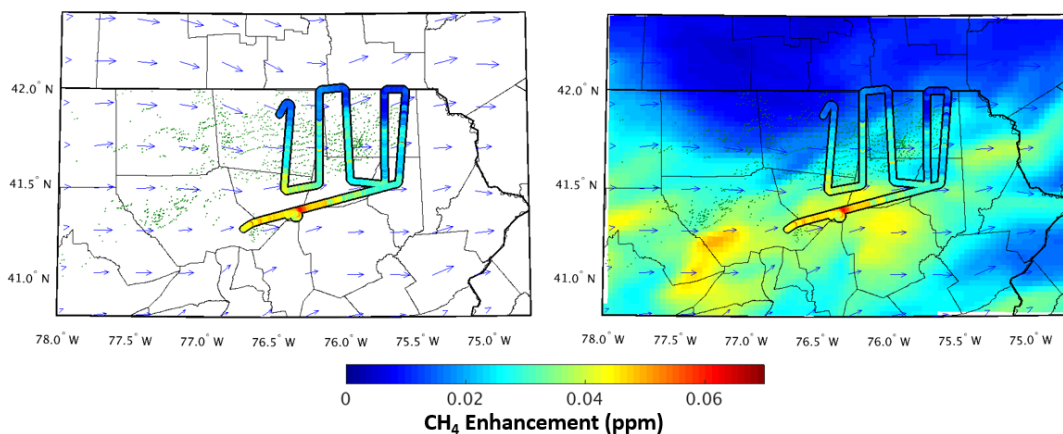


Figure 414: (left) Observed CH<sub>4</sub> enhancement from the late-afternoon flight on May 24<sup>th</sup>, 2015. (right) Observed CH<sub>4</sub> enhancement compared to the model projected CH<sub>4</sub> enhancement from the sum of all sources in the region. The colour scale of observed and projected enhancements is scaled 1:1, with matching colours indicating matching values. Modelled wind vectors and CH<sub>4</sub> concentrations are from 700 m model height level.

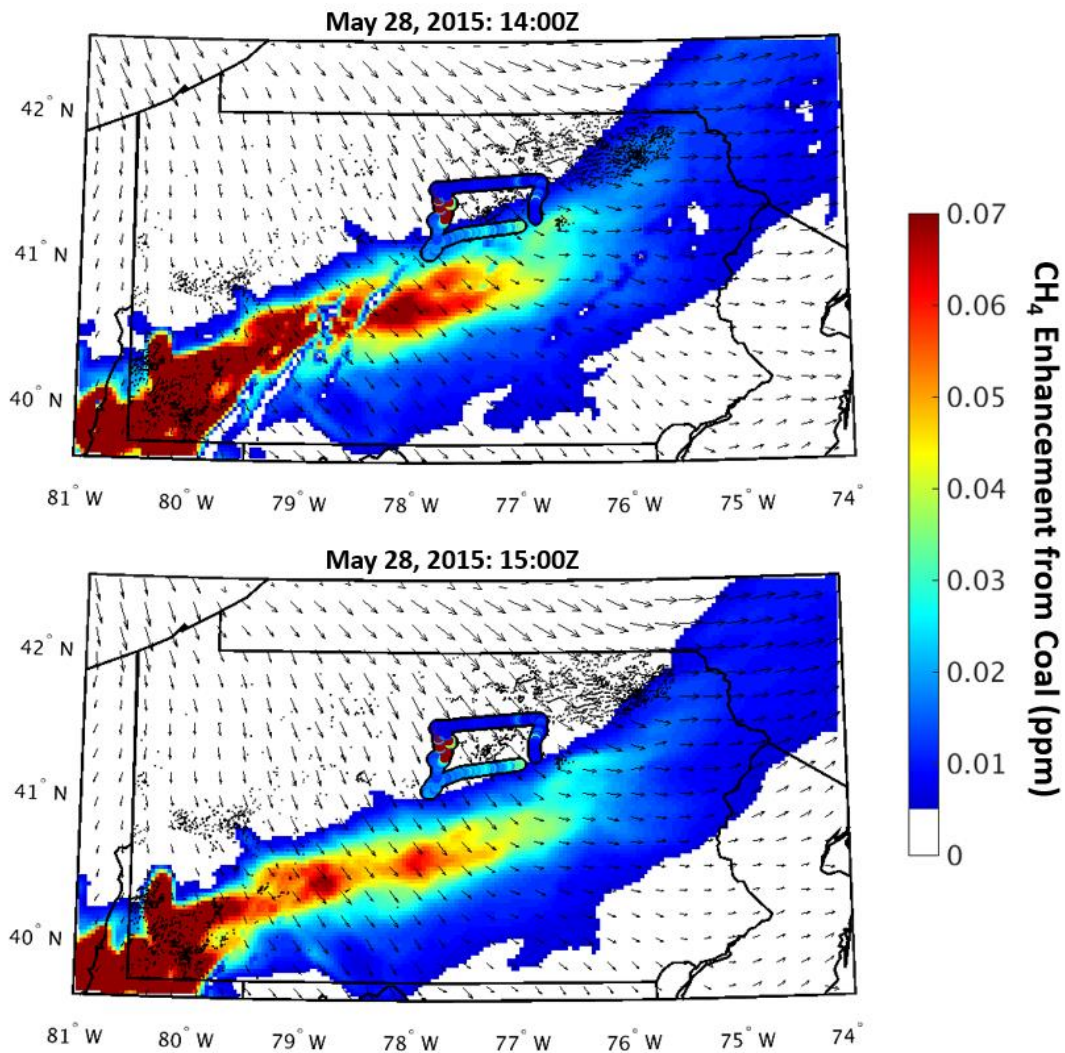


Figure 1315: Observed CH<sub>4</sub> enhancements from an early flight on May 28th, 2015 compared to projected CH<sub>4</sub> enhancements from coal emissions modelled at (top) 14:00Z and (bottom) 15:00Z. The one hour time difference results in vastly different projected enhancements across the southern portion of observations. Modelled wind vectors and CH<sub>4</sub> concentrations are from the 700 m model height level.

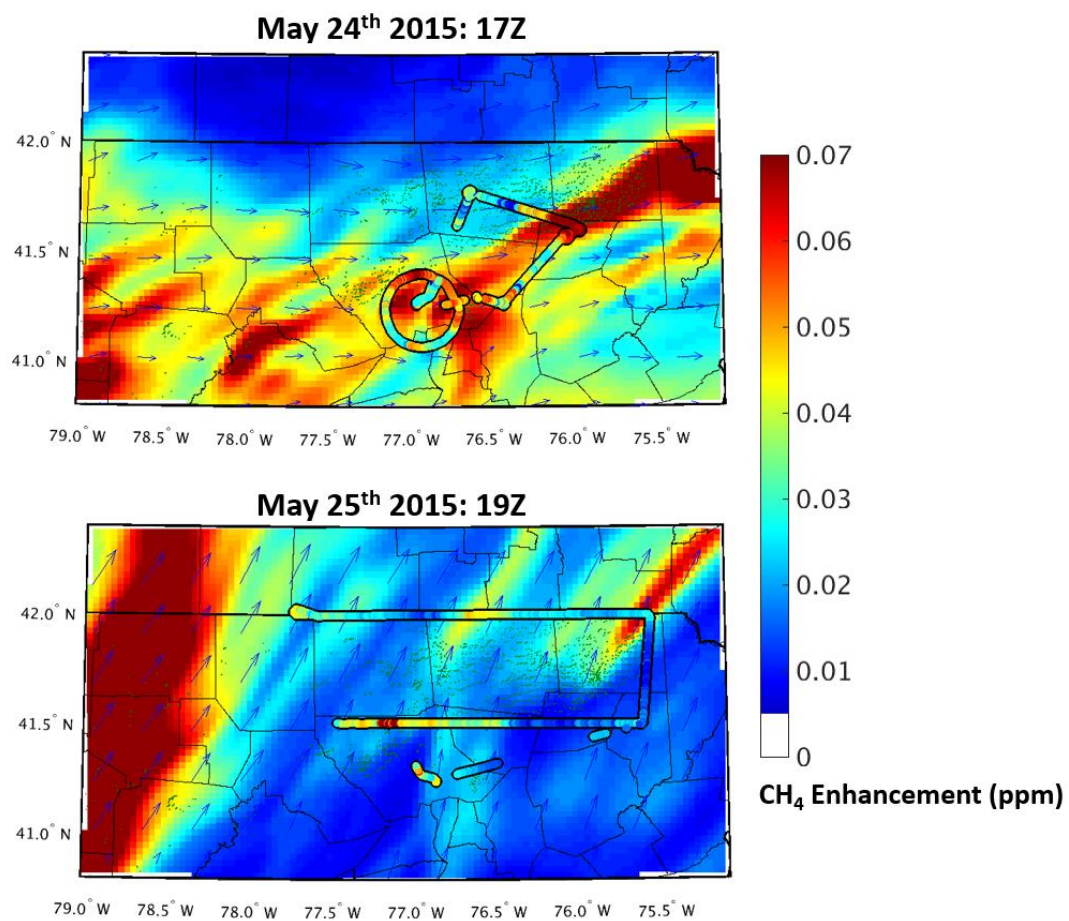
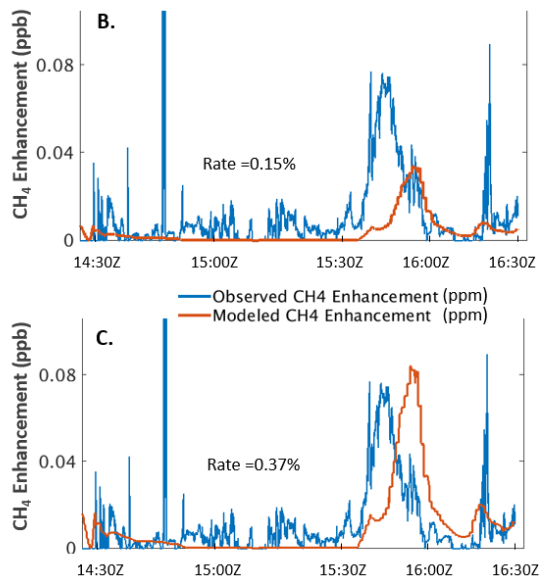
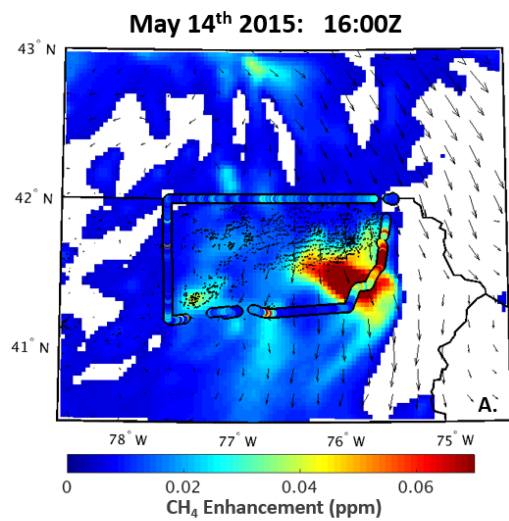


Figure 4416: Observed vs model projected CH<sub>4</sub> enhancements during (top) the early afternoon flight of May 24<sup>th</sup>, 2015 at 17Z and (bottom) the flight of May 25<sup>th</sup>, 2016 at 19Z. Modelled wind vectors and CH<sub>4</sub> concentrations are from 700 m model height level.



**Figure 15:** (a.) Observed vs model projected CH<sub>4</sub> enhancements during the May 14<sup>th</sup>, 2015 at 16Z. (b.) Comparison of observed natural gas enhancement to modelled natural gas enhancement along flight path, with upstream emission rate optimized by minimizing the absolute error between the datasets. (c.) Same as previous, but optimized by minimizing the sum of the error between the datasets.

**Formatted: Font: Bold**

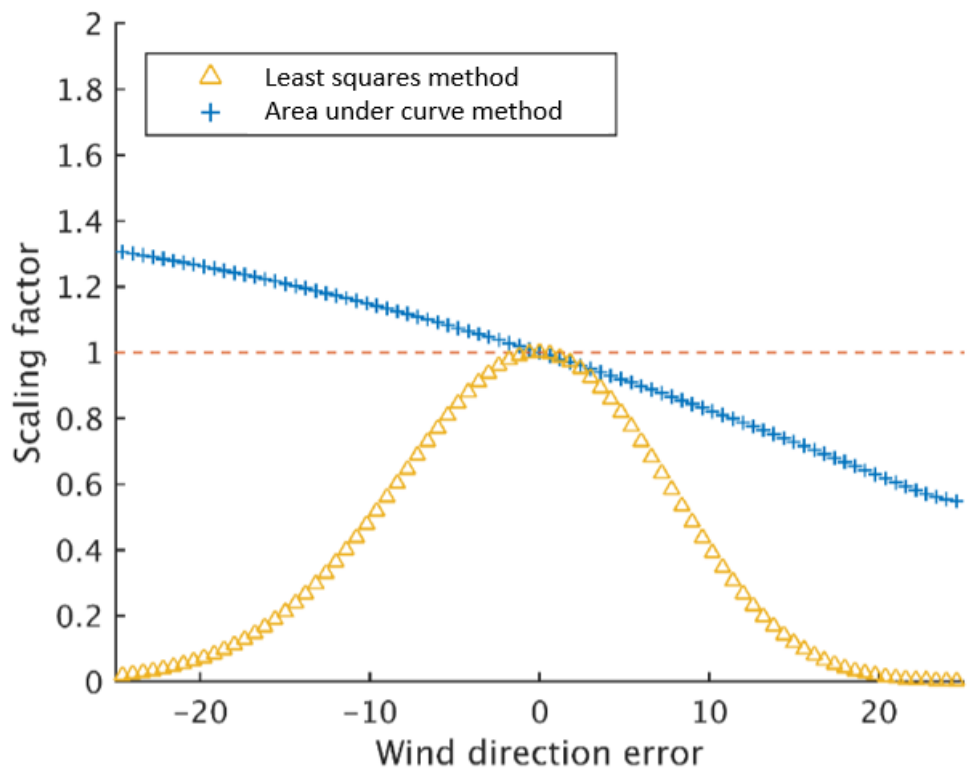
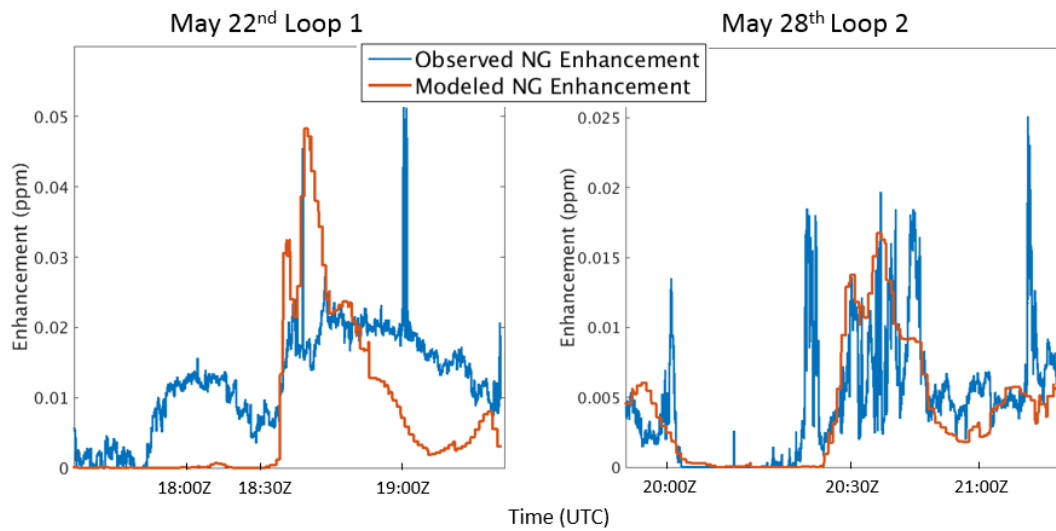
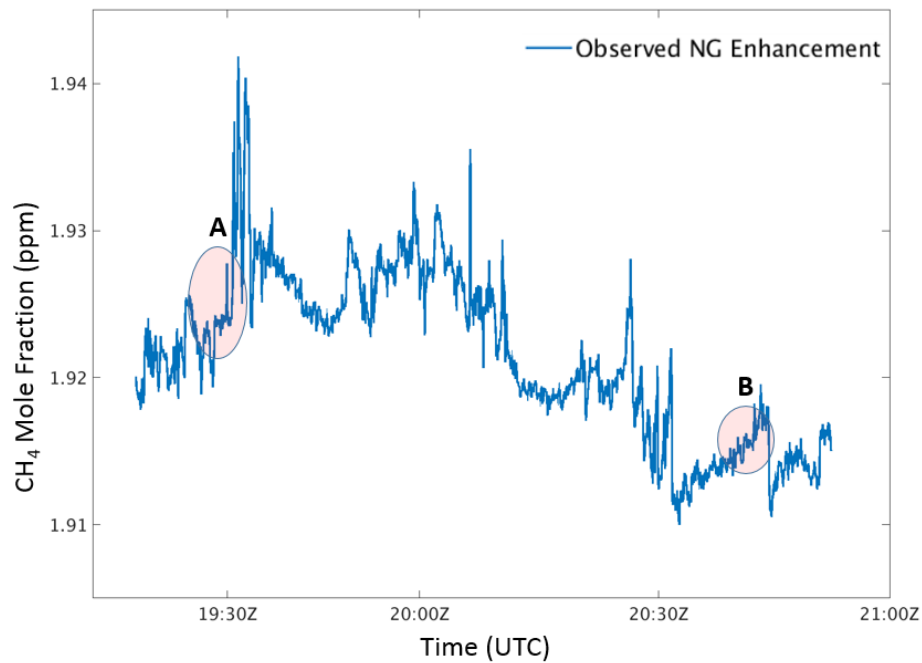


Figure 16: A demonstration of the effect of model transport error on the optimized emission rate using pseudo-observations transecting a modelled plume at a 45° angle. The scaling factor represents the change in the optimized emission rate compared to the true emission rate, with 1 representing a perfect rate.



**Formatted:** Caption

**Formatted:** Font: Not Bold

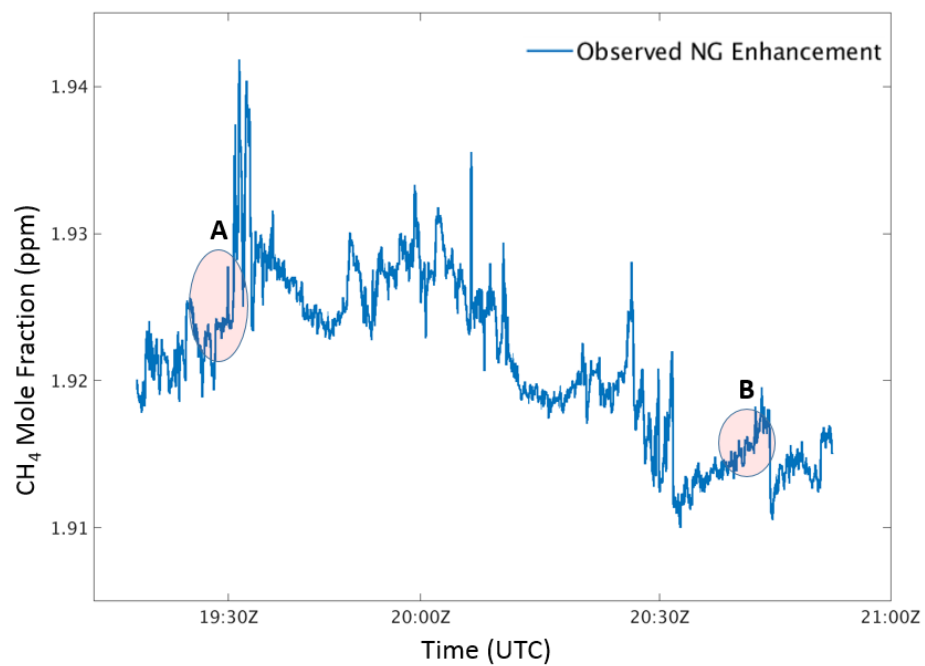


**Figure 17.** Comparison of observed natural gas enhancement to modelled natural gas enhancement for segments along the (left) May 22nd flight and (right) May 28th flight. A distinct lack of representativeness of the observations in the modelled enhancement can be seen in the May 22nd flight compared to the May 28th flight.

**Figure 17**

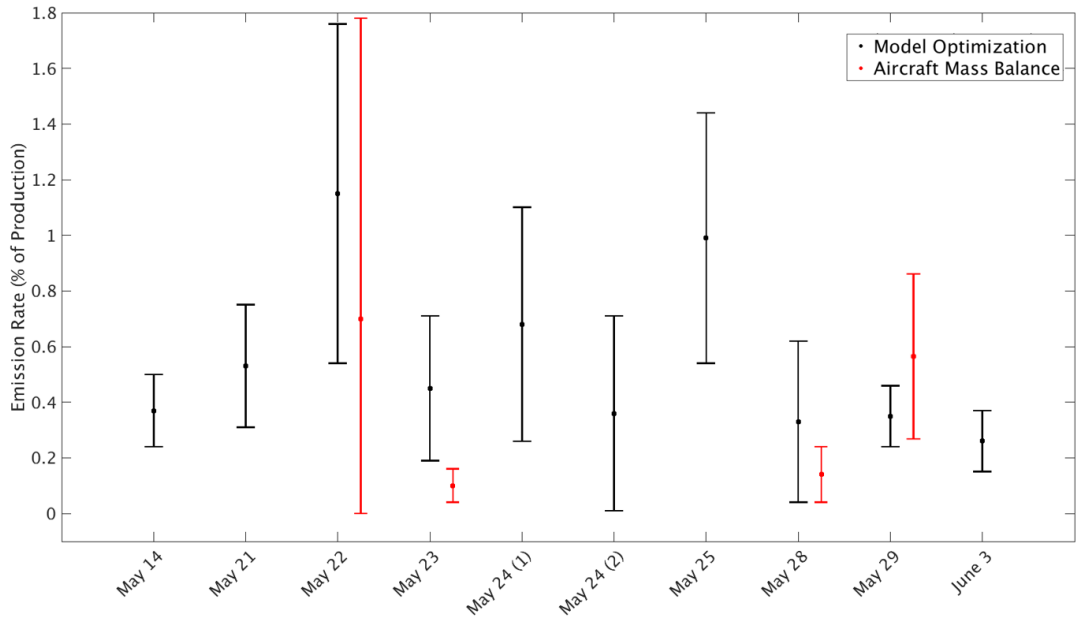
**Formatted:** Caption

**Formatted:** Font: Not Bold



**Figure 18:** Time series of CH<sub>4</sub> mole fractions from the second loop of the May 22<sup>nd</sup> flight. Observations at the shaded areas below A and B were taken at similar locations in space, showing the change in the background mole fraction across time.





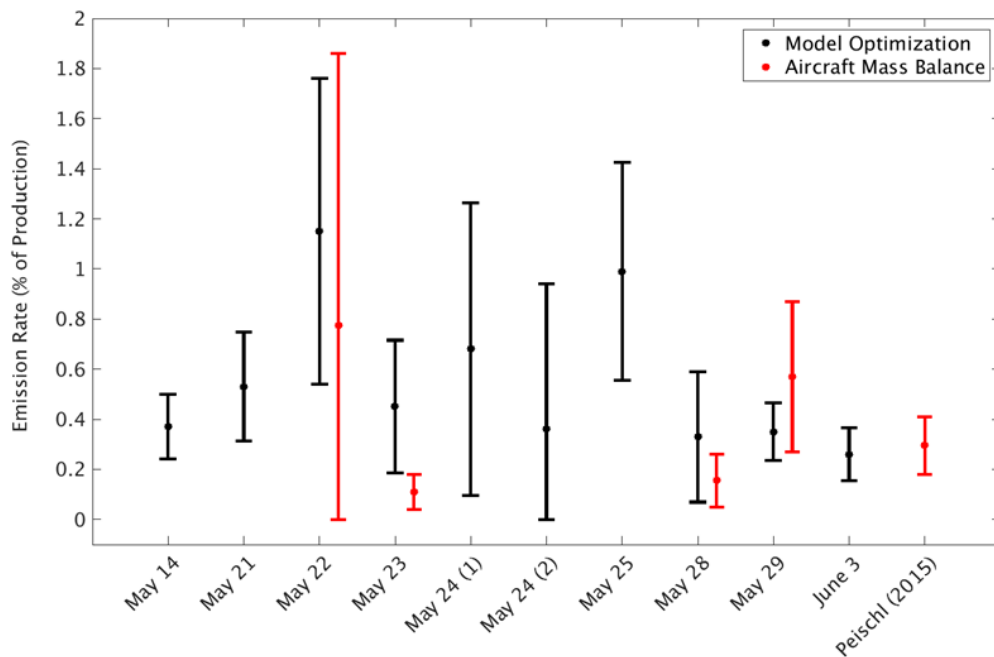


Figure 4918: Calculated upstream natural gas emission rates using (black) model optimization technique and (red) aircraft mass balance technique. Error bars represent the 2 $\sigma$  confidence interval for each flight. Mass balance performed in Peischl et al (2015) included for comparison.

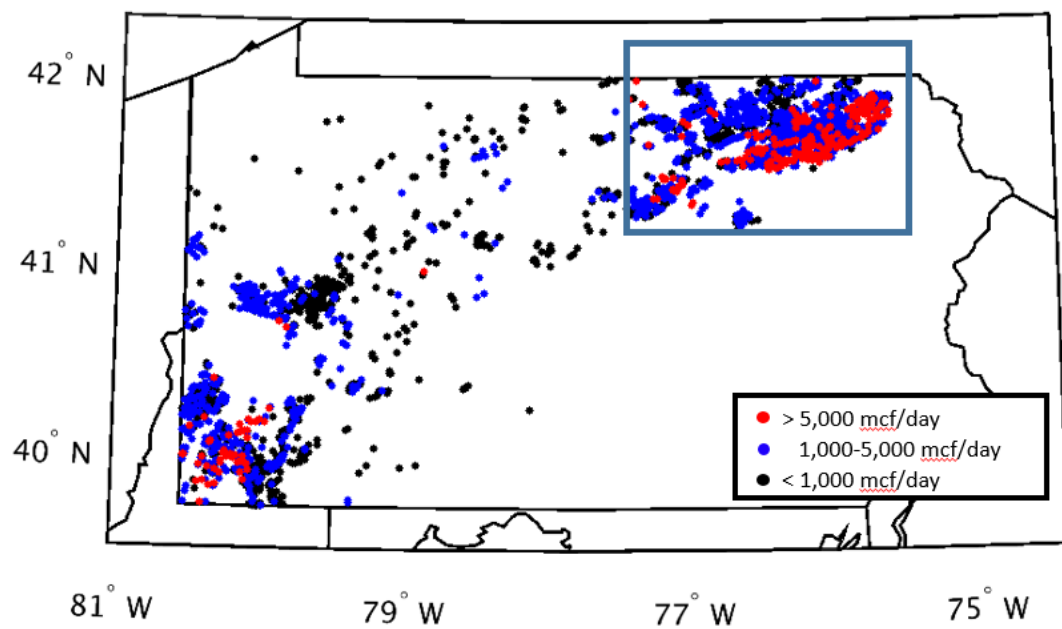


Figure 20: Well locations and daily production of unconventional wells in PA for May 2015. Boxed region is study region where flights took place.

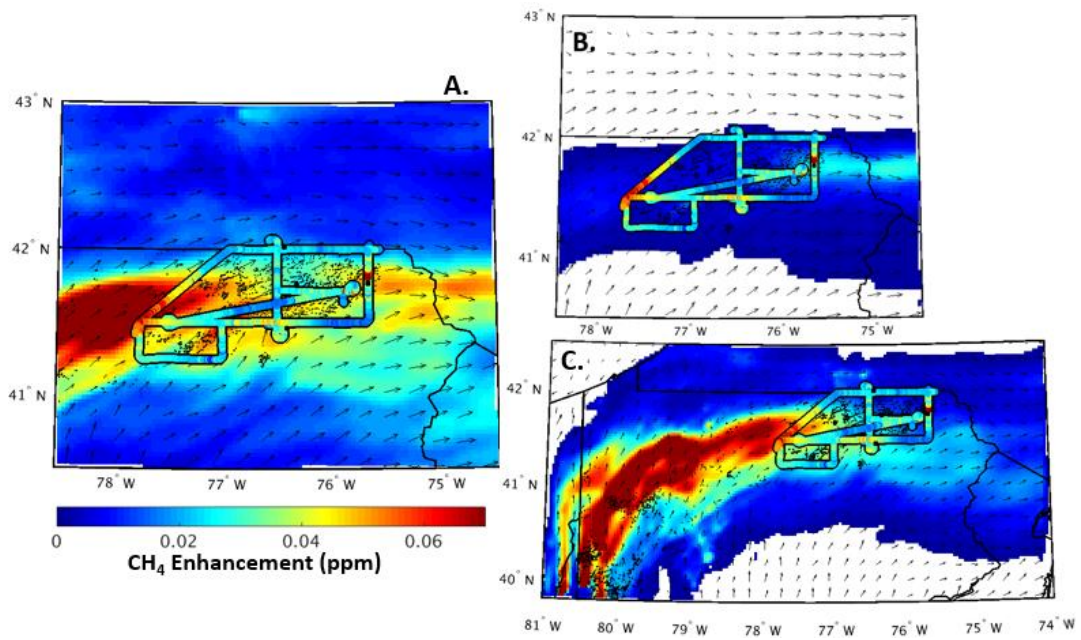
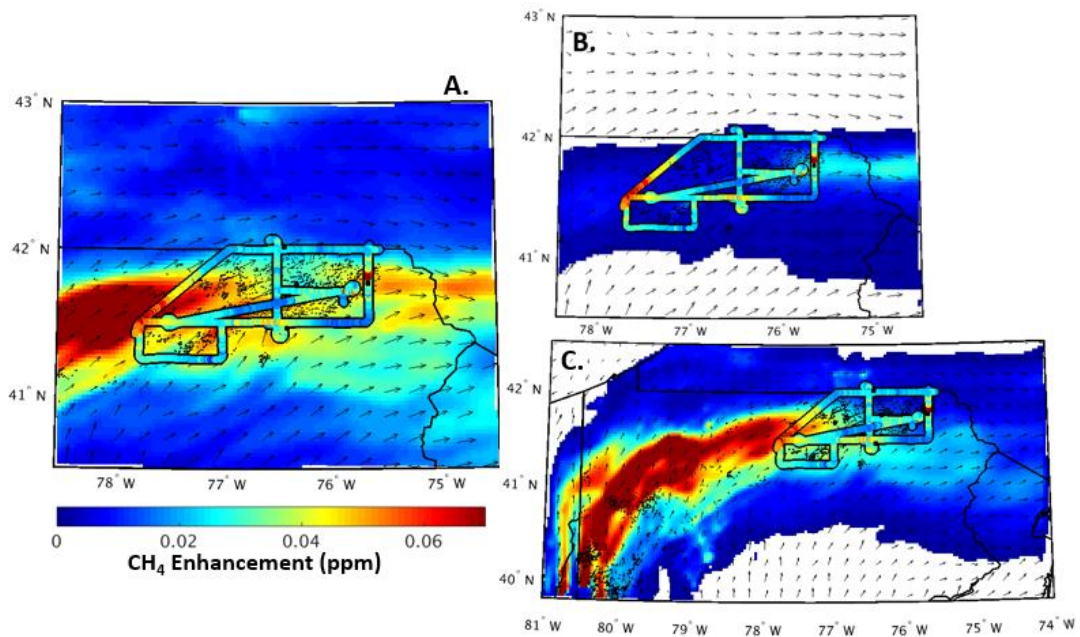


Figure 21



**Figure 19:** Observations vs modelled enhancements of the flight from Peischl et. al (2015) for July 6th, 2013. (a.) Observed enhancements from the flight over model projected enhancements from all sources at 21Z. (b.) Projected enhancement from upstream gas processes using a 0.4% emission rate. (c.) Projected enhancement from coal sources in southwestern PA. Modelled wind vectors and CH<sub>4</sub> concentrations are from 700 m model height level.